Doctoral thesis

Linear Perturbations of Spherically Symmetric Black Holes and Their Stability

球対称ブラックホールの線形摂動と安定性

Takuya Katagiri

Department of Physics, Graduate School of Science,
Rikkyo University

Abstract

Black holes are central in gravitational physics and have been intensively investigated not only from the perspective of astrophysics but also mathematics and quantum mechanics. In this thesis, we aim to reveal phenomenologically and mathematically rich features of spherically symmetric black holes in terms of the black hole perturbation theory and approach their fundamental problem: stability.

We study quasinormal mode frequencies of neutral and charged scalar field perturbations in the Reissner-Nordström-anti-de Sitter black holes and discuss the stability of the black holes in terms of the quasinormal mode frequencies. We apply the Robin boundary condition, which is the most general condition, parametrized by one parameter at the conformal infinity. We find that instability of the charged scalar field can be understood in terms of superradiance in that reflective boundary condition. We also find a condition in which the black hole is superradiantly unstable irrespectively of the Robin boundary condition parameter. On the other hand, if the condition is not satisfied, the stability crucially depends on the Robin boundary condition parameter and there appears a purely oscillating mode at the onset of the instability. We argue that as a result of the superradiant instability, the scalar field gains charge from the black hole and energy from its ambient electric field, while the black hole gives charge to the scalar field and gains energy from the scalar field but decreases its asymptotic mass parameter.

We investigate conserved quantities and instability on extremal black hole horizons called, respectively, the Aretakis constants and the Aretakis instability. As a first step, we study a massive Klein-Gordon field in two-dimensional anti-de Sitter spacetimes which emerge in the vicinity of an extremal black hole. We find out the geometrical meanings of the Aretakis constants and instability in a parallel-transported frame along a null geodesic: some components of the higher-order covariant derivatives of the field in the parallel-transported frame are constant or unbounded at the late time, respectively. We also show that the Aretakis instability in the two-dimensional anti-de Sitter spacetime is the result of singular behaviors of the higher-order covariant derivatives of the fields on the whole infinity, not a blowup on a specific null hypersurface. We further explicitly demonstrate that the Aretakis constants can be derived from ladder operators constructed from the spacetime conformal symmetry.

Acknowledgements

First of all, I deeply thank my supervisor Tomohiro Harada for his insightful suggestions, useful comments, constructive criticism, encouragement, and for setting an example of a researcher. From when I was an undergraduate student to the present, I have greatly benefited from him.

I would like to offer my special thanks to my collaborator Masashi Kimura for useful feedback, for providing valuable knowledge of how to study and cook, for taking a lot of time to discuss, and for giving me opportunities for invited talks and collaborations.

I would like to show my appreciation to Tsutomu Kobayashi, Takashi Hiramatsu, Yu Nakayama, Hidekazu Tanaka, and Yasuyuki Hatsuda for careful guidance, critical comments, and for giving me opportunities to improve my works. I am grateful to Shahar Hadar, Akihiro Ishibashi, Takaaki Ishii, Shunichiro Kinoshita, Keiju Murata, Shin Nakamura, Harvey S. Reall, and Norihiro Tanahashi for the informative comments and useful discussions.

I thank my colleagues, Koichiro Nakagawa and Keitaro Tomikawa for casual conversations, for sharing important pieces of information, and for taking the time to answer my basic questions. I would like to express my gratitude to Kuniko Kozai for administrative supports and informal communication at tee time.

I really thank Itsuki Hano, Yuta Ikeda, Aya Iyonaga, Yasutaka Koga, Hiroyuki Masunaga, Akihito Mitsugi, Masataka Nagashima, Keisuke Nakashi, Kota Ogasawara, Shun Okawa, Keishiro Okumoto, Masaki Shida, Tomo Tanaka, and Naoko Ueda for great time, a lot of encouragement, and (online) drinking. I sincerely thank my parents, Masumi and Takashi. Without their supports and encouragement, I could not have achieved my works and thesis. I appreciate the financial support from Rikkyo University Special Fund for Research.

Contents

Chapter 1

Introduction

General relativity formulated by Einstein in 1915 [1] is the classical theory of spacetime and gravity. Today, general relativity is in the mainstream of physics, in particular, lays the foundation for astrophysics. In recent years, general relativity has influenced several areas of physics such as particle physics, condensed matter physics, hydrodynamics, and mathematics such as information theory and differential geometry. In fact, gravity involves many key scientific questions of today: How did the Universe begin and evolve to the present one, and how will further do? How can we unify the classical theory of gravity and quantum mechanics? Do black holes really exist in the Universe, and if so, how do they interact with their surroundings? More fundamental questions also arise: Is general relativity right? How correct is it? At the Planck scale, no one knows a quantum description of gravity. At the cosmological scale, the modification of general relativity might explain the accelerating expansion of the present Universe without introducing dark energy. Motivated by those problems, many extended theories of general relativity have also been proposed. A wide set of topics related to gravity forms an area of a study named gravitational physics.

A black hole is one of the most fascinating objects and is central in gravitational physics. The only element in its construction is in essence the concept of spacetimes. In the standard scenario in astrophysics, black holes are formed as a result of the gravitational collapse of a massive star. Black holes are compact objects with strong gravity and involve accreting matter in their surroundings, and are expected to cause high energy phenomena in the neighborhood. From these properties, black holes are regarded as laboratories in the Universe for gravitational physics and high energy physics. Those existences are widely believed and are indeed strongly suggested by many observations. Since the first direct detection of gravitational waves by LIGO in September 2015 [2], many gravitational waves originating from

the black-hole binary systems have been observed [3, 4]. In 2019, the image of the shadow of the central object in M87, which is the candidate of a supermassive black hole, has been reported [5, 6, 7, 8, 9, 10]. In the recent remarkable progress of those observations, a deeper theoretical understanding of the dynamical property of black holes and phenomena arising from them are becoming more and more important.

Black holes have also been widely investigated as theoretical tools for studying physics other than gravity within anti-de Sitter/conformal field theory (AdS/CFT) correspondence proposed by Maldacena in 1997 [11]. That correspondence implies a profound connection between gravity in the higher-dimensional anti-de Sitter spacetime and strongly coupled quantum field theory. This method provides an effective description for the strongly coupled quantum field theory, in which a standard perturbative approach is not applicable, in terms of gravitational physics in the higher-dimensional anti-de Sitter spacetimes. In particular, black holes in the anti-de Sitter spacetime are dual to the quantum field theories at finite temperature. This leads to the expectation that equilibrium and non-equilibrium thermal states can be understood in terms of dynamical properties of the black holes in the anti-de Sitter spacetime. Within this framework, the black holes in the anti-de Sitter spacetime are now utilized as a standard tool in considering near-equilibrium behaviors in condensed matter physics and hydrodynamics [12, 13, 14, 15, 16, 17]. Besides, AdS/CFT correspondence also gives a new perspective for difficult problems in gravitational physics such as the Hawking radiation [18], the black hole information paradox [19, 20], the nature of spacetime singularities [21, 22], and quantum gravity [23, 24].

In mathematics as well, black holes have been investigated. Mathematically, a black hole is a manifold with a Lorentzian metric and a solution of nonlinear partial differential equations. For a black hole solution in general relativity and some extensions, several beautiful theorems have been shown. One of them is the no-hair theorem [25, 26], which claims that four-dimensional asymptotically flat black holes with an electric charge are completely characterized by three classical parameters: mass, electric charge, and spin. In other words, the black hole is remarkably simple geometry. Another one is the uniqueness theorem [27, 28, 29], which claims that a four-dimensional asymptotically flat stationary black hole in vacuum is unique to the Kerr solution [30]. Although it is in general hard to solve the field equations, the black hole solution in general relativity and some extensions are strongly restricted under reasonable assumptions. Sometimes those theorems do not hold in extended theories and the different black holes as those of general relativity are derived. In higher dimensions or other asymptotic spacetime structures such as anti-de Sitter spacetime as well, those theorems

seem not to hold even for general relativity and richer solution space emerges.

Perturbation theory plays a significant role in physics. The black hole perturbation theory is a useful method for studying black hole spacetimes. Analysis of the time evolution of perturbation fields reveals the dynamical properties of a black hole as a linear response to external disturbances. The time evolution of the fields is typically divided into three contributions [31, 32]: the prompt contribution which is the early-time signal directly traveling to an observer from the initial source, the quasinormal-mode contribution which describes a damped oscillation excited by the fields traveling to the near-horizon region from the source, the tail contribution which describes a late-time power-law falloff in time after the exponential damping.

The black hole perturbation theory is crucial for an analytical understanding of gravitational wave observations. In binary black holes, the waveforms at the so-called ringdown phase are described by a superposition of quasinormal modes whose frequency and decay rate are determined by parameters of the black hole formed at the final stage. Fitting the observational signal with the template based on the black hole perturbation theory and combining them with other observations together, the physical parameters of the black hole can be estimated. Furthermore, theoretical analysis of the ringdown gravitational wave enables us to test general relativity. If the no-hair theorem and the uniqueness theorem hold for the black hole in the Universe, the quasinormal modes should be completely determined by the parameters of the Kerr black hole, i.e., mass and spin. In particular, the precise evaluation of the deviation of the quasinormal mode frequencies from the case of the Kerr black hole leads to testing theories of gravity in the strong-gravity regime [33].

Studies of linear perturbations of fundamental fields other than gravitational waves are also important. Astrophysical black holes at the center of the galaxy are in perturbed states by photons, neutrinos, and strong magnetic fields, etc. The linear response to scalar, vector, and fermionic fields describes the dynamical property of a realistic black hole and brings insights into the environment in the vicinity. If dark matter particles are present near the black holes, they also perturb them. If characteristic phenomena are induced by those perturbing fields around the black hole, they could be observational evidence of the existence of such the fields. Actually, the observational signature of gravitational waves induced by the collapse of clouds formed by axion dark matter near the Kerr black holes has been intensively discussed [34, 35].

In AdS/CFT correspondence, the black hole perturbation theory in anti-de Sitter spacetimes, in particular, quasinormal modes, applies to the study of linear response of equilibrium thermal states to adding of an external source.

A phenomenon, which a perturbed state returns to a stable equilibrium state, is called a relaxation phenomenon which is subject of the non-equilibrium statistical mechanics and hydrodynamics. The important quantity characterizing that phenomenon is the transport coefficient, e.g., viscosity. In the strongly coupled quantum field theory, the theoretical analysis of the relaxation phenomenon is difficult because a standard perturbative approach is not applicable due to the strongly coupled property. On the gravitational theory side, quasinormal mode spectra of a black hole in the anti-de Sitter spacetime correspond to poles of the retarded Green function of the perturbation field, and many analytical methods for finding them have been proposed. The quasinormal mode frequency gives information about the locations of poles of the correlation function in the dual quantum field theory and supplies the transport coefficient. It is known that the value of the viscosity to entropy ratio in the strongly coupled quantum field theories calculated in terms of the quasinormal modes of black holes in the anti-de Sitter spacetime roughly agrees with the experimental results [36].

The perturbation analysis can also give an answer to the following question: Is the spacetime stable? Stability of spacetimes is one of the most important problems in wide topics. Mathematically, a spacetime is said to be stable if a perturbation field and all its derivatives are uniformly bounded in time. The Minkowski spacetime, which is an empty spacetime in the theories of gravity, and the Schwarzschild black hole spacetime, which is the simplest black hole spacetime in vacuum [37, 38], have been proved to be stable [39, 40]. It is hard to fully analyze and linear stability is discussed as a first step in many problems.

In astrophysics, the stability analysis leads to restricting a mathematical model of astrophysical black holes. In other words, a stable black hole solution may describe a real celestial object in the Universe. The Kerr black holes have been shown to be linearly stable for gravitational, electromagnetic, massless scalar, and fermionic perturbations in terms of the Fourier mode analysis [41]. This implies that the Kerr black hole may be a final state of the gravitational collapse and describe astrophysical black holes. Unstable black hole solutions cannot describe real objects in the Universe except for the case where the time scale of the instability is larger than the age of the Universe. However, instability of a black hole is not astrophysically meaningless but is meaningful. Instability of perturbation fields could be an observable characteristic dynamical phenomenon, and may indirectly prove the existence of undetected particles. For example, the Kerr black hole can be unstable for massive bosonic field perturbations and the growth rate of the instability is typically rather slow [42, 43]. That instability is called superradiant instability. It is expected that superradiant instability

results in matter condensation near the black hole. If a dark matter particle is present near the black holes, superradiant instability can be induced depending on the mass of the particle. Several investigations [44, 45, 46, 47] attempt to restrict mass ranges of axion dark matter by taking advantage of superradiant instability. Numerical investigation [48] suggests that superradiant instability will induce extra black hole hair, e.g., nontrivial bosonic fields.

Mathematically, stability analysis of a solution is a useful method for finding new solutions of field equations which are nonlinear partial differential equations. Stability of a solution roughly means that there are no families of other solutions in the neighborhood of the solution in a solution space. In many problems, linear instability of a solution implies the existence of the branch to other solutions. This suggests that the unstable solutions transit to other solutions in a nonlinear regime. It is hence possible to analytically construct a new solution in a perturbative manner from that branch. This perturbative approach has been used in exploring new black hole solutions in higher dimensions [49, 50], asymptotically anti-de Sitter solutions [51, 52, 53], and hairy black hole solutions in the extended theories of general relativity [54, 55].

In AdS/CFT correspondence, stability analysis is a standard method for investigating the phase space of dual field theories. Stability of black holes in the anti-de Sitter spacetime corresponds to the relaxation phenomenon. Instability of those implies phase transitions at finite temperature, in particular, a critical temperature and order parameter can be calculated in terms of perturbation analysis of the spacetime. Seminal works [56, 57] have argued that the near-extremal Reissner-Nordström black hole in the anti-de Sitter spacetime suffers from linear instability against a massive charged scalar field perturbation with a certain range of mass, and evolve into a new black hole with a nontrivial charged scalar field in the nonlinear regime. It has further been shown that the conductivity in the dual field theory diverges below the critical temperature which is determined by the relation among the scalar field mass and charge, and the black hole mass and charge. This description is dual to superconductivity at low temperature and is called holographic superconductor.

Perturbation analysis in the anti-de Sitter spacetime is of great interest because the anti-de Sitter spacetime has a mathematically and phenomenologically richer structure than the Minkowski spacetime case. In this sense, the AdS spacetime is a playground for gravitational physics. Infinity in the anti-de Sitter spacetime effectively behaves as a "wall" for the perturbation, and hence the spacetime becomes a confined system. This feature leads to a surprising property in the nonlinear regime: turbulence of gravity. Then, the

anti-de Sitter spacetime becomes nonlinearly unstable [58, 59]. It has been argued that as a result of the turbulence, the field configuration collapses, and a black hole forms. The effective wall of the anti-de Sitter spacetime also causes superradiant instability of rotating black holes. The endpoint is not clear yet. At the current stage, it has been shown that the rotating black holes evolve into dynamical rotating black holes dubbed black resonators [60, 61] but they are regarded as a transient state because of superradiant instability themselves [62].

To define initial value problem in the anti-de Sitter spacetime well, we need carefully specify not only initial data but also boundary conditions at infinity because the anti-de Sitter spacetime fails to be globally hyperbolic. If one considers linear massive scalar field perturbations in the anti-de Sitter spacetime, the degree of freedom to choice of the boundary condition arises depending on the scalar field mass, and some lead to the appearance of growing modes [63]. Through this linear instability, a static soliton is produced in the nonlinear regime [64]. The effect coming from the boundary conditions is also expected in the case of black holes in the anti-de Sitter spacetime. Many studies of superradiant instability in the anti-de Sitter spacetime have chosen a specific boundary condition at infinity. However, for the construction of a confined system, there is no special reason to persist in that boundary condition. The imposition of other boundary conditions might lead to finding the qualitatively and quantitatively new feature. In chapter 4, we analyze superradiant instability under all possible boundary conditions.

Black holes are defined by a boundary called the event horizon. Are the event horizons stable for perturbations? This is one of the theoretical challenges in gravitational physics. The singularity theorems of Penrose [65] claim that spacetime singularities generically appear in gravitational collapse. The appearance of the singularity represents a breakdown of general relativity that gives the classical descriptions of gravity and matter. However, it is believed that the singularity is hidden behind the event horizon and hence is causally disconnected from observers outside it. If the event horizon is unstable, the spacetime singularities might be exposed or the event horizon might become singularities. Perhaps, even if so, the black hole might evolve into a different black hole and keep the singularity hidden.

Mathematically, extremal black holes are a border between a black hole and a visible spacetime singularity from a distant observer in a solution space in general relativity. It is natural to investigate stability of the event horizon of extremal black holes with the above singularity problem in mind. Aretakis [66, 67, 68] has discussed late-time behaviors of massless scalar field perturbations of four-dimensional extremal Reissner-Nordström black holes and then argued that the field and its higher-order transverse deriva-

tives exhibit the polynomial growth in time only on the event horizon. This horizon-instability is called the Aretakis instability. The nonlinear evolution of the Aretakis instability has been investigated in [69, 70, 71, 72]. Mutara, Reall, and Tanahashi [70] have numerically found that the extremal Reissner-Nordström black holes generically settle down at the non-extremal Reissner-Nordström black holes but there exist fine-tuned initial data for which the instability never ends and the spacetime evolves into a dynamical extremal black hole with another classical hair on the horizon called the Aretakis constant. Interestingly, the horizon-instability also occurs in the nonlinear regime. It is also conjectured that with other fine-tuned initial data, the evolved spacetime contains a visible spacetime singularity from a distant observer [73].

Near-extremal black holes are ubiquitous in the Universe [74, 75, 76, 77, 78]. Furthermore, near-extremal black holes in the anti-de Sitter spacetime corresponds to the quantum field theories at low temperature. Thus, it is important for wide topics to study dynamics of test fields near the event horizon of extremal black holes. In chapter 5, we show that the Aretakis instability has a geometrical meaning and is a generic feature in linear fields of extremal black holes in arbitrary dimensions.

In this thesis, we aim to reveal the fundamental properties of black holes in terms of the black hole perturbation theory. We investigate analytically and numerically dynamical evolutions of linear scalar perturbations of the black holes and the vicinities. This thesis is based on our works [79, 80] and is organized as follows:

Chapter 2

We review the basic properties of maximally symmetric spacetimes, spherically symmetric spacetimes, two spherically symmetric black holes described by exact solutions of the Einstein equations, and general features of the black holes. We then see the global structure of the black holes. We further explore the motion of test particles and light rays in the black hole spacetimes.

Chapter 3

We briefly review the formalism of the linear perturbation theory of spacetimes. We first focus on the tensor field perturbations in the Minkowski background, i.e., gravitational waves, and explore scalar, vector, and tensor perturbations of the Schwarzschild black hole spacetime. We further see time evolution of the perturbation fields via the Green function, and define quasinormal modes and late-time tails. We also mention superradiant instability

and the Aretakis instability.

Chapter 4

We analytically and numerically study quasinormal mode frequencies of neutral and charged scalar fields in the Reissner-Nordström-anti-de Sitter black holes and discuss the stability of the black holes in terms of the quasinormal mode frequencies. We focus on the range of the mass squared of the scalar fields for which the Robin boundary condition parametrized by one parameter applies at the conformal infinity. We find that if the black hole is much smaller than the length scale of the anti-de Sitter spacetime, the instability of the charged scalar field can be understood in terms of superradiance in the reflective boundary condition. We also find a condition in which the black hole is superradiantly unstable irrespectively of the Robin boundary condition parameter. On the other hand, if the condition is not satisfied, the stability crucially depends on the Robin boundary condition parameter and there appears a purely oscillating mode at the onset of the instability. We argue that as a result of the superradiant instability, the scalar field gains charge from the black hole and energy from its ambient electric field, while the black hole gives charge to the scalar field and gains energy from the scalar field but decreases its asymptotic mass parameter. This chapter is based on T. Katagiri and T. Harada, "Stability of small charged anti-de Sitter black holes in the Robin boundary," Class. Quant. Grav., 38(13):135026, (2021) [79].

Chapter 5

The anti-de Sitter spacetime in two dimensions (AdS_2) emerges in the vicinity of an extremal black hole and hence it is expected that the study of AdS_2 brings us insight into fundamental properties near the horizon of the extremal black holes. We discuss dynamics of massive Klein-Gordon fields in AdS_2, in particular, conserved quantities and instability on the future Poincaré horizon called, respectively, the Aretakis constants and the Aretakis instability. We find out the geometrical meaning of the Aretakis constants and instability in a parallel-transported frame along a null geodesic, i.e., some components of the higher-order covariant derivatives of the field in the parallel-transported frame are constant or unbounded at the late time, respectively. Because AdS_2 is maximally symmetric, any null hypersurfaces have the same geometrical properties. Thus, if we prepare parallel-transported frames along any null hypersurfaces, we can show that the same instability emerges not only on the future Poincaré horizon but also on any null hypersurfaces. This implies

that the Aretakis instability in AdS_2 is the result of singular behaviors of the higher-order covariant derivatives of the fields on the whole AdS infinity, rather than a blowup on a specific null hypersurface. It is also discussed that the Aretakis constants and instability are related to the conformal Killing tensors. We further explicitly demonstrate that the Aretakis constants can be derived from ladder operators constructed from the spacetime conformal symmetry. This chapter is based on T. Katagiri and M. Kimura, "Revisiting the Aretakis constants and instability in two-dimensional anti-de Sitter spacetimes," Phys. Rev. D, 103(6):064011, (2021) [80].

Chapter 6

We summarize this thesis with discussions and give an outlook towards future works.

In this thesis, we adopt the sign convention $(-,+,+,+)$ and units in which $c = G = \hbar = 1$.

Chapter 2

Basic properties of spherically symmetric black holes

In this chapter, we review the basic properties of spherically symmetric black holes.

2.1 Maximally symmetric spacetimes

In this section, we review the concept of the symmetry of a spacetime. In particular, we explore the basic properties of a highly symmetric spacetime, which is called a *maximally symmetric spacetime*.

It is said that a spacetime $(\mathcal{M}, g_{ab})$ possesses a *symmetry* if the metric g_{ab} admits an isometry φ_t defined by $\varphi_t : \mathcal{M} \to \mathcal{M}$ such that $\varphi_t^* g_{ab} = g_{ab}$. The isometry group, φ_t, is generated by an infinitesimal coordinate transformation $x^a \to \bar{x}^a = x^a - \xi^a$ along a vector field ξ^a, which is called a *Killing vector field*. The Killing vector field obeys

$$\mathcal{L}_\xi g_{ab} = 0, \tag{2.1}$$

where $\mathcal{L}_\xi$ is the Lie derivative along the Killing vector field ξ^a. The above equation is written in the form

$$\nabla_a \xi_b + \nabla_b \xi_a = 0. \tag{2.2}$$

This is called the *Killing equation*. For an n-dimensional spacetime, there can exist at most $n(n+1)/2$ linearly independent Killing vector fields. It is said that an n-dimensional spacetime is *maximally symmetric* if the metric admits isometries generated by $n(n+1)/2$ Killing vector fields.

Now, we introduce the following important property of the Killing vector. Let us consider timelike or null geodesics with a tangent vector u^a in the

presence of a Killing vector field ξ^a. Then, a quantity $u^a\xi_a$ is conserved along the geodesics because $\mathcal{L}_u(u^b\xi_b) = \xi_b u^a \nabla_a u^b + u^a u^b \nabla_a \xi_b = 0$ due to the geodesic equation and the Killing equation (2.2). This quantity plays an important role in analyzing the motion of free particles or light rays in a symmetric spacetime as will be seen in sections 2.3.1 and 2.3.2 .

So far, we have not used the Einstein equations. We will review maximally symmetric spacetimes described by an exact solution of the Einstein equations below.

Minkowski spacetime

The simplest maximally symmetric spacetime is the *Minkowski spacetime*, which is an empty spacetime in general relativity. The Minkowski spacetime is the space of vanishing curvature, and the Minkowski metric η_{ab} satisfies the vacuum Einstein equations

$$R_{ab} - \frac{1}{2} R g_{ab} = 0. \tag{2.3}$$

In the cartesian coordinates (x^0, x, y, z), the metric is given in the form

$$ds^2 = -\left(dx^0\right)^2 + (dx)^2 + (dy)^2 + (dz)^2 . \tag{2.4}$$

In spherical coordinates (t, r, θ, ϕ), where $t = x^0$, $x^1 = r\sin\theta\sin\phi$, $x^2 = r\sin\theta\cos\phi$, $x^3 = r\cos\theta$, the metric takes the form

$$ds^2 = -dt^2 + dr^2 + r^2\left(d\theta^2 + \sin^2\theta d\phi^2\right), \tag{2.5}$$

where $-\infty < t < \infty$, $0 < r < \infty$, $0 < \theta < \pi$, and $0 < \phi < 2\pi$.

We have an alternative coordinate system defined by

$$u = t - r, \quad v = t + r, \tag{2.6}$$

where $-\infty < u < \infty$ and $-\infty < v < \infty$. In these coordinates, the Minkowski metric becomes

$$ds^2 = -dudv + \frac{1}{4}(u - v)^2\left(d\theta^2 + \sin^2\theta d\phi^2\right). \tag{2.7}$$

The absence of terms du^2 and dv^2 imply that the hypersurfaces $u =$ const. and $v =$ const. are null, i.e., $g^{ab}(\partial_a u)(\partial_b u) = g^{ab}(\partial_a v)(\partial_b v) = 0$.

To study the global structure, we introduce new coordinates,

$$\tilde{u} = \text{ArcTan } u, \quad \tilde{v} = \text{ArcTan } v, \tag{2.8}$$

where $-\pi/2 < \tilde{u} < \pi/2$, $-\pi/2 < \tilde{v} < \pi/2$, and $\tilde{v} \geq \tilde{u}$. In these coordinates, infinities $u = \pm\infty$ and $v = \pm\infty$ are transformed to finite values $\tilde{u} = \pm\pi/2$ and $\tilde{v} = \pm\pi/2$, respectively. Then, the Minkowski metric (2.7) takes the form

$$ds^2 = \frac{1}{\cos^2\tilde{u}\cos^2\tilde{v}}\left[-d\tilde{u}d\tilde{v} + \frac{1}{4}\sin^2(\tilde{u}-\tilde{v})\left(d\theta^2 + \sin^2\theta d\phi^2\right)\right]. \tag{2.9}$$

It follows that the Minkowski metric (2.9) is conformal to the metric $\bar{\eta}_{ab}$ defined by

$$d\bar{s}^2 = -4d\tilde{u}d\tilde{v} + \sin^2(\tilde{u}-\tilde{v})\left(d\theta^2 + \sin^2\theta d\phi^2\right). \tag{2.10}$$

This metric can be reduced to a useful form by using coordinates,

$$t' = \tilde{u} + \tilde{v}, \quad r' = -\tilde{u} + \tilde{v}, \tag{2.11}$$

where $-\pi < t' + r' < \pi$, $-\pi < t' - r' < \pi$, and $r' \geq 0$. Then, the metric $\bar{\eta}_{ab}$ in Eq. (2.10) is rewritten as

$$d\bar{s}^2 = -(dt')^2 + (dr')^2 + \sin^2 r'\left(d\theta^2 + \sin^2\theta d\phi^2\right). \tag{2.12}$$

This metric is that of the *Einstein static universe* which is a completely homogeneous spacetime. We can see that the whole of the Minkowski spacetime is conformal to the region $-\pi < t' + r' < \pi$, $-\pi < t' - r' < \pi$, $r' \geq 0$ of the Einstein static universe. Thus, the whole of the Minkowski spacetime can be embedded in the Einstein static universe. The boundary of the embedded Minkowski spacetime is called the *conformal infinity* of the Minkowski spacetime. It consists of the null surfaces at $\tilde{v} = \pi/2$ and $\tilde{u} = -\pi/2$, which are called *future and past null infinities*, respectively, and points at $(\tilde{u}, \tilde{v}) = (-\pi/2, \pi/2)$ called *spatial infinity*, at $(\tilde{u}, \tilde{v}) = (\pi/2, \pi/2)$ and $(\tilde{u}, \tilde{v}) = (-\pi/2, -\pi/2)$, which are called *future and past timelike infinities*, respectively. The global structure of the Minkowski spacetime in the (t', r') plane is presented in Figure 2.1. This is called a *Penrose diagram* of the Minkowski spacetime. In this diagram, the null geodesics are represented by straight lines at $\pm 45°$.

De Sitter spacetime

The space of positive constant curvature is called the *de Sitter spacetime*. The metric satisfies the Einstein equations with positive cosmological constant Λ,

$$R_{ab} - \frac{1}{2}Rg_{ab} + \Lambda g_{ab} = 0. \tag{2.13}$$

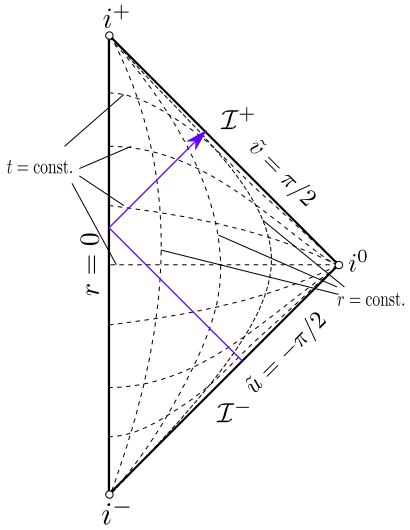

Figure 2.1: The Penrose diagram of the Minkowski spacetime. Future and past null infinities are denoted by $\mathcal{I}^+$ and $\mathcal{I}^-$, respectively. Future and past timelike infinities are denoted by i^+ and i^-, respectively, and spatial infinity is denoted by i^0. The dashed curves represent $t = \text{const.}$ surfaces and $r = \text{const.}$ surfaces. The blue arrow is the null geodesic reaching from $\mathcal{I}^-$ to $\mathcal{I}^+$ through the origin $r = 0$.

The de Sitter spacetime in four dimensions can be represented as the hyperboloid

$$-\left(X^0\right)^2 + \left(X^1\right)^2 + \left(X^2\right)^2 + \left(X^3\right)^2 + \left(X^4\right)^2 = \alpha^2, \tag{2.14}$$

where $\alpha = (3/\Lambda)^{1/2}$, in the five-dimensional Minkowski space described by

$$ds^2 = -\left(dX^0\right)^2 + \left(dX^1\right)^2 + \left(dX^2\right)^2 + \left(dX^3\right)^2 + \left(dX^4\right)^2. \tag{2.15}$$

Introducing coordinates (t, r, θ, ϕ) such that

$$\begin{aligned} X^0 &= \left(\alpha^2 - r^2\right)^{1/2} \sinh\left(\frac{t}{\alpha}\right), \\ X^1 &= \left(\alpha^2 - r^2\right)^{1/2} \cosh\left(\frac{t}{\alpha}\right), \\ X^2 &= r\cos\theta, \\ X^3 &= r\sin\theta\cos\phi, \\ X^4 &= r\sin\theta\sin\phi, \end{aligned} \tag{2.16}$$

the metric can be written in a useful form

$$ds^2 = -\left(1 - \frac{r^2}{\alpha^2}\right) dt^2 + \left(1 - \frac{r^2}{\alpha^2}\right)^{-1} dr^2 + r^2\left(d\theta^2 + \sin^2\theta d\phi^2\right). \tag{2.17}$$

The components of the metric are singular at $r = \alpha$ but this is just a result of a bad choice of the coordinates. This is called a *coordinate singularity* and is eliminated by the coordinate change. The current coordinates cover part of the whole spacetime.

In coordinates $(\tau, \chi, \theta, \phi)$ such that

$$\begin{aligned} X^0 =& \alpha \sinh \tau, \\ X^1 =& \alpha \cosh \tau \cos \chi, \\ X^2 =& \alpha \cosh \tau \sin \chi \cos \theta, \\ X^3 =& \alpha \cosh \tau \sin \chi \sin \theta \cos \phi, \\ X^4 =& \alpha \cosh \tau \sin \chi \sin \theta \sin \phi, \end{aligned} \tag{2.18}$$

where $-\infty < \tau < \infty$, $0 \leq \chi \leq \pi$, $0 \leq \theta \leq \pi$, and $0 \leq \phi \leq 2\pi$, the de Sitter metric takes the form

$$ds^2 = \alpha^2 \left[-d\tau^2 + \cosh^2 \tau \left\{ d\chi^2 + \sin^2 \chi \left(d\theta^2 + \sin^2 \theta d\phi^2 \right) \right\} \right], \tag{2.19}$$

These coordinates cover the whole spacetime. This metric corresponds to that of the closed Robertson-Walker spacetime. One can also introduce other coordinates which cover the different part of the whole de Sitter spacetime and in which the metric takes different forms.

To study the global structure, we introduce a new coordinate

$$t' = 2\mathrm{ArcTan}\left(e^{\tau}\right) - \frac{\pi}{2}, \quad r' = \chi, \tag{2.20}$$

where $-\pi/2 < t' < \pi/2$ and $0 \leq r' \leq \pi$. Then, the metric (2.19) can be rewritten as

$$ds^2 = \alpha^2 \cosh^2 \left(\frac{t'}{\alpha} \right) d\bar{s}^2, \tag{2.21}$$

where $d\bar{s}^2$ is the line element of the Einstein static universe (2.12). Infinities $\tau = \pm\infty$ are transformed to finite values $t' = \pm\pi/2$, and the de Sitter spacetime is conformal to the region for $-\pi/2 < t' < \pi/2$ of the Einstein static universe. Thus, the whole of the de Sitter spacetime can be represented by embedding in the Einstein static universe. The Penrose diagram of the de Sitter spacetime is presented in Figure 2.2. In contrast to the Minkowski spacetime case, there are spacelike infinities for timelike and null curves in future and past. Furthermore, the region where future observers can see does not cover the whole of the spacetime. For example, for a static observer at $(t', r') = (\pi/2, 0)$, all events outside the past light cone corresponding to the surface tangent to the blue arrow in Figure 2.2 can never be observable.

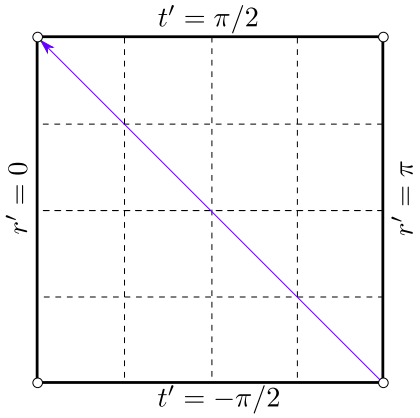

Figure 2.2: The Penrose diagram of the de Sitter spacetime. The dashed vertical lines represent $r' = \text{const.}$ surfaces The dashed horizontal lines represent $t' = \text{const.}$ surfaces. The blue arrow is the null geodesic reaching from $(t', r') = (-\pi/2, \pi')$ to $(t', r') = (\pi/2, 0)$.

Anti-de Sitter spacetime

The space of negative constant curvature is called the *anti-de Sitter spacetime*. The metric satisfies the Einstein equations with negative cosmological constant Λ,

$$R_{ab} - \frac{1}{2} R g_{ab} + \Lambda g_{ab} = 0. \tag{2.22}$$

The anti-de Sitter spacetime in four dimensions can be visualized as the hyperboloid

$$-\left(X^0\right)^2 - \left(X^1\right)^2 + \left(X^2\right)^2 + \left(X^3\right)^2 + \left(X^4\right)^2 = -\ell^2, \tag{2.23}$$

where $\ell = (-3/\Lambda)^{1/2}$, in the five-dimensional space with the metric

$$ds^2 = -\left(dX^0\right)^2 - \left(dX^1\right)^2 + \left(dX^2\right)^2 + \left(dX^3\right)^2 + \left(dX^4\right)^2. \tag{2.24}$$

Introducing coordinates (t, r, θ, ϕ) such that

$$\begin{aligned} X^0 &= \left(\ell^2 + r^2\right)^{1/2} \sin\left(\frac{t}{\ell}\right), \\ X^1 &= \left(\ell^2 + r^2\right)^{1/2} \cos\left(\frac{t}{\ell}\right), \\ X^2 &= r\cos\theta, \\ X^3 &= r\sin\theta\cos\phi, \\ X^4 &= r\sin\theta\sin\phi, \end{aligned} \tag{2.25}$$

the metric takes a form

$$ds^2 = -\left(1+\frac{r^2}{\ell^2}\right)dt^2 + \left(1+\frac{r^2}{\ell^2}\right)^{-1} dr^2 + r^2\left(d\theta^2 + \sin^2\theta d\phi^2\right). \qquad (2.26)$$

These coordinates cover part of the whole spacetime.

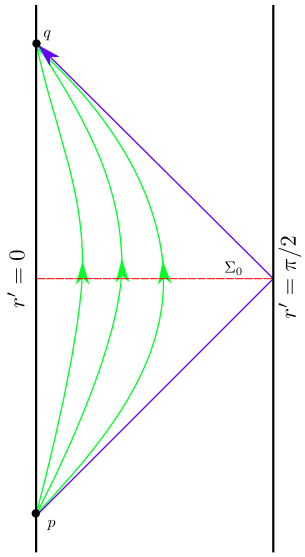

Figure 2.3: The Penrose diagram of the anti-de Sitter spacetime. The dashed red line represents a spacelike hypersurface denoted by Σ_0. The solid vertical lines represent spatial infinity at $r' = 0, \pi/2$. The blue arrow is the null geodesic from p to q. The green curves are timelike geodesics from p to q.

To study the global structure, we introduce a coordinate

$$t' = \frac{t}{\ell}, \quad r' = \mathrm{ArcTan}\left(\frac{r}{\ell}\right), \qquad (2.27)$$

where $-\infty < t' < \infty$ and $0 \leq r' \leq \pi/2$. Then, the metric (2.26) can be rewritten in the form

$$ds^2 = \frac{\ell^2}{\cos^2 r'} d\bar{s}^2, \qquad (2.28)$$

where $d\bar{s}^2$ is the line element of the Einstein static universe (2.12). Hence, the anti-de Sitter spacetime is conformal to the region for $0 \leq r' \leq \pi/2$ of the Einstein static universe. The Penrose diagram is presented in Figure 2.3. Spatial infinity is a timelike surface and are often called the *AdS boundary*.

Due to the presence of the timelike boundary, there are no surfaces such that every non-spacelike curves in the spacetime intersect. Hence, given initial data on any spacelike hypersurface such as Σ_0 in Figure 2.3, one cannot

predict the dynamical evolution in the whole spacetime. Namely, the initial data on Σ_0 can predict the evolution only in the triangle region surrounded by the line $r' = 0$ and the blue arrow. To predict it beyond that region, we need to specify information coming in from the timelike boundary. This will be discussed in chapter 4. Furthermore, as seen in Figure 2.3, the timelike geodesic from p does never reach the timelike boundary, while the null geodesic does.

2.2 Spherically symmetric spacetimes

In this section, we give a precise definition of the spherical symmetry of spacetimes. For that, let us first consider a two-dimensional unit sphere S^2. In spherical coordinates (θ, ϕ), the metric on S^2 is given in the form

$$ds^2 = d\theta^2 + \sin^2\theta d\phi^2. \tag{2.29}$$

This space possesses three linearly independent Killing vector fields

$$\begin{aligned} k^a_{(1)} &= (\partial/\partial\phi)^a\,, \\ k^a_{(2)} &= -\cos\phi\,(\partial/\partial\theta)^a + \cot\theta\sin\phi\,(\partial/\partial\phi)^a\,, \\ k^a_{(3)} &= \sin\phi\,(\partial/\partial\theta)^a + \cot\theta\cos\phi\,(\partial/\partial\phi)^a\,. \end{aligned} \tag{2.30}$$

The above vectors are generators of the $SO(3)$ group. Thus, the two-dimensional unit sphere possesses the $SO(3)$ group of isometries. Besides the continuous isometries generated by the Killing vector fields (2.30), the metric (2.29) possesses the following discrete symmetries

$$\phi \to -\phi, \qquad \theta \to \pi - \theta. \tag{2.31}$$

We are now ready to define the spherical symmetry of spacetimes. A spacetime is said to be *spherically symmetric* if its isometry group contains the $SO(3)$ group and the orbits of the subgroup are two-dimensional spheres. Physically, the $SO(3)$ isometry can be interpreted as rotations. Hence, a spherically symmetric spacetime is a spacetime whose metric remains invariant under the rotations.

For a spherically symmetric spacetime, in coordinates (x^0, x^1, θ, ϕ), the metric whose components all are independent of x^0 takes the form

$$ds^2 = -g_{00}(x^1)\left(dx^0\right)^2 + g_{11}(x^1)\left(dx^1\right)^2 + R\left(x^1\right)^2 d\Omega_2^2, \tag{2.32}$$

where R is a function of x^1 and $d\Omega_2^2$ is the line element of S^2 given in Eq. (2.29). Precisely, a spacetime described by Eq. (2.32) is a static and

spherically symmetric spacetime, which will be defined in the next section. As can be seen in Eq. (2.32), for fixed values of x^0 and x^1, the metric for the spherically symmetric spacetime induces a metric on S^2, i.e., the induced metric is proportional to the metric of S^2, and thus can be characterized by the total area of S^2. The total area is calculated to

$$A = 4\pi R^2. \tag{2.33}$$

For this reason, the function R have a well-defined geometrical meaning. It is convenient for a spherically symmetric spacetime to introduce a function r such that

$$r = \left(\frac{A}{4\pi}\right)^{1/2}. \tag{2.34}$$

Usually, the function R is denoted by r, then r is called the areal radius. Furthermore, the coordinate x^0 is usually denoted by t and called time. In coordinates (t, r, θ, ϕ), the metric (2.32) can be written as

$$ds^2 = -g_{00}(r)dt^2 + g_{11}(r)dr^2 + r^2 d\Omega_2^2. \tag{2.35}$$

It is also possible to define the spherical symmetry of spacetimes in arbitrary dimensions in the same manner.

2.3 Spherically symmetric black holes

We review the basic properties of two well-known spherically symmetric black holes described by exact solutions of the Einstein equations.

2.3.1 Schwarzschild black hole spacetime

We consider a spherically symmetric gravitational field in vacuum. Schwarzschild [37, 38] found an exact solution of the vacuum Einstein equations (2.3) in four dimensions representing such the gravitational field. The spacetime described by that solution is called the *Schwarzschild spacetime*. In coordinates (t, r, θ, ϕ), the metric is given in the form

$$ds^2 = -\left(1 - \frac{2M}{r}\right)dt^2 + \left(1 - \frac{2M}{r}\right)^{-1} dr^2 + r^2 d\Omega_2^2, \tag{2.36}$$

where M is an integration constant but as will be seen below it can be interpreted as the mass of the source of the gravitational field. We note here $r > 2M$ for the reasons mentioned below. Comparing the Schwarzschild

metric (2.36) with the spherically symmetric metric (2.35), it is obvious that the Schwarzschild spacetime is spherically symmetric.

One of the important properties is that the metric is independent of the time coordinate t and invariant under $t \to -t$. Physically, these features can be interpreted as time-translation and time-reflection symmetries of the spacetime. Mathematically, these are defined by the terms *stationary* and *static* as follows. A spacetime is said to be *stationary* if there exists a one-parameter group of isometries whose orbits are timelike curves. Namely, a stationary spacetime possesses a timelike Killing vector field, and then its metric is independent of the Killing parameter in appropriate coordinates. The Schwarzschild metric (2.36) admits the timelike Killing vector field $(\partial/\partial t)^a$ and t is the Killing parameter, i.e.,

$$\mathcal{L}_{\partial_t} g_{ab} = 0. \tag{2.37}$$

Furthermore, a spacetime is said to be *static* if it is stationary and there exist spacelike hypersurfaces that are orthogonal to the orbits of the isometry. This means that in appropriate coordinates such as the coordinates (t, r, θ, ϕ), the metric of a static spacetime is invariant under $t \to -t$. Thus, the Schwarzschild spacetime is static.

It is noticed that in the limit of $r \to \infty$, the metric components approach those of the Minkowski spacetime in the spherical coordinates, i.e.,

$$ds^2 = -\left(1 - \frac{2M}{r}\right) dt^2 + \left(1 + \frac{2M}{r} + \mathcal{O}\left(1/r^2\right)\right) dr^2 + r^2 d\Omega_2^2. \tag{2.38}$$

The Schwarzschild spacetime is asymptotically flat as the metric has the form $g_{ab} = \eta_{ab} + \mathcal{O}(1/r)$ as $r \to \infty$ for the Minkowski metric η_{ab} in Eq. (2.5) in the spherical coordinates. Noticing that far from the center of gravity, $r \to \infty$, the gravitational field can be described by the weak-field approximation, $-g_{tt} = 1 + 2\psi$, where $\psi = -M/r$ is the Newtonian gravitational potential for a source of mass M, the parameter M in Eq. (2.36) can be interpreted as the total mass of the gravitational source.

A remarkable feature of the Schwarzschild metric (2.36) is that the metric components are singular at both $r = 2M$ and $r = 0$. Therefore, one must cut these points out of the spacetime manifold in the current coordinates. The manifold is divided into two manifolds for $0 < r < 2M$ and $2M < r$. Then, we choose the one for $2M < r$, where contains an asymptotically flat region. This is why the Schwarzschild metric (2.36) is defined for $2M < r$. The singularity at $r = 2M$ is just a coordinate singularity. It can indeed be avoided by coordinate transformations as will be seen below. The null hypersurface located at $r = 2M$ has a geometrically special meaning and is directly associated with the concept of black holes. Actually, the Schwarzschild metric

describes a static and spherically symmetric black hole spacetime as will be seen below. On the other hand, the singularity at $r = 0$ cannot be removed and is called a *curvature singularity*. Strictly speaking, this singularity is not part of the spacetime.

According to Birkhoff's theorem, without the assumption of staticity, all spherically symmetric spacetimes of the vacuum Einstein equations (2.3) are static. This consequence implies that there exits no monopole radiation in gravity. Furthermore, according to the uniqueness theorem for static black holes [81], a static black hole solution of the vacuum Einstein equations (2.3) in four dimensions must be spherically symmetric. Namely, in general relativity, a four-dimensional static black hole spacetime in vacuum is unique to the Schwarzschild spacetime and is completely characterized by one parameter of the mass M.

We mention a natural generalization of the Schwarzschild spacetime to higher dimensions. The spacetime in n dimensions is called the *Schwarzschild-Tangherlini spacetime* [82] and described by

$$ds^2 = -\left(1 - \frac{\mu}{r^{n-3}}\right) dt^2 + \left(1 - \frac{\mu}{r^{n-3}}\right)^{-1} dr^2 + r^2 d\Omega_{n-2}^2, \tag{2.39}$$

where $d\Omega_{n-2}^2$ is the line element of $(n-2)$-dimensional unit sphere and μ is related to the mass parameter M via

$$\mu = \frac{16\pi M}{(n-2)A_{n-2}}. \tag{2.40}$$

Here, A_{n-2} is the volume of the $(n-2)$-dimensional unit sphere and defined as

$$A_{n-2} = \frac{2\pi^{(n-1)/2}}{\Gamma\left(\frac{n-1}{2}\right)}. \tag{2.41}$$

We also comment that four-dimensional static and spherically symmetric spacetimes described by exact solutions of the Einstein equations with the cosmological constant Λ. The spacetime is called the *Schwarzschild-(anti-) de Sitter spacetime* [83]. Its metric is given in the form

$$ds^2 = -\left(1 - \frac{2M}{r} - \frac{\Lambda r^2}{3}\right) dt^2 + \left(1 - \frac{2M}{r} - \frac{\Lambda r^2}{3}\right)^{-1} dr^2 + r^2 d\Omega_2^2. \tag{2.42}$$

When $\Lambda > (<) 0$, the metric components approach those of the (anti-) de Sitter spacetime in the limit of $r \to \infty$. For these spacetimes as well, generalizations to higher dimensions are known.

Global structure

As slightly stated above, the Schwarzschild metric (2.36) describes a static black hole in vacuum. In this subsection, we review the concept of black holes. For that, we need to introduce a new coordinate system avoiding the coordinate singularity at $r = 2M$ and investigate the global structure of the spacetime in terms of an extension of the spacetime manifold.

To avoid the singularity at $r = 2M$, we first define the *tortoise coordinate*,

$$\begin{aligned} r_* &= \int \left(1 - \frac{2M}{r}\right)^{-1} dr \\ &= r + 2M \ln\left(\frac{r}{2M} - 1\right) + \text{constant}, \end{aligned} \tag{2.43}$$

where $-\infty < r_* < \infty$ for $2M < r$. In the tortoise coordinate, $r \to 2M$ and $r \to +\infty$ correspond to $r_* \to -\infty$ and $r_* \to +\infty$, respectively. We also introduce null coordinates,

$$u = t - r_*, \quad v = t + r_*, \tag{2.44}$$

where $-\infty < u < \infty$ and $-\infty < v < \infty$. In coordinates (u, v, θ, ϕ), the Schwarzschild metric (2.36) can be rewritten as

$$ds^2 = -\frac{2Me^{-r/2M}}{r} e^{(u-v)/4M} du dv + r^2 d\Omega_2^2, \tag{2.45}$$

where r is now viewed as a function of u and v. Furthermore, introducing the so-called *Kruskal-Szekeres* coordinates

$$U = -e^{-u/4M}, \quad V = e^{v/4M}, \tag{2.46}$$

so that $-\infty < U < 0$ and $0 < V < \infty$, we can rewrite the metric (2.45) as

$$ds^2 = -\frac{32M^3 e^{-r/2M}}{r} dU dV + r^2 d\Omega_2^2, \tag{2.47}$$

where

$$-UV = \left(\frac{r}{2M} - 1\right) e^{r/2M - 1}. \tag{2.48}$$

It can be seen that the singularity at $r = 2M$, which corresponds to $U = 0$ or $V = 0$, is eliminated. Furthermore, we can now define the function $r = r(U, V)$ for $U \geq 0$ and $V \leq 0$ by Eq. (2.48). These facts reveal the existence of a larger manifold with the metric (2.47) than the manifold with the Schwarzschild metric (2.36). Namely, the spacetime manifold with the

Schwarzschild metric initially defined only in $-\infty < U < 0$ and $0 < V < \infty$ can be extended to the spacetime manifold with the metric (2.36), where $-\infty < U < \infty$ and $-\infty < V < \infty$. This extension is called the *Kruskal extension*. However, the singularity at $r = 0$ still exists. As $r \to 0$, the scalar quantity $R_{abcd}R^{abcd}$ blows up as M^2/r^6, and thus it is an unremovable singularity.

The Kruskal-Szekeres coordinates (U, V, θ, ϕ) make the global structure of the Schwarzschild spacetime clear. We introduce double null coordinates

$$\tilde{U} = \text{ArcTan } U, \quad \tilde{V} = \text{ArcTan } V, \tag{2.49}$$

where $-\pi/2 < \tilde{U} < \pi/2$ and $-\pi/2 < \tilde{V} < \pi/2$. In these coordinates, infinities $U = \pm\infty$ and $V = \pm\infty$ correspond to the finite values of $\tilde{U} = \pm\pi/2$ and $\tilde{V} = \pm\pi/2$, respectively. The Penrose diagram for the extended Schwarzschild spacetime is presented in Figure 2.4. Region II and region IV

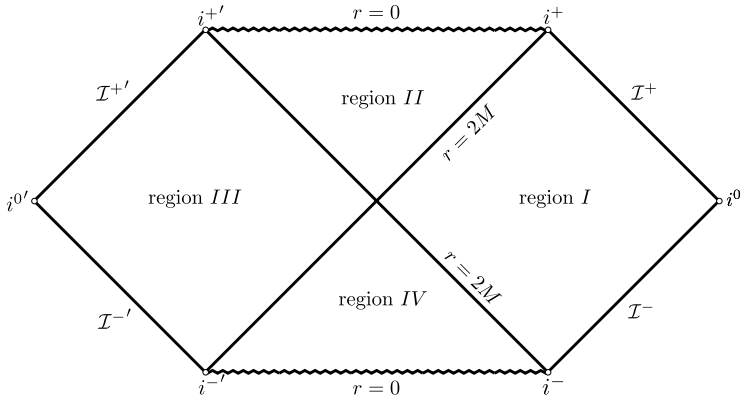

Figure 2.4: The Penrose diagram of the extended Schwarzschild spacetime. The symbols $\mathcal{I}^+$, $\mathcal{I}^-$, i^+, i^-, and i^0 represent future null infinity, past null infinity, future timelike infinity, past timelike infinity, and spatial infinity, respectively, of the asymptotically flat region denoted by region I. The symbols $\mathcal{I}^{+\prime}$, $\mathcal{I}^{-\prime}$, $i^{+\prime}$, $i^{-\prime}$, and $i^{0\prime}$ represent future null infinity, past null infinity, future timelike infinity, past timelike infinity, and spatial infinity, respectively, of another asymptotically flat region denoted by region III. The zigzag lines represent the curvature singularity at $r = 0$. The event horizon corresponds to the boundary of region I and region II.

are spacetime regions in $0 < r < 2M$, and there still exists the curvature singularity at $r = 0$. Region I and region III are asymptotically flat regions in $2M < r$. Region I and region III are isometric, and region II and region IV are also isometric.

Let us consider sending light rays from a point in regions I and II in Figure 2.4. Outside the surface at $r = 2M$ (region I), the outwards null geodesics reach future null infinity $V = \infty$ but the inwards null geodesics encounter the curvature singularity at $r = 0$. Inside $r = 2M$ (region II), both these geodesics hit the singularity within the finite affine parameter. Namely, it is impossible to send light rays from region II to region I. Thus, the surface at $r = 2M$ is the boundary such that the curvature singularity can be evaded outside but cannot inside. This geometrically special boundary is called the *event horizon*. Light rays emitted from region I toward region III go into region II and finally hit the curvature singularity at $r = 0$. This is also the case for light rays sent from region III toward region I.

The event horizon is directly related to the concept of a black hole. Now, we give a definition of a black hole in an asymptotically flat spacetime. A *black hole* in an asymptotically flat spacetime is defined by a region such that no causal curves from it connect future null infinity, where the causal curve is defined as a curve such that the tangent vector is timelike or null. Physically, no signals at a velocity less than or equal to that of light inside a black hole can be observed by any observer outside it. The event horizon is defined as the boundary of the black hole. In the same manner, a black hole in asymptotically (anti-) de Sitter spacetimes can also be defined.

Killing horizon and surface gravity

We introduce the notion of the Killing horizon, which has a close connection to the event horizon but is independent of it. For a stationary spacetime, a *Killing horizon* is defined as a null hypersurface to which the Killing vector field is normal. This implies that the Killing vector is tangent to the null geodesic generator of the null hypersurface. Although the concept of the Killing horizon is independent of the event horizon, it is shown that the event horizon of an asymptotically flat stationary black hole, which is described by a solution satisfying the Einstein equations, is a Killing horizon [84]. For example, the Killing vector field of the Schwarzschild spacetime, $t^a = (\partial/\partial t)^a$, is null at the event horizon $r = 2M$ as can be seen from $g_{ab}t^a t^b = -(1-2M/r)$, and thus the event horizon of the Schwarzschild black hole is indeed the Killing horizon.

We review some geometrical properties of the Killing horizon. By definition, for a Killing vector field ξ^a we have

$$\xi^a \xi_a = 0, \tag{2.50}$$

at the Killing horizon. Since the gradient of $\xi^a \xi_a$ is also normal to the horizon,

i.e., $\xi^a \nabla_a (\xi^b \xi_b) = 0$ at the horizon, there exists a function κ such that

$$\nabla^a \left(\xi^b \xi_b\right) = -2\kappa \xi^a. \tag{2.51}$$

The quantity κ is called the *surface gravity*. Taking the Lie derivative of Eq. (2.51) along ξ^a, we obtain

$$\mathcal{L}_\xi \kappa = 0. \tag{2.52}$$

Thus, κ is constant along the Killing horizon. For example, the surface gravity of the Schwarzschild spacetime is calculated to

$$\kappa = \frac{1}{4M}. \tag{2.53}$$

It can be seen that κ is indeed constant.

Equation (2.51) can be rewritten as

$$\xi^a \nabla_a \xi^b = \kappa \xi^a. \tag{2.54}$$

This is the geodesic equation with non-affine parametrization. Thus, κ measures the failure of the Killing parameter, v, defined by

$$\xi^a \nabla_a v = 1, \tag{2.55}$$

to coincide with the affine parameter, λ, on the Killing horizon. Then, we have

$$\lambda = e^{\kappa v}, \tag{2.56}$$

if $\kappa \neq 0$. Actually, we have already seen this relation at Eq. (2.46); V is the affine parameter and $\kappa = (4M)^{-1}$ in the Schwarzschild spacetime. Defining a vector k^a such that

$$k^a = e^{-\kappa v} \xi^a, \tag{2.57}$$

we find

$$k^a \nabla_a k^b = 0. \tag{2.58}$$

The vector k^a is the affinely parametrized tangent to the null geodesic horizon generator.

Motion of test particles and light rays in the Schwarzschild spacetime

We review the motion of test particles and light rays outside the event horizon of the Schwarzschild black hole spacetime. We first consider a freely falling massive particle into the black hole. The Lagrangian is given by

$$\mathcal{L} = \frac{1}{2} \mu g_{ab} u^a u^b, \tag{2.59}$$

where μ is the particle mass and u^a is a tangent vector of the orbit of the particle. The behavior of the particle is described by timelike geodesics. Hence, u^a is the tangent vector of the timelike geodesic: $u^a \nabla_a u^b = 0$. In particular, with the aid of the spherical symmetry of the spacetime, we can restrict the geodesic motion in the equatorial plane $\theta = \pi/2$ without loss of generality.

Since the Lagrangian (2.59) is constant along the geodesic, we have

$$-1 = g_{ab}u^a u^b = -\left(1 - \frac{2M}{r}\right)\dot{t}^2 + \left(1 - \frac{2M}{r}\right)^{-1}\dot{r}^2 + r^2\dot{\phi}^2, \tag{2.60}$$

where the dot denotes the derivative with respect to the proper time of the particle. Here, we have used the property of the equatorial motion, i.e., $\theta = \pi/2$ and $\dot{\theta} = 0$. Solving this equation, we can see the motion of the particle. For that, we further take an advantage of the spacetime symmetry. As stated in section 2.1, there exist conserved quantities along a geodesic in a spacetime in the presence of a Killing vector field. From the Euler-Lagrange equation of the Lagrangian (2.59), we find two conserved quantities:

$$\begin{aligned} E :=& -\mu g_{ab}u^a \xi^b_{(t)} = \mu\left(1 - \frac{2M}{r}\right)\dot{t}, \\ L :=& \mu g_{ab}u^a \xi^b_{(\phi)} = \mu r^2\dot{\phi}, \end{aligned} \tag{2.61}$$

where $\xi^a_{(t)} = (\partial/\partial t)^a$ and $\xi^a_{(\phi)} = (\partial/\partial\phi)^a$ are the Killing vectors associated with the time-translation and the rotation, respectively. Physically, E/μ and L/μ can be interpreted as the total energy including the gravitational potential energy and the angular momentum per unit rest mass for a static observer at infinity, respectively.

Using Eq. (2.61), Eq. (2.60) is reduced to an equation for the radial motion,

$$\frac{1}{2}\dot{r}^2 + V(r) = \frac{1}{2}\frac{E^2}{\mu^2}, \tag{2.62}$$

where

$$V(r) = \frac{1}{2}\left(1 - \frac{2M}{r}\right)\left(1 + \frac{L^2}{\mu^2 r^2}\right). \tag{2.63}$$

Hence, the radial motion of the geodesic is the same as that of a particle with the energy E in one-dimensional non-relativistic mechanics with the potential $V(r)$.

Let us consider the shape of $V(r)$. If $L^2 < 12M^2\mu^2$, there are no extrema, and $V(r)$ is a monotonically increasing function of r. Hence, all particles towards the black hole will fall into the event horizon and finally hit the

curvature singularity at $r = 0$. If $L^2 = 12M^2\mu^2$, there are no extrema but exists an inflection point at $r = 6M$. If $L^2 > 12M^2\mu^2$, $V(r)$ has two extrema at $r = R_\pm$ where

$$R_\pm = \frac{L^2 \pm (L^4 - 12L^2M^2\mu^2)^{1/2}}{2M\mu^2}. \tag{2.64}$$

The maximum and minimum are located at $r = R_-$ and $r = R_+$, respectively. Hence, unstable circular orbits $\dot{r} = 0$ exist at $r = R_-$ and stable circular orbits exist at $r = R_+$. In particular, $R_+ > 6M$. Thus, the radius $r = 6M$ is the critical radius inside which no stable circular orbits exist, and is called the *innermost stable circular orbits* (ISCO). There is no analog of the ISCO in the Newtonian theory.

The binding energy per unit rest mass of the particle at the ISCO is calculated to

$$E_b = 1 - E/\mu \simeq 0.058. \tag{2.65}$$

This is the fraction of the rest energy released by gravity when a particle initially at infinity spirals towards the black hole and then plunges into the event horizon. The fraction $0.058 \sim 6\%$ is much higher than for nuclear reaction, which releases at most 0.9%. For this reason, it is widely expected that high energy phenomena occur around astrophysical black holes, in particular, at an accretion disk. The ISCO is regarded as the inner edge of the accretion disks.

We next consider light rays, which are described by null geodesics,

$$0 = g_{ab}u^a u^b = -\left(1 - \frac{2M}{r}\right)\dot{t}^2 + \left(1 - \frac{2M}{r}\right)^{-1}\dot{r}^2 + r^2\dot{\phi}^2, \tag{2.66}$$

where u^a is the tangent vector to the geodesic and the dot denotes the derivative with respect to the affine parameter. The conserved quantities along the geodesics as in Eq. (2.61) can also be defined, and hence the same form equation as Eq. (2.62) with $\mu^2 = 1$ is derived but the effective potential is

$$V(r) = \frac{L^2}{2r^2}\left(1 - \frac{2M}{r}\right). \tag{2.67}$$

The shape of the potential is independent of L. The only extremum is a maximum and is located at $r = 3M$. Thus, there exist unstable circular orbits for photons. This shows that gravity affects the propagation of photons.

2.3.2 Reissner-Nordström black hole spacetime

We review a static and spherically symmetric charged black hole spacetime which is described by a solution of the Einstein equations with the Maxwell

field A_a,

$$R_{ab} - \frac{1}{2} R g_{ab} = 2F_{ac}F^{c}_{\ b} - \frac{1}{2} g_{ab} F_{cd} F^{cd}, \tag{2.68}$$

where $F_{ab} = \partial_a A_b - \partial_b A_a$. The *Reissner-Nordström spacetime* [85, 86] describes the static and spherically symmetric gravitational field with an electric charge. In coordinates (t, r, θ, ϕ), the metric takes a form

$$ds^2 = -\left(1 - \frac{2M}{r} + \frac{Q^2}{r^2}\right) dt^2 + \left(1 - \frac{2M}{r} + \frac{Q^2}{r^2}\right)^{-1} dr^2 + r^2 d\Omega_2^2, \tag{2.69}$$

and the Maxwell field is given by

$$A_a = -\frac{Q}{r} (dt)_a \,, \tag{2.70}$$

where M and Q denote the mass and electric charge of the charged gravitational source, respectively. The Reissner-Nordström spacetime is asymptotically flat as $g_{ab} = \eta_{ab} + O(1/r)$ for the Minkowski metric η_{ab} in $r \to \infty$. The components of the metric are singular at $r = r_\pm := M \pm (M^2 - Q^2)^{1/2}$ if $M \geq |Q|$ and at $r = 0$. The former is just a coordinate singularity as in the Schwarzschild metric (2.36), while the latter is a curvature singularity. The Reissner-Nordström metric (2.69) is defined for $r_+ < r$ but it can be extended to a larger manifold as will be seen later.

The properties of the spacetime are different depending on the relation between M and Q. If $M > |Q|$, there exist two null hypersurfaces at $r = r_\pm$, and in particular, the surface at $r = r_+$ is the event horizon as will be seen below. The event horizon is the Killing horizon and the surface gravity is defined as

$$\kappa = \frac{(M^2 - Q^2)^{1/2}}{{r_+}^2}. \tag{2.71}$$

The event horizon of the Reissner-Nordström spacetime is often called the *outer horizon*. The null hypersurface at $r = r_-$ is called the *Cauchy horizon* or the *inner horizon*. The presence of the Cauchy horizon implies that general relativity suffers from a lack of the predictability in the sense that we cannot uniquely determine what happens beyond it from initial data. However, it is believed that the Cauchy horizon to be unstable and thus the above problem is solved. That is the strong cosmic censorship conjecture.

If $M = |Q|$, the Reissner-Nordström metric (2.69) becomes

$$ds^2 = -\left(1 - \frac{r_+}{r}\right)^2 dt^2 + \left(1 - \frac{r_+}{r}\right)^{-2} dr^2 + r^2 d\Omega_2^2, \tag{2.72}$$

where $r_+ = M = |Q|$. This metric describes the *extremal Reissner-Nordström spacetime*. In particular, the Killing horizon at $r = r_+$ is a *degenerate Killing*

horizon whose precise definition will be given in section 2.4. The remarkable feature of the extremal Reissner-Nordström spacetime is that the surface gravity vanishes as can be seen from Eq. (2.71). This implies the absence of the redshift effect, which plays a key role in the stability problem as will be explained in section 3.4. Also, the local structure near the surface $r = r_+$ is intensively discussed in the context of the AdS/CFT correspondence. We will give a detailed discussion in chapter 5.

If $|Q| > M$, there are no null hypersurfaces such the outer and inner horizons as seen above. Then, the metric (2.69) is regular except for $r = 0$ and represents a *naked singularity*, which is a spacetime such that the curvature singularity is visible from a distant observer. However, it is believed that the situation $|Q| > M$ does not happen in physically reasonable situations. That is the weak cosmic censorship conjecture.

The uniqueness theorem holds for both the non-extremal and extremal Reissner-Nordström spacetimes: a solution representing a static black hole spacetime to the Einstein equations with the Maxwell field, Eq. (2.68), is spherically symmetric.

As in the Schwarzschild spacetime case, there is a generalization to higher dimension and other asymptotic structure at infinity $r \to \infty$. The most general spacetime is the *n-dimensional Reissner-Nordström-(anti-) de Sitter spacetime*. In coordinates $(t, r, \theta^2, \theta^3, \cdots, \theta^{n-1})$, the metric takes the form

$$\begin{aligned} ds^2 = &- \left(1 - \frac{\mu}{r^{n-3}} + \frac{q}{r^{2(n-3)}} - \frac{2\Lambda r^2}{(n-2)(n-1)}\right) dt^2 \\ &+ \left(1 - \frac{\mu}{r^{n-3}} + \frac{q}{r^{2(n-3)}} - \frac{2\Lambda r^2}{(n-2)(n-1)}\right)^{-1} dr^2 + r^2 d\Omega_{n-2}^2, \end{aligned} \tag{2.73}$$

and the gauge field is given by

$$A_a = \left(-\frac{q}{r^{n-3}} + \phi_0\right) (dt)_a \,, \tag{2.74}$$

where ϕ_0 is an integration constant. Here, μ in Eq. (2.73) is defined in Eq. (2.40) and q is related to the electric charge Q as

$$q = \frac{8\pi Q}{(2(n-2)(n-3))^{1/2} A_{n-2}}, \tag{2.75}$$

where A_{n-2} is the volume of the $(n-2)$-dimensional unit sphere and defined in Eq. (2.41).

Global structure

To investigate the global structure, we first introduce the tortoise coordinate

$$r_* = \int \left(1 - \frac{2M}{r} + \frac{Q^2}{r^2}\right)^{-1} dr, \tag{2.76}$$

where $-\infty < r_* < \infty$. If $M > |Q|$, it is calculated to

$$r_* = r + \frac{{r_+}^2}{r_+ - r_-} \ln(r - r_+) - \frac{{r_-}^2}{r_+ - r_-} \ln(r - r_-) + \text{constant}, \tag{2.77}$$

for $r_+ < r$. In this coordinate, $r \to r_+$ and $r \to \infty$ correspond to $r_* \to -\infty$ and $r_* \to \infty$, respectively. If $M = |Q|$,

$$r_* = r + 2M \ln(r - M) - \frac{2}{r - M} + \text{constant}, \tag{2.78}$$

for $M < r$ and if $M < |Q|$,

$$r_* = r + M \ln\left(r^2 - 2Mr + Q^2\right) + \frac{2}{Q^2 - M^2} \text{ArcTan}\left(\frac{r - M}{Q^2 - M^2}\right) + \text{constant}, \tag{2.79}$$

for $0 < r$. Note that the asymptotic form of r_* in the limit of $r \to r_+$, are $\sim \ln(r - r_+)$ for the non-extremal case and $\sim -(r - M)^{-1}$ for the extremal case, that is, r is written in the form of an exponential of r_* for $M > |Q|$ and inverse power for $M = |Q|$ near the horizon.

In any case, defining coordinates

$$u = t - r_*, \quad v = t + r_*, \tag{2.80}$$

where $-\infty < u < \infty$ and $-\infty < v < \infty$, the Reissner-Nordström metric (2.69) takes the form

$$ds^2 = -\left(1 - \frac{2M}{r} + \frac{Q^2}{r^2}\right) du dv + r^2 d\Omega_2^2, \tag{2.81}$$

where r is a function of u and v.

For the case $M > |Q|$, we introduce coordinates

$$U_+ = -e^{-\frac{r_+ - r_-}{2{r_+}^2} u}, \quad V_+ = e^{\frac{r_+ - r_-}{2{r_+}^2} v}, \tag{2.82}$$

so that $-\infty < U_+ < 0$ and $0 < V_+ < \infty$. Noticing that

$$-U_+ V_+ = (r - r_+)(r - r_-)^{-\frac{{r_-}^2}{{r_+}^2}} e^{\frac{r_+ - r_-}{{r_+}^2} r}, \tag{2.83}$$

we can define the function r such that $0 \leq U_+$ and $V_+ \leq 0$. Note that the outer horizon $r = r_+$ is located at $U_+ = 0$ or $V_+ = 0$. Furthermore, near $r = r_+$, the metric takes the form

$$ds^2 \simeq -\frac{8{r_+}^4}{(r_+ - r_-)^2} dU_+ dV_+ + {r_+}^2 d\Omega_2^2, \tag{2.84}$$

and hence the metric components are regular at the outer horizon. We can thus analytically extend the spacetime manifold beyond the surface $r = r_+$. However, it follows from Eq. (2.83) that the current chart breaks down at the inner horizon $r = r_-$, i.e., $U_+ = \infty$ or $V_+ = -\infty$ at $r = r_-$. Hence, the coordinates (U_+, V_+, θ, ϕ) cover only the region $r_0 < r < \infty$, where $r = r_0$ is some cutoff radius such that $r_- < r_0 < r_+$.

We can further extend the above spacetime manifold by introducing new coordinates

$$U_- = -e^{\frac{r_+ - r_-}{2{r_-}^2} u_-}, \quad V_- = -e^{-\frac{r_+ - r_-}{2{r_-}^2} v_-}, \tag{2.85}$$

where $-\infty < U_- < 0$ and $-\infty < V_- < 0$, and

$$\begin{aligned} u_- &= t - r - \frac{{r_+}^2}{r_+ - r_-} \ln(r_+ - r) + \frac{{r_-}^2}{r_+ - r_-} \ln(r - r_-), \\ v_- &= t + r + \frac{{r_+}^2}{r_+ - r_-} \ln(r_+ - r) - \frac{{r_-}^2}{r_+ - r_-} \ln(r - r_-), \end{aligned} \tag{2.86}$$

for $r_- < r < r_+$. Noticing that

$$U_- V_- = (r - r_-)(r_+ - r)^{-\frac{{r_+}^2}{{r_-}^2}} e^{-\frac{r_+ - r_-}{{r_-}^2} r}, \tag{2.87}$$

we can define the function r such that $0 \leq U_-$ and $0 \leq V_-$, i.e., $0 < r < r_-$. The inner horizon $r = r_-$ is located at $U_- = 0$ or $V_- = 0$. Furthermore, in the current coordinates, the metric near $r = r_-$ becomes

$$ds^2 \simeq -\frac{8{r_-}^4}{(r_+ - r_-)^2} dU_- dV_- + {r_-}^2 d\Omega_2^2, \tag{2.88}$$

and thus we can extend the spacetime manifold to a manifold for $0 < r < r_-$. It can be seen from Eq. (2.87) that these coordinates are singular at the outer horizon $r = r_+$ but at the cutoff radius $r = r_0$ such that $r_- < r_0 < r_+$ we can match each manifold for the coordinates (U_-, V_-, θ, ϕ) and (U_+, V_+, θ, ϕ).

For the coordinates $(U_\pm, V_\pm)$, defining coordinates

$$\tilde{U}_\pm = \text{ArcTan } U_\pm, \quad \tilde{V}_\pm = \text{ArcTan } V_\pm, \tag{2.89}$$

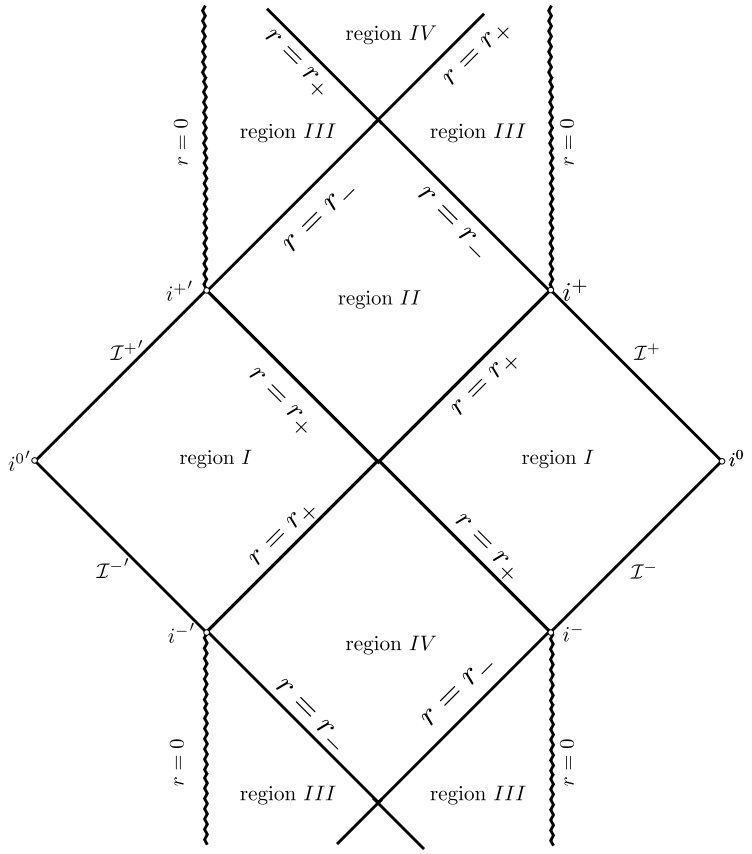

Figure 2.5: The Penrose diagram of the extended non-extremal Reinnser-Nordström spacetime. The symbols $\mathcal{I}^+$, $\mathcal{I}^-$, i^+, i^-, and i^0 represent future null infinity, past null infinity, future timelike infinity, past timelike infinity, and spatial infinity, respectively, of the asymptotically flat region denoted by right region I. The symbols $\mathcal{I}^{+\prime}$, $\mathcal{I}^{-\prime}$, $i^{+\prime}$, $i^{-\prime}$, and $i^{0\prime}$ represent future null infinity, past null infinity, future timelike infinity, past timelike infinity, and spatial infinity, respectively, of another asymptotically flat region denoted by left region I. The zigzag line represents the curvature singularity at $r = 0$.

the metric (2.81) can be rewritten as

$$ds^2 = \frac{16{r_\pm}^4}{r^2\left(r_+ - r_-\right)^2}\frac{\left(r - r_+\right)\left(r - r_-\right)}{\sin\left(2\tilde{U}_\pm\right)\sin\left(2\tilde{V}_\pm\right)}d\tilde{U}_\pm d\tilde{V}_\pm + r^2 d\Omega_2^2, \tag{2.90}$$

where r is now viewed as a function of $\tilde{U}$ and $\tilde{V}$. Then, $U_\pm = \pm\infty$ and $V_\pm = \pm\infty$ are transformed to finite values. Hence, these coordinates make the global structure of the spacetime clear. The Penrose diagram is presented in Figure 2.5. There are infinite numbers of asymptotically flat regions $r_+ < r$ denoted by region I. Region II and region IV are the spacetime region $r_- < r < r_+$ and region III is the spacetime region $0 < r < r_-$. There still exists the curvature singularity at $r = 0$ in region III. In contrast to the Schwarzschild spacetime case, the singularity is timelike and hence can be avoided by timelike curves from region I into region III through region II. Such curves can pass region III and region IV, and thus reemerge into another asymptotically flat region denoted by region I.

For the case $M = |Q|$, i.e., the extremal Reinnser-Nordström black hole case, one can see the global structure in the same manner. The Penrose diagram is presented in Figure 2.6. In this case as well, there are infinite numbers of asymptotically flat regions denoted by region I. Region II is the spacetime region $0 < r < r_+$ and there still exists the curvature singularity at $r = 0$. Since the singularity is timelike, timelike curves can avoid the singularity, and hence they can pass region II and emerge into another asymptotically flat region again.

The Penrose diagram for the case $M < |Q|$, i.e., the naked singularity case, is presented in Figure 2.7. There exists the timelike curvature singularity $r = 0$. Timelike and null curves can reach from the singularity to future null infinity $\mathcal{I}^+$. This means that the curvature singularity is visible by a distant observer.

Motion of a test charged particle and generalized ergosphere

We review the motion of a test charged particle in the Reissner-Nordström spacetime and a structure near the event horizon, which emerges arising from the interaction between the particle and the charged black hole, called the *generalized ergosphere* [87].

We consider a freely falling charged massive particle towards the black hole. The charged particle of the mass μ is described by a timelike geodesic

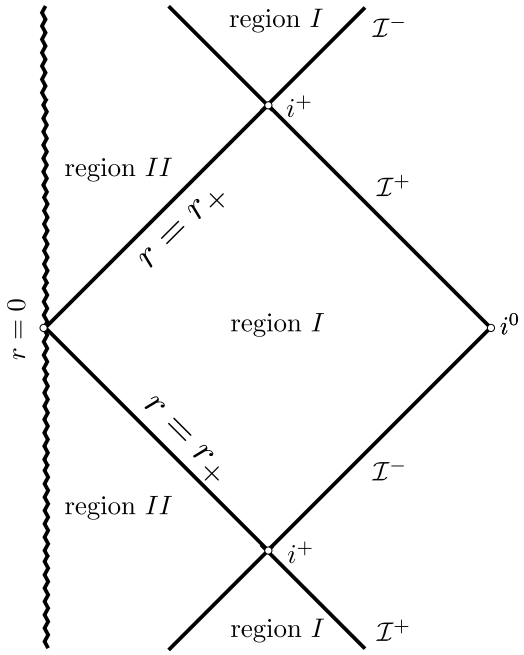

Figure 2.6: The Penrose diagram of the extended extremal Reinnser-Nordström spacetime. The symbols $\mathcal{I}^+$, $\mathcal{I}^-$, i^+, i^-, and i^0 represent future null infinity, past null infinity, future timelike infinity, past timelike infinity, and spatial infinity, respectively. The zigzag line represents the curvature singularity at $r = 0$.

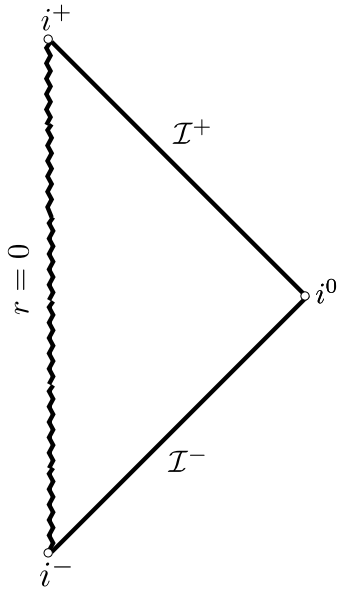

Figure 2.7: The Penrose diagram of the naked singularity. The symbols $\mathcal{I}^+$, $\mathcal{I}^-$, i^+, i^-, and i^0 represent future null infinity, past null infinity, future timelike infinity, past timelike infinity, and spatial infinity, respectively. The zigzag line represents the curvature singularity at $r = 0$.

with a tangent vector u^a,

$$-1 = g_{ab}u^a u^b = -\left(1 - \frac{2M}{r} + \frac{Q^2}{r^2}\right)\dot{t}^2 + \left(1 - \frac{2M}{r} + \frac{Q^2}{r^2}\right)^{-1}\dot{r}^2 + r^2\dot{\phi}^2, \tag{2.91}$$

where the dot denotes the derivative with respect to the proper time. Here, we have restricted the motion in the equatorial plane $\theta = \pi/2$ because of the spherical symmetry of the spacetime. Furthermore, there exist conserved quantities,

$$\begin{aligned} E :=& \mu\left(1 - \frac{2M}{r} + \frac{Q^2}{r^2}\right)\dot{t} + \frac{eQ}{r}, \\ L :=& \mu r^2\dot{\phi}, \end{aligned} \tag{2.92}$$

where e is the electric charge of the particle, and $\xi^a_{(t)} = (\partial/\partial t)^a$, $\xi^a_{(\phi)} = (\partial/\partial\phi)^a$. As in the particle motion in the Schwarzschild spacetime, E/μ and L/μ can be interpreted as energy and angular momentum per unit rest mass for a static observer at infinity, respectively. Using E and L, Eq. (2.91) is reduced to

$$\frac{1}{2}\dot{r}^2 + \frac{1}{2}\left(1 - \frac{2M}{r} + \frac{Q^2}{r^2}\right)\left(1 + \frac{L^2}{\mu^2 r^2}\right) = \frac{1}{2\mu^2}\left(E - \frac{eQ}{r}\right)^2. \tag{2.93}$$

On circular orbits $\dot{r} = 0$, we have

$$E = E_\pm := \frac{eQ}{r} \pm \mu \left[\left(1 - \frac{2M}{r} + \frac{Q^2}{r^2} \right) \left(1 + \frac{L^2}{\mu^2 r^2} \right) \right]^{1/2}. \tag{2.94}$$

Note that E_+ is the same as E_- for the reverse sign of eQ and t. Equation (2.94) shows that there are two states with $E = E_\pm$. This separation goes to zero at the event horizon, i.e.,

$$\lim_{r \to r_+} E_\pm = \frac{eQ}{r_+}. \tag{2.95}$$

At infinity, $\lim_{r\to\infty} E_\pm = \pm\mu$.

The important feature implied by Eq. (2.94) is that if $eQ < 0$ there can exist a negative energy state for E_+. For example, E_+ of the particle with $L = 0$ is negative in the region such that

$$r_+ \leq r < M + \sqrt{M^2 - Q^2 \left(1 - \frac{e^2}{\mu^2} \right)}. \tag{2.96}$$

For nonzero L as well, there exists such a region. This region is called the *generalized ergosphere*. The generalized ergosphere arises from the presence of the electric charge of the particle. The generalized ergosphere is similar to the ergoregion of rotating black holes. The ergoregion originates from the spin of the black hole and therefore can exist even for a neutral particle. In contrast, the generalized ergosphere can exist even in non-rotating black holes but instead needs the electromagnetic interaction between the black hole and a particle.

In the presence of the ergoregion, a particle can extract mass and angular momentum from rotating black holes. This phenomenon is known as the *Penrose process*. Similarly, it can be expected that the Reissner-Nordström black hole discharges due to the generalized ergosphere. Denardo and Ruffini [87] have argued the energetics of the Reissner-Nordström black hole and have shown that a charged particle indeed extracts charge of the black hole.

In a similar context, it is known that bosonic waves with angular momentum can extract mass and angular momentum of a rotating black hole as will be reviewed in section 3.4. This is called *superradiance*. As will be investigated in chapter 4, a charged black hole discharges by a charged boson field. We refer to this charge extraction phenomenon as *electromagnetic superradiance*.

2.4 Back holes in Gaussian null coordinates

We have explored the basic property of the Schwarzschild black hole and the Reissner-Nordström black hole. It is convenient to describe a black hole spacetime in a general manner. In this section, we review the general form of the line element describing the vicinity of Killing horizons.

We consider a smooth codimension-one null hypersurface $\mathcal{N}$ in an n-dimensional spacetime. In a neighborhood of any such hypersurface, we can adopt chart called the *Gaussian null coordinates* (v, ρ, θ^A), where $A = 2, 3, \ldots, n-2$ [88]. Here, θ^A are coordinates on $(n-2)$-dimensional spacelike hypersurface. With respect to the coordinate basis, a vector $n^a = (\partial/\partial v)^a$ is normal to $\mathcal{N}$ and its integral curves are null geodesic generators of $\mathcal{N}$, i.e., $n^a n_a = 0$ on $\mathcal{N}$. The normal vector n^a also satisfies $n^A(\partial/\partial\theta^A) = 0$ and

$$n^a \nabla_a n^b = \kappa n^b, \tag{2.97}$$

where κ is some function, on $\mathcal{N}$. Besides, a vector $L^a = (\partial/\partial\rho)^a$ is null, i.e., $L^a L_a = 0$ everywhere, and satisfies $L^a n_a = 1$ and $L^A(\partial/\partial\theta^A) = 0$ everywhere. Coordinates (v, ρ, θ^A) are assigned to points at the affine distance ρ along the null geodesic starting at the point on $\mathcal{N}$ with coordinates (v, θ^A) with the tangent vector L^a. Using those Gaussian null coordinates (v, ρ, θ^A), the line element near $\mathcal{N}$ located at $\rho = 0$ takes the form

$$ds^2 = \rho f\left(v, \rho, \theta^A\right) dv^2 + 2dvd\rho + 2\rho h_A\left(v, \rho, \theta^A\right) dvdx^A + \gamma_{AB}\left(v, \rho, \theta^A\right) dx^A dx^B, \tag{2.98}$$

where $B = 2, 3, \ldots, n-2$, and $f(v, \rho, \theta^A)$, $h_A(v, \rho, \theta^A)$, and $\gamma_{AB}(v, \rho, \theta^A)$ are smooth functions.

Let $\mathcal{N}$ be the Killing horizon. Namely, the Killing vector field ξ^a in the spacetime is normal and tangent to $\mathcal{N}$ and we can set $\xi^a = n^a$. Then, the metric (2.98) is independent of v and Eq. (2.97) can be rewritten as

$$\xi^a \nabla_a \xi^b = \kappa \xi^b. \tag{2.99}$$

Comparing this with Eq. (2.54), we can regard κ as the surface gravity. We thus obtain in the Gaussian null coordinates (v, ρ, θ^A) the general form of the metric in the vicinity of a stationary black hole spacetime with nonzero surface gravity,

$$ds^2 = \rho f\left(\rho, \theta^A\right) dv^2 + 2dvd\rho + 2\rho h_A\left(\rho, \theta^A\right) dvdx^A + \gamma_{AB}\left(\rho, \theta^A\right) dx^A dx^B. \tag{2.100}$$

We now define the *degenerate Killing horizon* as the Killing horizon such that the Killing vector field ξ^a normal to $\mathcal{N}$ is tangent to affinely parametrized

null geodesics on $\mathcal{N}$, i.e., $\kappa = 0$. The event horizon of the extremal Reissner-Nordström black hole is the degenerate Killing horizon. Equation (2.51) then shows that $\nabla^a(\xi^b\xi_b) = 0$ on $\mathcal{N}$ and therefore $\partial_\rho g_{vv}|_{\mathcal{N}} = 0$, i.e., $g_{vv} = \rho^2 F(\rho, \theta^A)$ for a function $F(\rho, \theta^A)$ so that $g_{vv} = \mathcal{O}(\rho^2)$. Thus, in the Gaussian null coordinates (v, ρ, θ^A), the line element near the degenerate Killing horizon is written in the form

$$ds^2 = \rho^2 F\left(\rho, \theta^A\right) dv^2 + 2dvd\rho + 2\rho h_A\left(\rho, \theta^A\right) dvdx^A + \gamma_{AB}\left(\rho, \theta^A\right) dx^A dx^B. \tag{2.101}$$

The degenerate Killing horizon has the following remarkable feature. We now perform the coordinate transformation,

$$v = \frac{\tilde{v}}{\epsilon}, \quad \rho = \epsilon\tilde{\rho}, \tag{2.102}$$

where $\epsilon > 0$. This is the scale transformation generated by $\xi = v\partial_v - \rho\partial\rho$. Further, taking the scaling limit, $\epsilon \to 0$, we obtain

$$ds^2 = \tilde{\rho}^2 F\left(0, \theta^A\right) d\tilde{v}^2 + 2d\tilde{v}d\tilde{\rho} + 2\tilde{\rho} h_A\left(0, \theta^A\right) d\tilde{v}dx^A + \gamma_{AB}\left(0, \theta^A\right) dx^A dx^B. \tag{2.103}$$

The resulting metric is invariant under the transformation (2.102), and is called a *near-horizon geometry*. Intuitively, the scaling limit corresponds to focus on the spacetime structure near the degenerate Killing horizon. Thus, the scaling invariant structure appears in the vicinity of degenerate Killing horizons. This property plays an important role in analysis of linear perturbations of extremal black holes [66, 67, 68] and in AdS/CFT correspondence [56, 57]. Note that the Killing horizon to be degenerate, i.e., $g_{vv} = \mathcal{O}(\rho^2)$, is crucial for the emergence of the near-horizon geometry.

Chapter 3

Linear perturbations in black hole spacetimes

In this chapter, we review the basic features of linear perturbations in black hole spacetimes.

3.1 Tensor field perturbations in the Minkowski spacetime

As a preliminary, we first review the linearized theory of gravity in the Minkowski spacetime. For that, we first consider tensor field perturbations in the Minkowski background, namely, the *gravitational wave*. The linear field in the Minkowski spacetime is denoted by h_{ab} and takes the form

$$g_{ab} = \eta_{ab} + h_{ab}, \tag{3.1}$$

where η_{ab} is the Minkowski metric (2.5) and we assume $|h_{ab}| \ll 1$. From the vacuum Einstein equations, we obtain equations for h_{ab} at the first order,

$$-\Box\bar{h}_{ab} - \eta_{ab}\partial^c\partial^d\bar{h}_{cd} + \partial^c\partial_a\bar{h}_{bc} + \partial^c\partial_b\bar{h}_{ac} = 0, \tag{3.2}$$

where $\Box$ is the d'Alembertian in the Minkowski spacetime and

$$\bar{h}_{ab} = h_{ab} - \frac{1}{2}\eta_{ab}h, \tag{3.3}$$

with

$$h = h^a_a = \eta^{ab}h_{ab}. \tag{3.4}$$

We now use the gauge freedom to choose the *harmonic gauge*,

$$\partial^a\bar{h}_{ab} = 0. \tag{3.5}$$

Note that the harmonic gauge condition is in general defined by $\partial_a(g^{ab}\sqrt{-g}) = 0$ but this condition reduces to Eq. (3.5) in the linear order of h_{ab}. Equation (3.5) gives four conditions and therefore reduces 10 independent components of $\bar{h}_{ab}$ to six independent components.

Imposing the harmonic gauge condition (3.5), Eq. (3.2) is reduced to

$$\Box\bar{h}_{ab} = 0. \tag{3.6}$$

The gauge condition does not fix the gauge completely. Actually, Eq. (3.5) changes as

$$\partial^a\bar{h}_{ab} \to \partial^a\bar{h}_{ab} - \Box\xi_b, \tag{3.7}$$

against the infinitesimal coordinate transformation ξ^a such that $x^a \to x^a + \xi^a$. Then, we also have

$$\bar{h}_{ab} \to \bar{h}_{ab} - \xi_{ab}, \tag{3.8}$$

where $\xi_{ab} = \partial_a\xi_b + \partial_b\xi_a - \eta_{ab}\partial_c\xi^c$. It can be seen from Eq. (3.7) that the harmonic gauge condition is not spoiled by the transformation if we choose

$$\Box\xi^a = 0. \tag{3.9}$$

With this condition, Eq. (3.6) is also invariant under the transformation because $\Box\xi_{ab} = 0$.

We can further reduce six independent components of $\bar{h}_{ab}$ to two independent components by choosing the function ξ^a subject to Eq. (3.9) which gives four conditions. In particular, we can choose ξ^0 so that $\bar{h} = 0$. Note that then $\bar{h}_{ab} = h_{ab}$. We also choose ξ^i so that $h_{0i} = 0$. The harmonic gauge condition (3.5) then implies

$$\partial^0 h_{00} = 0, \tag{3.10}$$

and hence h_{00} is constant in time. This time independent part is interpreted as the Newtonian potential of the source generating the tensor field h_{ab}. The above equation means that the dynamical part of h_{00} is zero, i.e., $h_{00} = 0$ as long as we concern dynamical evolution of h_{ab}. In conclusion, we have set

$$h_{0a} = 0, \quad h^i_i = 0, \quad \partial^i h_{ij} = 0. \tag{3.11}$$

This is called the *transverse-traceless gauge*. As stated above, initially 10 independent components of $\bar{h}_{ab}$ is reduced to six independent components by the harmonic gauge condition (3.5) and the residual gauge is further reduced to two degrees of freedom by the condition (3.9). The resulting two degrees of freedom are physical degrees of freedom of the gravitational wave described by Eq. (3.6).

Equation (3.6) takes the form of a wave equation in the Minkowski spacetime. We indeed have a wave solution that describes a plane wave traveling the $+z$ direction in the coordinates (t, x, y, z),

$$h_{ab} = \begin{pmatrix} 0 & 0 & 0 & 0 \\ 0 & h_+ & h_\times & 0 \\ 0 & h_\times & -h_+ & 0 \\ 0 & 0 & 0 & 0 \end{pmatrix} \cos\left[\omega(t-z)\right], \tag{3.12}$$

where ω is the frequency of the wave. The quantities h_+ and $h_\times$ are physical degrees of freedom of the gravitational wave and are called the amplitude of the *plus* and *cross* polarization, respectively.

3.2 Black hole perturbation theory in spherically symmetric black hole spacetimes

We review the black hole perturbation theory in the Schwarzschild black hole spacetime. We first focus on scalar filed perturbations and next on tensor field perturbations. It is useful to consider the dynamical evolution of a scalar field in a black hole spacetime background. Besides the interest to its own, the investigation of scalar field perturbations brings us insight into the basic property of how the spacetime reacts to the external perturbation in a much simpler form and therefore is suitable as a first step to the future study in tensor perturbations.

3.2.1 Scalar field perturbations

We consider a massless Klein-Gordon field in the Schwarzschild black hole spacetime background (2.36). The scalar field is described by

$$\Box\Phi(t, r, \theta, \varphi) = 0, \tag{3.13}$$

where $\Box$ is the d'Alembertian in the Schwarzschild spacetime. In the spherically symmetric spacetime, it is convenient to expand Φ in terms of the spherical harmonics $Y_{\ell m}$ as

$$\Phi(t, r, \theta, \varphi) = \sum_{\ell=0}^{\infty} \sum_{m=-\ell}^{\ell} \frac{u_{\ell m}(t, r)}{r} Y_{\ell m}(\theta, \varphi). \tag{3.14}$$

The spherical harmonics satisfies

$$\left[\frac{1}{\sin\theta}\partial_\theta\left(\sin\theta\partial_\theta\right) + \frac{1}{\sin^2\theta}\partial_\varphi^2\right] Y_{\ell m} = -\ell(\ell+1) Y_{\ell m}. \tag{3.15}$$

Using this, we obtain an equation for $u_{\ell m}$. With the tortoise coordinate r_* defined in Eq. (2.43), the equation for $u_{\ell m}$ is written in the form

$$\left[\partial_{r_*}^2 - \partial_t^2 - V_\ell(r)\right] u_{\ell m} = 0, \tag{3.16}$$

where

$$V_\ell = \left(1 - \frac{2M}{r}\right)\left[\frac{\ell(\ell+1)}{r^2} + \frac{2M}{r^3}\right]. \tag{3.17}$$

Furthermore, performing the Fourier transform with respect to t,

$$u_{\ell m}(t, r) = \frac{1}{2\pi}\int_{-\infty}^{\infty} d\omega\ \tilde{u}_{\ell m}(\omega, r) e^{-i\omega t}, \tag{3.18}$$

we arrive at

$$\left[\frac{d^2}{dr_*^2} + \omega^2 - V_\ell(r)\right]\tilde{u}_{\ell m} = 0. \tag{3.19}$$

This is equivalent to the Schrödinger equation with potential V_ℓ in one dimension. The effective potential corresponds to a single barrier and the maximum is roughly located at $r = 3M$, where the unstable circular orbit of photon exists as seen in section 2.3.1. Note that with the spherical harmonics, massless and massive Klein-Gordon equations in other spherically symmetric spacetime can also be reduced to the Schrödinger-type equation in the same manner.

3.2.2 Tensor field perturbations

We next review the tensor field perturbations in the Schwarzschild spacetime. As explained in Appendix A, a symmetric second-rank tensor can be expanded into 10 parts depending on (t, r) in terms of the scalar and vector spherical harmonics. Each part is labelled by ℓ and m as $u_{\ell m}(t, r)$ in Eq. (3.14). Tensor field perturbations can also be expanded into 10 parts in the spherical harmonics. Under the parity transformation $\theta \to \pi - \theta$ and $\varphi \to \varphi + \pi$, the scalar harmonics pick up a factor $(-1)^\ell$, while the vector harmonics pick up a factor $(-1)^{\ell+1}$. The perturbations with $(-1)^\ell$ are called *polar perturbations*, while the perturbations with $(-1)^{\ell+1}$ are called *axial perturbations*. Those are also called *even-party perturbations* and *odd-party perturbations*, respectively. Namely, the tensor perturbations h_{ab} can be separated into

$$h_{ab} = h_{ab}^{polar} + h_{ab}^{axial}, \tag{3.20}$$

where h_{ab}^{polar} and h_{ab}^{axial} denote the polar perturbations and the axial perturbations, respectively, and are written in the form of a sum of the expansion

in the spherical harmonics which is given in Eq. (A.14) in Appendix A. Note that since the Schwarzschild metric (2.36) is invariant under the parity transformation, the polar and axial perturbations do not mix.

As in the tensor perturbations in the Minkowski spacetime in section 3.1, we use the gauge freedom to simplify Eq. (3.20) by an infinitesimal coordinate transformation $x^a \to x'^a = x^a + \xi^a$. In the gauge used by Regge and Wheeler [89] which is explained in detail in Appendix A, the degrees of freedom of the polar perturbations are reduced from seven to four, and that of the axial perturbations is reduced from three to two. The line elements are then explicitly written in the forms

$$\begin{aligned} h^{polar}_{\mu\nu} dx^\mu dx^\nu =& -\left(1-\frac{2M}{r}\right)\left[1-\sum_{\ell=0}^{\infty}\sum_{m=-\ell}^{\ell} H^{(0)}_{\ell m}(t,r)Y_{\ell m}\right]dt^2 \\ &+2\left[\sum_{\ell=1}^{\infty}\sum_{m=-\ell}^{\ell} H^{(1)}_{\ell m}(t,r)Y_{\ell m}\right]dtdr \\ &+\left(1-\frac{2M}{r}\right)^{-1}\left[1+\sum_{\ell=0}^{\infty}\sum_{m=-\ell}^{\ell} H^{(2)}_{\ell m}(t,r)Y_{\ell m}\right]dr^2 \\ &+\left[1+\sum_{\ell=2}^{\infty}\sum_{m=-\ell}^{\ell} K_{\ell m}(t,r)Y_{\ell m}\right]r^2\left(d\theta^2+\sin^2\theta d\varphi^2\right), \end{aligned} \tag{3.21}$$

and

$$\begin{aligned} h^{axial}_{\mu\nu} dx^\mu dx^\nu =& -2\left[\sum_{\ell=2}^{\infty}\sum_{m=-\ell}^{\ell} h^{(0)}_{\ell m}(t,r)\frac{\partial_\varphi Y_{\ell m}}{\sin\theta}\right]dtd\theta \\ &+2\left[\sum_{\ell=2}^{\infty}\sum_{m=-\ell}^{\ell} h^{(0)}_{\ell m}(t,r)\sin\theta\partial_\theta Y_{\ell m}\right]dtd\varphi \\ &-2\left[\sum_{\ell=1}^{\infty}\sum_{m=-\ell}^{\ell} h^{(1)}_{\ell m}(t,r)\frac{\partial_\varphi Y_{\ell m}}{\sin\theta}\right]drd\theta \\ &+2\left[\sum_{\ell=1}^{\infty}\sum_{m=-\ell}^{\ell} h^{(1)}_{\ell m}(t,r)\sin\theta\partial_\theta Y_{\ell m}\right]drd\varphi. \end{aligned} \tag{3.22}$$

The functions $H^{(0)}_{\ell m}(t,r)$, $H^{(1)}_{\ell m}(t,r)$, $H^{(2)}_{\ell m}(t,r)$, and $K_{\ell m}(t,r)$ describe the polar perturbations, while $h^{(0)}_{\ell m}(t,r)$, $h^{(1)}_{\ell m}(t,r)$ describe the axial perturbations.

Axial perturbation equations

We can now write down the perturbation equations in the gauge of Regge and Wheeler. We first introduce the equations for the axial perturbations. For the metric (3.22), the linearized Einstein equations in vacuum can be reduced to an equation involving $h^{(1)}_{\ell m}$ only:

$$\begin{aligned}&\partial_t^2 h^{(1)}_{\ell m} - \left(1-\frac{2M}{r}\right)\left(\partial_r - \frac{2}{r}\right)\partial_r\left[\left(1-\frac{2M}{r}\right)h^{(1)}_{\ell m}\right] \\ &+\left(1-\frac{2M}{r}\right)\frac{(\ell-1)(\ell+2)}{r^2}h^{(1)}_{\ell m} = 0.\end{aligned} \tag{3.23}$$

Introducing the gauge-invariant valuable (see Eq. (A.24))

$$Q_{\ell m}(t,r) = \frac{1}{r}\left(1-\frac{2M}{r}\right)h^{(1)}_{\ell m}(t,r), \tag{3.24}$$

Eq. (3.23) becomes

$$\left[\partial_{r_*}^2 - \partial_t^2 - V_\ell^{RW}(r)\right]Q_{\ell m} = 0, \tag{3.25}$$

where r_* is the tortoise coordinate and

$$V_\ell^{RW}(r) = \left(1-\frac{2M}{r}\right)\left[\frac{\ell(\ell+1)}{r^2} - \frac{6M}{r^3}\right]. \tag{3.26}$$

Equation (3.25) is called the *Regge-Wheeler equation* and $V_\ell^{RW}(r)$ in Eq. (3.26) is called the *Regge-Wheeler potential*. We notice that the Regge-Wheeler equation (3.25) is the same form as Eq. (3.16), and the Regge-Wheeler potential (3.26) is slightly different from the scalar field case (3.17). The effective potentials for scalar, vector, and tensor field perturbations can be written in a unified manner as

$$V_\ell^\sigma(r) = \left(1-\frac{2M}{r}\right)\left[\frac{\ell(\ell+1)}{r^2} + \frac{2M(1-\sigma^2)}{r^3}\right], \tag{3.27}$$

where σ denotes the spin of the perturbations, namely, $\sigma = 0$ for the scalar perturbations, $\sigma = 1$ for the vector perturbations, $\sigma = 2$ for the tensor perturbations. Equation (3.27) shows that the effective potentials go to zero at the horizon $r = 2M$ and at infinity $r \to \infty$, in particular, decay exponentially in the tortoise coordinate near the horizon, while decay in a power law near infinity. This power-law form in the asymptotically flat region leads to a remarkable feature of linear perturbations as will be explained in section 3.3.2.

Polar perturbation equations

We next introduce equations for the polar perturbations (3.21). We first perform the following Fourier transform with respect to t,

$$\hat{H}^{(0)}_{\ell m}(\omega, r) = \int_{-\infty}^{\infty} dt H^{(0)}_{\ell m}(t, r)\, e^{i\omega t}, \tag{3.28}$$

$$\hat{H}^{(1)}_{\ell m}(\omega, r) = \int_{-\infty}^{\infty} dt H^{(1)}_{\ell m}(t, r)\, e^{i\omega t}, \tag{3.29}$$

$$\hat{H}^{(2)}_{\ell m}(\omega, r) = \int_{-\infty}^{\infty} dt H^{(2)}_{\ell m}(t, r)\, e^{i\omega t}, \tag{3.30}$$

$$\hat{K}_{\ell m}(\omega, r) = \int_{-\infty}^{\infty} dt K_{\ell m}(t, r)\, e^{i\omega t}. \tag{3.31}$$

We also define

$$\lambda = \frac{(\ell - 1)(\ell + 2)}{2}, \tag{3.32}$$

and introduce the gauge-invariant valuable (see Eq. (A.32))

$$\hat{Z}_{\ell m}(\omega, r) = \frac{r^2}{\lambda r + 3M}\hat{K}_{\ell m} + \frac{r}{i\omega(\lambda r + 3M)}\left(1 - \frac{2M}{r}\right)\hat{H}^{(1)}_{\ell m}. \tag{3.33}$$

Then, all dynamical equations for the perturbations are reduced to an equation for $\hat{Z}_{\ell m}(\omega, r)$ [90],

$$\left[\frac{d^2}{dr_*^2} + \omega^2 - V^Z_\ell(r)\right]\hat{Z}_{\ell m} = 0, \tag{3.34}$$

where

$$V^Z_\ell(r) = \left(1 - \frac{2M}{r}\right)\frac{2\lambda^2(\lambda + 1)r^3 + 6\lambda^2 M r^2 + 18\lambda M^2 r + 18M^3}{r^3(\lambda r + 3M)^2}. \tag{3.35}$$

Equation (3.34) is called the *Zerilli equation* and $V^Z_\ell(r)$ in Eq. (3.35) is called the *Zerilli potential*. Although the Zerilli potential is more complicated than the Regge-Wheeler potential (3.26), they are numerically almost indistinguishable. As in the Regge-Wheeler potential, the Zerilli potential also tends to zero at the horizon and at infinity, and in particular, decays in the same power law at $r \to \infty$. Furthermore, those potentials have the remarkable feature called the *isospectrality*, i.e., they posses the same quasinormal modes which will be precisely defined in the next section.

3.3 Properties of linear perturbations in spherically symmetric black hole spacetimes

We review the important properties of linear perturbations in spherically symmetric black hole spacetimes. We first see that the wave has a characteristic oscillation that describes the response with ringing of a black hole. After that, we see that the late-time asymptotic behavior of linear perturbations is dominated by a power law in time, not an exponentially decaying.

3.3.1 Quasinormal modes

We consider the problem of an equation of the form

$$\left[\frac{d^2}{dx^2} + \omega^2 - V(x)\right]\phi(\omega, x) = 0, \tag{3.36}$$

where $-\infty < x < \infty$. We set the locations of a black hole horizon and infinity at $x = -\infty$ and at $x = +\infty$, respectively. Equations for linear perturbations in a static and spherically symmetric spacetime, e.g., the Regge-Wheeler equation (3.25) and the Zerilli equation (3.34), typically take the above form.

We are now interested in the situation in which a black hole spacetime is perturbed by an extra field and how the field will evolve in time from initial data outside the black hole horizon. The response of the black hole spacetime is described by Eq. (3.36) and can be understood by solving the eigenvalue problem for ω under appropriate boundary conditions. In general, the effective potential $V(x)$ in Eq. (3.36) vanishes in $x \to -\infty$ and hence the asymptotic solution near the horizon is written in the form of the linear combination of $e^{+i\omega x}$ and $e^{-i\omega x}$. Taking the time-dependence, $e^{-i\omega t}$, into account, the former and the latter describe the outgoing wave and ingoing wave, respectively. Since nothing should radiate from the horizon in our situation, we discard the outgoing wave at the horizon, i.e.,

$$\phi(\omega, x) \sim e^{-i\omega x}, \quad x \to -\infty. \tag{3.37}$$

Suitable boundary conditions at $x \to +\infty$ depend on the asymptotic structure of the spacetime. In asymptotically flat spacetimes, $V(x)$ in Eq. (3.36) vanishes at infinity $x = +\infty$ as well. Hence, we have two asymptotic solutions, $e^{+i\omega x}$ and $e^{-i\omega x}$, and the general solution takes a form of a superposition of those outgoing and ingoing waves. Our interest is in a wave such that part of the wave propagates from finite distances to infinity and does not enter from infinity. Thus, the appropriate boundary condition at infinity in the

asymptotically flat spacetime is

$$\phi(\omega, x) \sim e^{+i\omega x}, \quad x \to +\infty. \tag{3.38}$$

In asymptotically anti-de Sitter spacetimes, $V(x)$ in Eq. (3.36) does not vanish due to the presence of the cosmological constant. Then, the asymptotic form of the solution takes the forms[1]

$$\phi(\omega, x) \sim \frac{A}{x^2} + Bx, \quad x \to +\infty, \tag{3.39}$$

for massless scalar field perturbations and

$$\phi(\omega, x) \sim \frac{A}{x} + B, \quad x \to +\infty, \tag{3.40}$$

for vector and tensor field perturbations. For the scalar perturbation, a popular choice is $B = 0$, which is called the *Dirichlet boundary condition*. Other choices are also meaningful depending on the problem, and the boundary conditions at the AdS boundary play an important role in the context of AdS/CFT correspondence. The topic of the boundary conditions at the AdS boundary will be more discussed in chapter 4. In the case for the vector and tensor perturbations, there seems to be no compelling reason for a specific boundary condition but $B = 0$ is usually chosen.

Imposing the above conditions, Eq. (3.36) picks up discrete complex values of ω, which are called *quasinormal (mode) frequencies*. The corresponding eigenfunctions are called *quasinormal modes*. If the imaginary part of ω is negative, the amplitude of $\phi(\omega, x)$ decays exponentially in time. Then, the wave has a damped oscillation. Physically, this describes the dissipation effect of the field into the black hole and infinity in asymptotically flat spacetimes. On the other hand, if the imaginary part is positive, the amplitude grows in time. This means that the system is linearly unstable. The topic of stability will be explained in section 3.4.

In the following discussion, we focus on the perturbation under the boundary conditions (3.37) and (3.38), and assume that the imaginary part of ω

[1] Asymptotic behaviors of a massive scalar field with mass squared μ^2 at infinity of the anti-de Sitter spacetime with the curvature scale ℓ are given in Eq. (4.25). Redefining ψ in Eq. (4.25) with $\chi = \ell/x$ as $\phi(x) = x\psi(x)$, the new scalar field ϕ satisfies the Schrödinger-type equation as in Eq. (3.36). Then, it can be checked that the asymptotic behavior of ϕ with $\mu^2\ell^2 = 0$ at $x = \infty$ takes the form of Eq. (3.39). As for vector and tensor field perturbations in the four-dimensional anti-de Sitter spacetime, both the scalar- and vector-type components satisfy the same equation as the massive scalar field ψ with $\mu^2\ell^2 = -2$ which is a conformally invariant scalar field [63]. Therefore, asymptotic behaviors of vector and tensor field perturbations at $x = \infty$ are the same as ϕ with $\mu^2\ell^2 = -2$. It can be checked that the asymptotic behavior takes the form of Eq. (3.40).

is negative. By definition, quasinormal modes satisfy the boundary conditions (3.37) and (3.38), i.e.,

$$\phi(\omega, x) \propto e^{i|\omega|x} = e^{i\mathrm{Re}[\omega]|x|}e^{-\mathrm{Im}[\omega]|x|}, \quad x \to \pm\infty. \tag{3.41}$$

This shows that the quasinormal modes diverge both at the horizon and at infinity. Therefore, the quasinormal mode cannot describe a physical state of the system for all values of x at a given time, rather describes the behavior of $\phi(\omega, x)$ at a fixed value of x and at a sufficiently large value of t. Then, the growing factor $e^{-\mathrm{Im}[\omega]|x|}$ is compensated by the time dependence $e^{+\mathrm{Im}[\omega]t}$.

Quasinormal modes in terms of the time-domain Green function

To obtain further perspective of quasinormal modes, we study an equation

$$\left[\partial_x^2 - \partial_t^2 - V(x)\right]\phi(t, x) = 0, \tag{3.42}$$

in terms of the Green function. We assume that the potential $V(x)$ tends to zero in $x \to \pm\infty$. We define the Laplace transform

$$\hat{\phi}\,(\omega, x) = \int_0^\infty dt\ e^{i\omega t}\phi(t, x), \tag{3.43}$$

where $\mathrm{Im}[\omega] > 0$ and $t \geq 0$. Acting $e^{i\omega t}$ on Eq. (3.42) and integrating it with respect to t from $t = 0$ to $t = \infty$, we obtain

$$\int_0^\infty dt\ e^{i\omega t}\left[\partial_x^2 - \partial_t^2 - V(x)\right]\phi(t, x) = 0. \tag{3.44}$$

Integrating the second term of the left-hand side by part, we can rewrite it to

$$-\int_0^\infty dt\ e^{i\omega t}\partial_t^2\phi(t, x) = \omega^2\int_0^\infty dt\ e^{i\omega t}\phi(t, x) - \mathcal{I}(\omega, x), \tag{3.45}$$

where

$$\mathcal{I}(\omega, x) = \left[i\omega\phi(t, x) - \partial_t\phi(t, x)\right]\big|_{t=0}. \tag{3.46}$$

Here, we have assumed $e^{i\omega t}\phi|_{t=\infty} = 0$ and $e^{i\omega t}\partial_t\phi|_{t=\infty} = 0$ from $\mathrm{Im}[\omega] > 0$. Furthermore, using Eq. (3.43), Eq. (3.44) is rewritten as

$$\left[\frac{d^2}{dx^2} + \omega^2 - V(x)\right]\hat{\phi}(\omega, x) = \mathcal{I}(\omega, x). \tag{3.47}$$

Thus, the partial differential equation (3.42) is reduced to an ordinary differential equation. We also define

$$G\left(t,x,x'\right)=\frac{1}{2\pi}\int_{-\infty+i\epsilon}^{\infty+i\epsilon}d\omega\ e^{-i\omega t}\hat{G}\left(\omega,x,x'\right), \tag{3.48}$$

where $t\geq 0$ and $\epsilon>0$, and $\hat{G}\left(\omega,x,x'\right)$ is the Green function of Eq. (3.47), i.e.,

$$\left[\frac{d^2}{dx^2}+\omega^2-V(x)\right]\hat{G}\left(\omega,x,x'\right)=\delta(x-x'). \tag{3.49}$$

Then, the corresponding solution of Eq. (3.47) is written in the form

$$\hat{\phi}(\omega,x)=\int_{-\infty}^{\infty}dx'\ \hat{G}\left(\omega,x,x'\right)\mathcal{I}(\omega,x). \tag{3.50}$$

Setting the condition $G(t,x,x')=0$ for $t<0$, Eq. (3.48) defines the retarded Green function of the operator $[\partial_x^2-\partial_t^2-V(x)]$, i.e.,

$$\left[\partial_x^2-\partial_t^2-V(x)\right]G\left(t,x,x'\right)=\delta\left(x-x'\right)\delta(t). \tag{3.51}$$

Performing the inverse Laplace transform of Eq. (3.50) by

$$\phi(t,x)=\frac{1}{2\pi}\int_{-\infty+i\epsilon}^{\infty+i\epsilon}d\omega\ e^{-i\omega t}\hat{\phi}\left(\omega,x\right), \tag{3.52}$$

where $t\geq 0$ and $\epsilon>0$, and using Eq. (3.46), the general solution for $\phi(t,x)$ is written in the form

$$\phi(t,x)=-\int_{-\infty}^{\infty}dx'\ \left[\partial_t G\left(t,x,x'\right)\phi(t=0,x)+G\left(t,x,x'\right)\partial_t\phi(t,x)\big|_{t=0}\right]. \tag{3.53}$$

Thus, given the initial data $\phi(t=0,x)$ and $\partial_t\phi(t,x)\big|_{t=0}$, the Green function $G\left(t,x,x'\right)$ constructs the solution $\phi(t,x)$.

Before obtaining $G\left(t,x,x'\right)$, we discuss the asymptotic behaviors of $\hat{\phi}_+(\omega,x)$ and $\hat{\phi}_-(\omega,x)$ which are linearly independent solutions of the homogeneous equation

$$\left[\frac{d^2}{dx^2}+\omega^2-V(x)\right]\hat{\phi}(\omega,x)=0. \tag{3.54}$$

We define the Wronskian of them as

$$W(\omega)\equiv\hat{\phi}_-(\omega,x)\partial_x\hat{\phi}_+(\omega,x)-\hat{\phi}_+(\omega,x)\partial_x\hat{\phi}_-(\omega,x). \tag{3.55}$$

Note that $W(\omega)$ is independent of x, i.e., $\partial_x W(\omega)=0$. Since $V(x)$ goes to zero at $x=\pm\infty$ in the system we concern, the asymptotic behaviors of a

general solution of Eq. (3.54) at both the boundaries are written in the form of the linear combination of $e^{-i\omega x}$ and $e^{+i\omega x}$. Taking this into account, we choose $\hat{\phi}_+(\omega, x)$ and $\hat{\phi}_-(\omega, x)$ such that

$$\hat{\phi}_+(\omega, x) \sim \begin{cases} e^{-i\omega x}, & x \to -\infty, \\ a_1(\omega)e^{-i\omega x} + a_2(\omega)e^{+i\omega x}, & x \to +\infty, \end{cases} \tag{3.56}$$

and

$$\hat{\phi}_-(\omega, x) \sim \begin{cases} b_1(\omega)e^{-i\omega x} + b_2(\omega)e^{+i\omega x}, & x \to -\infty, \\ e^{+i\omega x}, & x \to +\infty. \end{cases} \tag{3.57}$$

From these asymptotic behaviors, $W(\omega)$ in Eq. (3.55) is computed to

$$W(\omega) = 2i\omega b_2(\omega), \tag{3.58}$$

at $x = -\infty$ and

$$W(\omega) = 2i\omega a_1(\omega), \tag{3.59}$$

at $x = +\infty$. Since $W(\omega)$ is independent of x, we have $a_1(\omega) = b_2(\omega)$.

We are now ready to express $G(\omega, x, x')$. We consider compactly supported initial data such that the function $\mathcal{I}(\omega, x)$ in Eq. (3.46) is non-vanishing only in $x_L < x' < x_R$ with $\mathcal{R} \ll x_L$, where $\mathcal{R}$ is the length scale of the spacetime. We then discuss the response of the black hole seen by a distant observer at $x_R < x$. Then, for $x' < x$ we have

$$\hat{G}\,(\omega, x, x') = \frac{1}{W(\omega)}\hat{\phi}_+(\omega, x)\hat{\phi}_-(\omega, x'). \tag{3.60}$$

Thus, we can obtain $G(\omega, x, x')$ by calculating Eq. (3.48) in terms of $\hat{\phi}_+(\omega, x)$ and $\hat{\phi}_-(\omega, x')$ through Eq. (3.60).

In the case of the Schwarzschild spacetime, the complex integral in Eq. (3.48) can be performed by the integration along the contour illustrated in Figure 3.1. There are three contributions in the integral [31, 32]: the contribution from two quarter-circles at $|\omega| \to \infty$, from poles of the integrand due to zeros of $a_1(\omega)$, and from the branch cut along the negative imaginary axis. The branch-cut contribution depends on the asymptotic form of the effective potential at boundaries.

The contribution from the two quarter-circles at $|\omega| \to \infty$ corresponds to the early-time response of the black hole. In the limit of $|\omega| \to \infty$, the wave freely propagates and hence directly travels from the source to a distant observer at the speed of light.

The second contribution from the pole corresponds to the quasinormal mode. Let $\omega = \omega_n$ be a set of zeros of $a_1(\omega)$, i.e., $a_1(\omega_n) = 0$. Then,

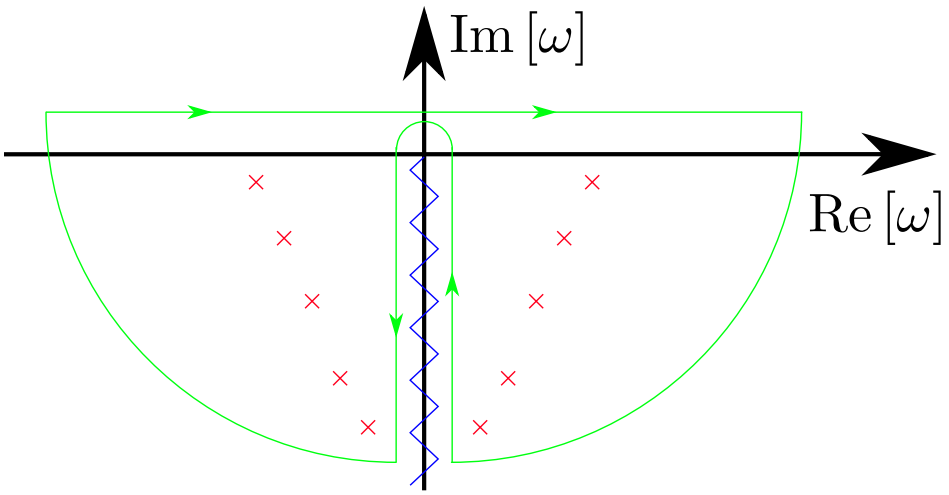

Figure 3.1: The schematic figure of the contour of the integration in Eq. (3.48) in the complex ω-plane. The green line is the contour. The red cross marks represent the poles from $a_1(\omega)$ and the blue zigzag line is the branch cut.

$a_1(\omega_n) = 0$ determines the quasinormal mode frequencies. The vanishing of $a_1(\omega)$ at $\omega = \omega_n$ means that $W(\omega_n) = 0$ from Eq. (3.59), and therefore $\hat{\phi}_+(\omega_n, x)$ and $\hat{\phi}_-(\omega_n, x)$ are no longer linearly independent. Expanding $a_1(\omega)$ near $\omega = \omega_n$ and picking the residual of the poles, we derive the quasinormal-mode contribution

$$G_{QNM}\left(t, x, x'\right) \sim -\mathrm{Re}\left[\sum_n \frac{a_2(\omega_n)}{\omega_n a_1'(\omega_n)} e^{-i\omega_n(t-x-x')}\right], \tag{3.61}$$

where

$$a_1'(\omega_n) = \frac{d}{d\omega} a_1(\omega)\big|_{\omega=\omega_n}. \tag{3.62}$$

We can see that $G_{QNM}(t, x, x')$ takes the form of a sum over a discrete term.

The branch cut leading to the third contribution is a general feature if the effective potential $V(x)$ in Eq. (3.42) goes to zero slower than an exponential at $x = +\infty$, e.g., power-law as in the Regge-Wheeler potential (3.26) and the Zerilli potential (3.34), except for the centrifugal potential barrier [91, 92]. The branch-cut contribution yields a *power-law tail* as will be more explained in the next subsection. Late-time behaviors of the perturbation are dominated by the power law of time rather than the quasinormal mode.

As observed above, the quasinormal-mode contribution (3.61) does not represent the full signal. Namely, quasinormal modes do not form a complete set of perturbations. This means that stability analysis of a system focusing

on the Fourier mode such as in Eq. (3.18) is incomplete. In particular, even if the system is stable in the sense of the absence of exponentially growing quasinormal modes, a late-time power-law tail could have a singular behavior, for example, its derivatives are unbounded at late times. This will be reviewed in section 3.4.

3.3.2 Power-law tails

We briefly review the branch-cut contribution in Eq. (3.48). To compute it, the exact solution to Eq. (3.42) is needed. It is in general complicated but can be simplified in the limit of $t \gg x + x'$. In the Schwarzschild spacetime case, Leaver [31] has found that the leading behavior in the limit of $t \to \infty$ takes the form

$$G_{tail}\,(t, x, x') \sim (-1)^{\ell+1} \frac{4M(2\ell+2)!}{[(2\ell+1)!!]^2} \frac{(xx')^{\ell+1}}{t^{2\ell+3}}. \tag{3.63}$$

This shows that the late-time behavior seen by a distant observer at $x \gg M$ is expressed by a power law of time. Such the power-law behavior is called the *power-law tail*. In the limit of $t \to \infty$ with t/x fixed, the tail at future null infinity is also calculated to

$$G_{tail}\,(t, x, x') \sim (-1)^{\ell+1} \frac{2M(\ell+1)!}{(2\ell+1)!!} \frac{(x')^{\ell+1}}{u^{\ell+2}}, \tag{3.64}$$

where $u = t - x$.

Price [93] has first found the power-law behaviors at late times in the asymptotically flat region of a spherically symmetric stellar collapse. The exponent depends on the initial data, namely, the static initial data near the stellar surface evolve to $\sim t^{-2\ell-3}$ at late times, while those far from the surface do $\sim t^{-2\ell-2}$. Several authors [91, 92, 94, 95] have shown that the power is the same if the asymptotic form of the effective potential is the same. Namely, the power-law tail at infinity is independent of the detail of the central object, e.g., black holes or stars. It is believed that the power-law tail is generated by backscattering off the spacetime curvature potential at large distances.

For a better understanding of the response of a black hole to the linear perturbations we have discussed so far, as an example, let us consider the situation in which the source is localized around a distance x' from the Schwarzschild black hole at initial time $t = 0$, and a distant observer located at x, where $x' < x$, will see the signal at $t > 0$. Then, the signal observed at t is separated into the following main contributions:

(i) For $t < x - x'$, no signal reaches the observer because of the causality.

(ii) At $t \simeq x - x'$, the signal begins to be observed. This is part of the initial outward wave, which is described by the two-quarter circles in the integral in the Green function (3.48), and the signal directly travels to the observer at the speed of light.

(iii) At $t \simeq x + x'$, the signal from the quasinormal mode arrives at the observer. Part of the initial wave towards the black hole takes a time $\sim x'$ to propagate, and excites the quasinormal mode in the vicinity of the black hole. The resulting excitation takes a time $\sim x$ to propagate to the observer. This signal has an exponentially damping in time and is called the ringdown wave. This contribution is given by Eq. (3.61).

(iv) When the signal from the quasinormal mode sufficiently decays, the power-law tail begins to be observed. This contribution is described by the branch cut in the Green function (3.48) and is given by Eq. (3.63).

3.4 Stability problems

We review stability problems of a spacetime in this section. The black hole perturbation theory we have reviewed is a useful method for judging linear stability as a first step of the investigation of the nonlinear dynamical evolution of the system. Mathematically, linear stability problem of a black hole is reduced to investigations whether or not there is an upper bound for the amplitude and all derivatives of the perturbation field at all the points on and outside the black hole horizon to the future from the initial surface. If not, the spacetime is linearly unstable.

In this section, we focus on linear stability of black hole spacetimes. The seminal work of linear stability of the exact black hole solution to the Einstein equations is [89] by Regge and Wheeler. The authors have proposed the formalism of the linear perturbations of the Schwarzschild spacetime as explained in section 3.2.2, i.e., the Regge-Wheeler equation (3.25). Focusing on the Fourier mode with respect to time, several works have shown that there is no exponentially growing quasinormal mode and thus the Schwarzschild metric (2.36) is linearly stable. Such the stability of the Fourier mode is called the mode stability. Kay and Wald [96] have rigorously proved the stability of the Schwarzschild metric beyond the mode stability. As for a wide range of non-extremal black holes with the nonnegative cosmological constant as well, the linear stabilities are completely shown in [97].

In the rest of the final section, we review two linear instabilities, which will be discussed later.

Superradiance and superradiant instability

Superradiance is a phenomenon that extracts energy and angular momentum from rotating black holes by bosonic waves [98, 99, 100]. In this process, the wave is amplified by scattering off the effective potential near the black hole horizon. For superradiance occurring, the bosonic wave of a frequency ω is required to satisfy an inequality

$$0 < \omega < m\Omega_H, \tag{3.65}$$

where m is the azimuthal number of the wave and Ω_H is the angular velocity of the rotating black hole. This phenomenon essentially arises from the presence of the ergoregion in the vicinity of the rotating black hole, in which the asymptotic timelike Killing vector fields associated with time-translation at spatial infinity become spacelike due to the rotation, and hence the negative energy state is allowed. Superradiance does not occur for fermionic waves.

If superradiance occurs in a confined system, the scattering wave near the black hole horizon will travel outwardly and arrive at the "wall", then will be reflected and go back to the black hole again. If the ingoing wave also satisfies the condition (3.65), the wave is amplified again. Repeating a series of the process, the amplitude of the wave unboundedly grows in time. This can be interpreted as linear instability and is called the *black hole bomb* or *superradiant instability*. Precisely speaking, a rotating black hole suffers from superradiant instability if the quasinormal mode frequency satisfies the condition (3.65). The confined system can be constructed by the imposition of perfectly reflective boundary conditions at large distances [101, 102], mass of a boson field [103], and the negative cosmological constant [104, 105]. In the context of astrophysics, superradiant instability for a massive boson field is intensively discussed to seek ultralight bosons as a candidate of dark matter. The nonlinear evolution of the instability for an asymptotically anti-de Sitter black hole is also discussed in the context of AdS/CFT correspondence and mathematical relativity.

As seen in section 2.3.2, the Reissner-Nordström black hole has the generalized ergoregion for massive charged particles. Therefore, it is expected that the amplification phenomenon also emerges for charged bosonic waves. The condition for the process is given by

$$0 < \omega < \frac{eQ}{r_+}, \tag{3.66}$$

where e and Q are charge of a boson field and the black hole, respectively, and r_+ is the horizon radius. In this process, the boson field gains charge from the black hole and energy from its ambient electric field, while the black

hole gives charge to the boson field and gains energy from the boson field but decreases its mass. We will discuss the detail in chapter 4. Furthermore, superradiant instability also appears [106]. We will discuss the instability as well in chapter 4.

The Aretakis instability

The Schwarzschild spacetime and the non-extremal Reissner-Nordström spacetime have shown to be linearly stable beyond the mode analysis [96, 97]. In those proofs, the presence of the redshift effect plays a key role. As a result, the extra field and all its derivatives are bounded on and outside the event horizon at the future from the initial surface.

To get the picture of how the redshift effect plays, let us consider the situation in which there are two observers, $\mathbf{O}_p$ and $\mathbf{O}_f$, crossing the event horizon at different times, where $\mathbf{O}_p$ falls into the black hole earlier than $\mathbf{O}_f$, and $\mathbf{O}_p$ sends photons to $\mathbf{O}_f$. Then, the energy of the photons sent from $\mathbf{O}_p$ along the horizon undergoes the redshift proportional to $e^{-\kappa v}$, where κ is the surface gravity and v is the Killing parameter along the horizon. Hence, all components of the energy-momentum tensor exponentially decay at late times $v \to \infty$. Using the analogy of photons and massless scalar waves, this redshift effect implies that the wave and its derivative on and outside the horizon also decay at late times.

In contrast, by definition, extremal black holes have the vanishing surface gravity and hence no redshift effect. Therefore, the above picture breaks down and photons can stay on the horizon for a long time. Aretakis [66, 67, 68] has shown that a test massless scalar field in the extremal Reissner-Nordström black hole spacetime decays on and outside the horizon at late times and its transverse derivatives decay only outside but do not decay on. This implies that some component of the energy-momentum tensor of the field on the horizon does not decay at late times. For example, first-and second-order radial derivatives of the spherically symmetric mode ψ_0 on the horizon $\mathcal{H}_+$ at late times $\tau \to \infty$ take the forms

$$\partial_r \psi_0\big|_{\mathcal{H}_+} \sim -\frac{H_0}{M^3}, \quad \partial_r^2 \psi_0\big|_{\mathcal{H}_+} \sim \frac{H_0}{M^5}\tau, \quad \text{as } \tau \to \infty, \tag{3.67}$$

where M is the black hole mass and H_0 is a constant called the *Aretakis constant*. The first-order derivative on the horizon approaches the Aretakis constant at late times, and the second-order derivative blows up linearly in time. The higher-order derivatives also blow up polynomially in time at the late time. These late-time divergent behaviors of the derivatives of the field on the horizon are called the *Aretakis instability*. The Aretakis constant H_0

is a conserved quantity along the horizon. That existence implies that the radial-radial component of the energy-momentum tensor of the field on the horizon does not decay at the late time; hence an infalling observer measures the local energy density at the horizon. In this sense, the Aretakis constant is interpreted as "horizon hair". For higher multipoles labeled by ℓ as well, there exist the Aretakis constants H_ℓ which are also conserved quantities along the horizon. Then, $(\ell+1)$th-order radial derivatives of the field on the horizon approach the Aretakis constants H_ℓ at late times, and $(\ell+2)$th-and higher-order derivatives blow up.

One might think that the Aretakis instability does not directly imply the singular behavior of physical quantities from the fact that the second- and higher-order derivatives, not the first-order, are unbounded at late times. However, the observational signature of the Aretakis instability is suggested [107]. In [107], precise expressions for the leading late-time behavior of the field at finite distances and future null infinity are derived, and the Aretakis constant can be read off from those expressions. In other words, we can measure, in principle, the horizon-hair from observations away from the event horizon. This result suggests that (near-)extremal black holes admit classical measurable horizon-hair and the Aretakis instability potentially serves as an observational signature.

What happens by taking the backreaction into account? According to [70], with generic initial data, the extremal Reissner-Nordström black hole spacetime finally settles down into the non-extremal one. However, with fine-tuning, the extremality remains and the Aretakis' divergent behavior lasts forever. Namely, the extremal Reissner-Nordström spacetimes evolve into a dynamical extremal black hole involving with the Aretakis instability. It is conjectured that with other fine-tuned initial data, the extremal Reissner-Nordström black hole evolves into a naked singularity [73].

The physical interpretations and origin of the Aretakis constant and instability are not clear. Those will be discussed in chapter 5.

Chapter 4

Stability of small charged anti-de Sitter black holes in the Robin boundary

The content in this chapter was originally published as:
T. Katagiri and T. Harada, "Stability of small charged anti-de Sitter black holes in the Robin boundary," Class. Quant. Grav., 38(13):135026, (2021)

As explained in Chapter 1, for the study of stability, it is useful to investigate quasinormal mode frequencies (QNFs). Uchikata and Yoshida [106] discuss the QNFs of neutral and charged massless scalar fields in the asymptotically AdS charged black hole. They claim that the spacetime can suffer from the superradiant instability only if $eQ > 0$, while the spacetime is stable if $eQ \leq 0$, where e and Q are the scalar field charge and the black hole charge, respectively. As we will show later, the result of the instability caused by superradinace is just a consequence of the assumption that the real part of the QNFs is positive. We will discuss that the negative real part of the QNFs should also be discussed because there is no physical reason to rule out this possibility. In this respect, their analysis does not suffice.

In addition, their analysis has room to be extended with respect to boundary conditions at the conformal infinity. The boundary conditions play important roles in the dynamical evolution of a test field in spacetimes without global hyperbolicity [108, 63, 109]. Hence, for the classification of the stability of (asymptotically) AdS spacetimes, the perturbation analysis should be done for all possible boundary conditions at the conformal infinity. For massless neutral scalar fields, in order to define well-posed and stable evolution, the suitable one is unique to the Dirichlet boundary condition. Of

course, Uchikata and Yoshida [106] follow this and obtain desirable results. In contrast, for *massive* neutral fields with some range of the (effective) mass squared, e.g. in the case of a conformally coupled massless scalar field, the Robin boundary condition is allowed. This is characterised by one parameter and includes the Dirichlet and Neumann boundary conditions. In this sense, the Robin boundary condition is more general [110]. Also, even for charged fields, it can be adopted if the electromagnetic interaction between the black hole and the field is sufficiently small at the asymptotic infinity. For the above reasons, the study of QNFs of the neutral and charged massive scalar fields in the charged AdS black hole under the Robin boundary condition can shed light on a relation between the boundary conditions and the dynamical evolution of the fields, such as the time scale of the (in)stability. Then, it is possible to directly compare the result with that of [106].

It is meaningful to discuss the stability of spacetimes against linear perturbations imposed the Robin boundary condition in many directions. In gravitational physics, there emerge new solutions through the analysis of linear perturbation on the pure AdS background [64, 111, 112]. Through the analysis in the current paper, it is suggested that there are new black hole solutions which are asymptotically AdS and satisfy the Robin boundary condition at the conformal infinity. Since the background scalar field is trivial, the "backreaction" contributions of the scalar field to the metric and Maxwell fields appear only from the second order. This is why the dynamics of a scalar field as a test field in the background metric and Maxwell fields provides a fully consistent linear perturbation solution. The appearance of a zero-mode linear perturbation solution of the scalar field suggests a branch off of a sequence of hairy-black-hole solutions there for it has been shown that this is the case in similar systems [113, 114, 115, 116]. In the context of the AdS/CFT, the Robin boundary condition corresponds to a double-trace or multi-trace deformation [117] and the parameter of the boundary condition determines its coupling constant [118].

In this chapter, we analytically and numerically investigate the QNFs of neutral and charged massive scalar fields in the anti-de Sitter spacetime (AdS) and in the Reissner-Nordström-AdS black holes with the Robin boundary condition at the conformal infinity. In the latter case, we assume that black holes are much smaller than the AdS length scale. We take this assumption for the following reasons. First, the most profound growing and decaying modes usually appear in the small-horizon limit [106]. Second, two kinds of instability caused by charged fields in Reissner-Nordström-AdS spacetimes, the superradiant instability and the near-horizon scalar condensation, are mutually entangled in general but should be of different natures in appropriate limits: in the small (large)-horizon limit, the superradiant in-

stability (the near-horizon scalar condensation) is singled out [114]. Third, in the current paper, we are interested in the qualitative change of the QNFs and the stability of black holes caused by the boundary conditions which are generalized due to the presence of even an infinitesimally small negative cosmological constant, rather than in the quantitative change caused by the large negative one. Finally, as long as the authors know, no one has ever fully numerically evaluated the QNFs because of potential difficulty in handling the Robin boundary condition. In this context, it is useful to obtain the QNFs in the small-black-hole limit in the Robin boundary for future fully numerical studies for more general situations. For these reasons, we shall obtain the QNFs under the small-black-hole assumption as a first step. We then discuss the dynamical properties of the scalar field in terms of the QNFs.

This chapter is organized as follows. In Section 4.1, we introduce the system and the basic equations. In Section 4.2, we briefly review Ref. [63] for a massive scalar field in the AdS spacetime and present a numerical result consistent with their result. In Section 4.3, we introduce symmetries in the QNFs and justify the matched asymptotic expansion method for the neutral and charged scalar fields in the charged small AdS black holes. In Section 4.4, we analytically show that the small charged AdS black hole suffers from superradiant instability if the QNFs in the pure AdS satisfy the superradaint condition. In Section 4.5, we show numerical results for QNFs for the neutral and charged scalar fields in the charged small AdS black hole. In Section 4.6, we give physical interpretation of the superradiant instability in the AdS black hole. In Section 4.7, we summarize this chapter. In the Appendix B, we present mathematical notions, show the validity of the matching procedure in the matched asymptotic expansion, derive the asymptotic behaviors of the solutions, and explicitly confirm the symmetry in the QNFs.

4.1 System and basic equations

We consider the Einstein-Maxwell-scalar system with a negative cosmological constant. The action is given by

$$S = \int d^{d+2}x\sqrt{-g}\left[\frac{1}{16\pi}(R-2\Lambda) + L_m + L_{em}\right] \tag{4.1}$$

with

$$L_m = -\left[(D_a\Psi)\,(D^a\Psi)^* + \mu^2|\Psi|^2\right], \tag{4.2}$$

$$L_{em} = -\frac{1}{16\pi}F_{ab}F^{ab}, \tag{4.3}$$

where R is the scalar curvature and $\Lambda(<0)$ is the cosmological constant, $F_{ab} = \nabla_a A_b - \nabla_b A_a = \partial_a A_b - \partial_b A_a$ is the field strength, $D_a := \nabla_a - ieA_a$, ∇_a is the Levi-Civita covariant derivative, A_a is a gauge field, e and μ^2 are the charge and mass of the complex scalar field Ψ, respectively. We assume $e \geq 0$ without loss of generality and do not specify the sign of μ^2.

Varying Eq. (4.1) with respect to g_{ab}, we obtain Einstein's equations

$$G_{ab} + \Lambda g_{ab} = 8\pi T_{ab}, \tag{4.4}$$

where $T_{ab} = T_{(m)ab} + T_{(em)ab}$ with

$$\begin{aligned} T_{(m)ab} =& (D_a\Psi)(D_b\Psi)^* + (D_a\Psi)^*(D_b\Psi) - g_{ab}\left[(D_c\Psi)(D^c\Psi)^* + |\Psi|^2\right], \\ T_{(em)ab} =& \frac{1}{4\pi}\left(F_{ac}F_b{}^c - \frac{1}{4}g_{ab}F_{cd}F^{cd}\right). \end{aligned} \tag{4.5}$$

Varying Eq. (4.1) with respect to A_a, we obtain some components of Maxwell's equations

$$\nabla_b F^{ba} = -4\pi j^a_{(e)}, \tag{4.6}$$

where $j^a_{(e)}$ is the conserved electric current density given by

$$j^a_{(e)} = -ie\left[\Psi^*(D^a\Psi) - \Psi(D^a\Psi)^*\right]. \tag{4.7}$$

The rest of the components of Maxwell's equations

$$\nabla_{[a}F_{bc]} = 0 \tag{4.8}$$

are automatically satisfied by construction. Varying Eq. (4.1) with respect to Ψ, we obtain the equation of motion for Ψ

$$\left[(\nabla_a - ieA_a)\,(\nabla^a - ieA^a) - \mu^2\right]\Psi = 0. \tag{4.9}$$

For non-minimally coupled scalar field, μ^2 is replaced with $\mu^2 + \xi R$ in the above, where ξ is a coupling constant to gravity. From the above, we can find the conserved particle number current density j^a [119]:

$$j^a = -i[\Psi^*(D^a\Psi) - \Psi(D^a\Psi)^*]. \tag{4.10}$$

Since the electric current density $j^a_{(e)}$ is related to j^a through $j^a_{(e)} = ej^a$, we can identify the charge of the associated particle with e.

In the presence of the timelike Killing vector ξ^a, we can define the conserved energy current J^a as $J^a := -T^a_b\xi^b$, which can be decomposed as $J^a = J^a_{(m)} + J^a_{(em)}$, where $J^a_{(m)} := -T^a_{(m)b}\xi^b$ and $J^a_{(em)} := -T^a_{(em)b}\xi^b$. In spherical symmetry, the conserved charge associated with J^a is the Misner-Sharp quasi-local energy $E_{\rm MS}$ [120].

We will focus on Eq. (4.9) regarding Ψ as a test field in the fixed spacetime and gauge field in Sections II–V. In Sections VI and VII, we will also discuss the other equations and the effect of the scalar field onto the spacetime and the gauge field.

4.2 Scalar field in the AdS spacetime

4.2.1 Brief review of exact results

We briefly review a neutral scalar field in the AdS spacetime based on Ishibashi and Wald [63]. From Eq. (4.9), the scalar field obeys the following equation:

$$\left(\nabla_\mu\nabla^\mu - \mu^2\right)\Psi = 0. \tag{4.11}$$

Since the AdS spacetime is static, Eq. (4.11) can be written in the form of

$$-\frac{\partial^2}{\partial t^2}\Psi = A\Psi, \tag{4.12}$$

where t is a Killing parameter and A is given by $A = -VD^i\left(VD_i\right) + \mu^2V^2$, $V \equiv \left(-\xi^\mu\xi_\mu\right)^{1/2}$, $\xi^\mu = (\partial/\partial t)^\mu$ is a timelike Killing vector and D^i is the Levi-Civita covariant derivative on a constant t spacelike hypersurface.

Now we can view A as a linear operator $A : D \to K$, where D and K are the subspaces of the Hilbert space $\mathcal{H} = L^2$. The definitions of mathematical notions are given in Appendix B.1. If A in Eq. (4.12) is symmetric and positive, A has at least one self-adjoint extension A_E which is positive [121]. Moreover, if the boundary condition is specified, A_E is uniquely determined [109] . If we find a positive and unique A_E, we can define stable and unique evolution of Ψ from initial data [108] . Therefore, the problem of how to define stable and unique evolution in the non-globally hyperbolic (static) spacetime boils down to choose the boundary condition such that A_E is positive.

In the coordinates $(t, \chi, \theta^1, \theta^2, \ldots, \theta^d)$, the metric of the unit $(d+2)$-dimensional AdS spacetime is given by

$$ds^2 = \frac{\ell^2}{\sin^2\chi}\left(-dt^2 + d\chi^2 + \cos^2\chi d\Omega_d^2\right), \tag{4.13}$$

where $\chi \in [0, \pi/2]$ is a radial coordinate, $(\theta^1, \theta^2, \ldots, \theta^d)$ correspond to angular coordinates, $d\Omega_d^2$ is the metric of the d dimensional sphere, and $\ell \equiv \sqrt{d(d+1)/(-2\Lambda)}$ is the AdS length scale. The origin is located at $\chi = \pi/2$, while $\chi = 0$ corresponds to the conformal infinity.

We assume that Ψ is in the form,

$$\Psi(t, \chi, \theta^1, \ldots, \theta^d) = (\ell \cot\chi)^{-d/2}\psi(\chi)Y_{\boldsymbol{k}}(\theta^1, \ldots, \theta^d)e^{-i\omega t}, \tag{4.14}$$

where $Y_{\boldsymbol{k}}(\theta^1, \ldots, \theta^d)$ are spherical harmonics and $\omega \in \mathbb{C}$ is the frequency. Now Eq. (4.12) is rewritten as

$$A\psi(\chi) = \omega^2\psi(\chi), \tag{4.15}$$

where

$$A = -\frac{d^2}{d\chi^2} + \frac{\nu^2 - 1/4}{\sin^2\chi} + \frac{\rho^2 - 1/4}{\cos^2\chi} \tag{4.16}$$

with $\nu^2 = 1/4 + d(d+2)/4 + \mu^2\ell^2$ and $\rho^2 = 1/4 + l(l+d-1) + d(d-2)/4$. Note that A given by Eq. (4.16) is a symmetric operator.

We require that the general solution of Eq. (4.15) be regular at the origin. On the other hand, the asymptotic behavior of the solution near the conformal infinity is given by

$$\psi(\chi) \sim C_1\psi_{fast}(\chi) + C_2\psi_{slow}(\chi)\ ,\ C_1, C_2 \in \mathbb{C}, \tag{4.17}$$

where $\psi_{fast}(\chi)$ and $\psi_{slow}(\chi)$ show the faster and slower cutoffs in the limit to the conformal infinity $\chi \to 0$, respectively. In analogy, we refer to the boundary condition $C_2 = 0$ and $C_1 = 0$ as the Dirichlet and Neumann boundary conditions, respectively. Besides, we call the boundary condition such that C_1/C_2 is a real constant the Robin boundary condition. Ref. [63] summarises the relation between the positivity of the self-adjoint extension of A and the boundary conditions at the conformal infinity as the following theorem.

Theorem 1: *Let A and A_E be the symmetric operator given by Eq. (4.16) and its self-adjoint extension, respectively. For the solution (4.17) which satisfies the regularity condition at the origin, the relation between the positivity of A_E and the boundary condition imposed at the conformal infinity is as*

follows:
(1) *If* $-(d+3)(d-1)^2/4 \leq \mu^2\ell^2$, *there exists unique* A_E, *and it is positive.*
(2) *If* $-(d+1)^2/4 < \mu^2\ell^2 < -(d+3)(d-1)^2/4$, A_E *is positive if and only if*

$$\kappa \geq \kappa_c = -\left|\frac{\Gamma(-\nu)}{\Gamma(\nu)}\right| \frac{\Gamma(\zeta^0_{\nu,\rho})^2}{\Gamma(\zeta^0_{-\nu,\rho})^2}, \tag{4.18}$$

where $C_1 = \kappa C_2$ $(\kappa \in \mathbb{R})$ *and* $\zeta^0_{\nu,\rho} \equiv (\nu+\rho+1)/2$.
(3) *If* $\mu^2\ell^2 = -(d+1)^2/4$, A_E *is positive if and only if* $\kappa_{BF} \leq \kappa_{BF,c} = 2\gamma + 2P(\zeta^0_{0,\rho})$, *where* $C_1 = C_2/\kappa_{BF}$ $(\kappa_{BF} \in \mathbb{R})$, $P(\zeta^0_{0,\rho}) \equiv d\log\Gamma(\chi)/d\chi|_{\chi=\zeta^0_{0,\rho}}$ *and* γ *is the Euler number.*
(4) *If* $\mu^2\ell^2 < -(d+1)^2/4$, A *is unbounded below. Then, any* A_E *are unbounded below.*

4.2.2 Numerical investigation

Let us investigate the scalar field for the case **(2)** of this theorem. For this purpose, we shall solve Eq. (4.15) in the 4-dimensional AdS spacetime. Now we introduce a new variable

$$y = 1 + \frac{1}{\tan^2\chi}, \tag{4.19}$$

and a function $g(y)$ such that

$$\psi(y) = y^{\frac{\omega\ell}{2}}(y-1)^{\frac{l}{2}}g(y). \tag{4.20}$$

Then Eq. (4.15) is reduced to an equation for $g(y)$,

$$y(1-y)\frac{d^2}{dy^2}g(y) + \{\gamma - (\alpha+\beta+1)y\}\frac{d}{dy}g(y) - \alpha\beta g(y) = 0 \tag{4.21}$$

with

$$\begin{aligned}
\alpha &= \frac{\omega\ell}{2} + \frac{l}{2} + \frac{3}{4} + \frac{1}{4}\sqrt{9+4\mu^2\ell^2}, \\
\beta &= \frac{\omega\ell}{2} + \frac{l}{2} + \frac{3}{4} - \frac{1}{4}\sqrt{9+4\mu^2\ell^2}, \\
\gamma &= \omega\ell + 1.
\end{aligned} \tag{4.22}$$

Eq. (4.21) has two independent solutions

$$g(y) = y^{-\alpha}F\left(\alpha, \alpha-\gamma+1; \alpha-\beta+1; \frac{1}{y}\right) \ , \ y^{-\beta}F\left(\beta, \beta-\gamma+1; \beta-\alpha+1; \frac{1}{y}\right), \tag{4.23}$$

where $F(\ ,\ ;\ ;\frac{1}{y})$ is the Gaussian hypergeometric function. We thus obtain the general solution of Eq. (4.15),

$$\begin{aligned}\psi(y) =& Cy^{-\frac{l}{2}-\frac{3}{4}-\frac{1}{4}\sqrt{9+4\mu^2\ell^2}}(y-1)^{\frac{l}{2}}F\left(\alpha,\alpha-\gamma+1;\alpha-\beta+1;\frac{1}{y}\right)\\ &+Dy^{-\frac{l}{2}-\frac{3}{4}+\frac{1}{4}\sqrt{9+4\mu^2\ell^2}}(y-1)^{\frac{l}{2}}F\left(\beta,\beta-\gamma+1;\beta-\alpha+1;\frac{1}{y}\right),\end{aligned} \tag{4.24}$$

where C and D are arbitrary constants in $\mathbb{C}$.

Near the conformal infinity, Eq. (4.24) behaves as

$$\psi(\chi)\sim C\chi^{\frac{3}{2}+\frac{1}{2}\sqrt{9+4\mu^2\ell^2}}+D\chi^{\frac{3}{2}-\frac{1}{2}\sqrt{9+4\mu^2\ell^2}}. \tag{4.25}$$

This is an explicit form of Eq. (4.17). According to Theorem 1, we have a degree of freedom in choosing the boundary condition depending on the value of $\mu^2\ell^2$. We here focus on the case $-9/4<\mu^2\ell^2<-5/4$ and impose the Robin boundary condition

$$C=\kappa D,\quad \kappa\in\mathbb{R} \tag{4.26}$$

on Eq. (4.25). Then, the AdS spacetime behaves as a confined system because Eq. (4.26) gives a reflecting boundary condition [110]. In the context of AdS/CFT correspondence, this boundary condition corresponds to the double-trace deformation and the one parameter of the boundary condition determines its coupling constant [118]. We thus obtain the solution of Eq. (4.15) satisfying the boundary condition at the conformal infinity as follows:

$$\begin{aligned}\psi(y)=D\Bigg[&\kappa y^{-\frac{l}{2}-\frac{3}{4}-\frac{1}{4}\sqrt{9+4\mu^2\ell^2}}(y-1)^{\frac{l}{2}}F\left(\alpha,\alpha-\gamma+1;\alpha-\beta+1;\frac{1}{y}\right)\\ &+y^{-\frac{l}{2}-\frac{3}{4}+\frac{1}{4}\sqrt{9+4\mu^2\ell^2}}(y-1)^{\frac{l}{2}}F\left(\beta,\beta-\gamma+1;\beta-\alpha+1;\frac{1}{y}\right)\Bigg].\end{aligned} \tag{4.27}$$

As shown in Appendix B.3, in the limit of $y\to 1$, or $\chi\to\pi/2$, Eq. (4.27) behaves as

$$\psi(y)\sim D\Gamma(\alpha+\beta-\gamma)\left[D_1(\tilde{\omega},\kappa)\left(\frac{\pi}{2}-\chi\right)^{-l-1}+D_2(\tilde{\omega},\kappa)\left(\frac{\pi}{2}-\chi\right)^{l}\right], \tag{4.28}$$

where

$$\begin{aligned}D_1(\omega,\kappa)&=\frac{\kappa\Gamma(\alpha-\beta+1)}{\Gamma(\alpha)\Gamma(\alpha-\gamma+1)}+\frac{\Gamma(\beta-\alpha+1)}{\Gamma(\beta)\Gamma(\beta-\gamma+1)},\\ D_2(\omega,\kappa)&=\frac{\Gamma\left(\gamma-\alpha-\beta\right)}{\Gamma\left(\alpha+\beta-\gamma\right)}\left(\frac{\kappa\Gamma(\alpha-\beta+1)}{\Gamma(1-\beta)\Gamma(\gamma-\beta)}+\frac{\Gamma(\beta-\alpha+1)}{\Gamma(1-\alpha)\Gamma(\gamma-\alpha)}\right).\end{aligned} \tag{4.29}$$

We can see that the first term in the square brackets on the right-hand side of Eq. (4.28) diverges at $\chi = \pi/2$ if $D_1(\omega, \kappa) \neq 0$. Therefore, to guarantee the regularity at the origin, we require

$$D_1(\omega, \kappa) = 0. \tag{4.30}$$

This equation determines the eigenfrequency or the QNF of the mode which satisfies the boundary condition. It also gives us the relation between the evolution and the boundary condition at the conformal infinity. Here we can see that the functions $D_1(\omega, \kappa)$ and $D_2(\omega, \kappa)$ have a symmetry under the transformation $\omega \to -\omega$, and moreover satisfy the relation $D_1(\omega, \kappa) = {D_1}^*(-\omega^*, \kappa)$ and $D_2(\omega, \kappa) = {D_2}^*(-\omega^*, \kappa)$. Thus, if ω is a QNF, then, both of $-\omega$ and $-\omega^*$ and therefore ω^* are.

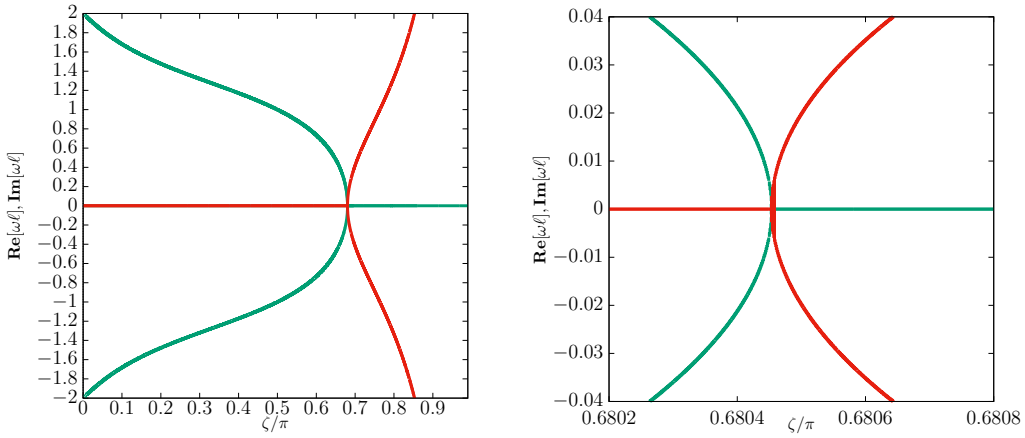

(a) The relation between ζ and ω.

(b) The enlarged figure of Figure 4.1(a).

Figure 4.1: The relation between ζ and ω of QNFs with $d = 2$, $l = 0$, and $\mu^2\ell^2 = -2$. The real and imaginary parts of ω are denoted by green and red lines, respectively.

Now we redefine the parameter of the boundary condition as $\zeta \equiv \mathrm{ArcTan}\,[1/\kappa] \in (0, \pi)$, where ζ is a monotonically decreasing function of $\kappa \in \mathbb{R}$ with $\zeta = 0$ and $\zeta = \pi/2$ corresponding to the Dirichlet and Neumann conditions, respectively. Then the stability criterion $\kappa \geq \kappa_c$ corresponds to $\zeta \leq \zeta_c$ in terms of ζ, where we have defined

$$\zeta_c \equiv \mathrm{ArcTan}\left[-\left|\frac{\Gamma(\nu)}{\Gamma(-\nu)}\right| \frac{\Gamma(\zeta^0_{-\nu,\rho})^2}{\Gamma(\zeta^0_{\nu,\rho})^2}\right]. \tag{4.31}$$

For s-wave ($l = 0$) in the 4-dimensional AdS spacetime, substituting $d = 2$, $\mu^2\ell^2 = -2$, and $l = 0$, we find

$$\zeta_c \simeq 0.68045\pi. \tag{4.32}$$

We numerically solve Eq. (4.30) by the Newton-Raphson method. Figures 4.1(a) and 4.1(b) present the relation between ζ and ω. Here we choose $d = 2,\ l = 0$, and $\mu^2\ell^2 = -2$. The vertical axis denotes $\mathrm{Re}[\omega\ell]$ and $\mathrm{Im}[\omega\ell]$. The horizontal axis denotes the normalised parameter ζ/π. The green and red lines denote $\mathrm{Re}[\omega\ell]$ and $\mathrm{Im}[\omega\ell]$, respectively. Figure 4.1(b) is the enlarged figure of Figure 4.1(a) in the region given by $\mathrm{Re}[\omega\ell], \mathrm{Im}[\omega\ell] \in [-0.04, 0.04]$ and $\zeta/\pi \in [0.6802, 0.6808]$. These figures show that $\mathrm{Re}[\omega\ell]$ decreases as ζ increases for $\zeta \leq \zeta_c \simeq 0.68\pi$ and $\mathrm{Re}[\omega\ell] = 0$ for $\zeta_c < \zeta$. We can also see that $\mathrm{Im}[\omega\ell]$ is zero for $\zeta \leq \zeta_c$, while it takes two values, the one is positive and the other negative with the same absolute value for $\zeta_c < \zeta$. Hence, the operator A of Eq. (4.15) fails to be positive for $\zeta_c < \zeta$ because there is a mode of which the imaginary part of frequency is positive. This means that the mode is unstable for $\zeta_c < \zeta$ or $\kappa < \kappa_c$.

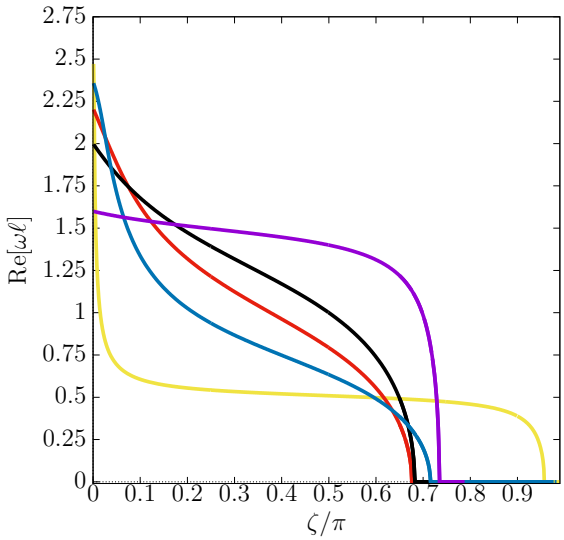

Figure 4.2: The relation between ζ and $\mathrm{Re}[\omega\ell]$ of QNFs with $d = 2,\ l = 0$, and $\mu^2\ell^2 = -1.26, -1.50, -1.75, -2.00$, and -2.24, which are denoted by the yellow, blue, red, black, and purple lines, respectively.

Figure 4.2 gives the relation between ζ and $\mathrm{Re}[\omega\ell]$ with $d = 2$, $l = 0$, and $\mu^2\ell^2 = -1.26, -1.50, -1.75, -2.00, -2.24$, which are denoted by yellow, blue, red, black, and purple lines, respectively. The vertical and horizontal axes denote $\mathrm{Re}[\omega\ell]$ and ζ, respectively. At $\zeta = 0$, $\mathrm{Re}[\omega] = (3 + \sqrt{9 + 4\mu^2\ell^2})/2$ is larger as $\mu^2\ell^2$ is increased. We have checked that for all the mass squared cases, the behavior of ω is the same as that in Figures 4.1(a) and 4.1(b) qualitatively. Namely, as ζ is increased for $0 < \zeta < \zeta_c$, ω is real and is monotonically decreasing, and for $\zeta_c < \zeta$ it vanishes and then ω be-

comes pure imaginary. The critical value ζ_c becomes larger in the order $\mu^2\ell^2 = -2.24, -2.00, -1.75$, while it takes smaller values in the order $\mu^2\ell^2 = -1.75, -1.50, -1.26$. We have also checked that as $\mu^2\ell^2$ is further increased for $-1.26 < \mu^2\ell^2 < -5/4$, ζ_c monotonically increases and approaches π.

4.3 Neutral and charged scalar fields in AdS black holes

4.3.1 Field equations, boundary conditions, and symmetries

Using the Schwarzschild-like coordinates (t, r, θ, ϕ), the line element in the Reissner-Nordström-AdS spacetime in 4 dimensions is written in the form

$$ds^2 = -\frac{\triangle}{r^2}dt^2 + \frac{r^2}{\triangle}dr^2 + r^2\left(d\theta^2 + \sin^2\theta d\phi^2\right) \tag{4.33}$$

with

$$\triangle := r^2 - 2Mr + Q^2 + \frac{r^4}{\ell^2} = (r - r_+)(r - r_-)R(r), \tag{4.34}$$

$$R(r) := 1 + \left(\frac{r}{\ell}\right)^2 + \left(\frac{r_+}{\ell} + \frac{r_-}{\ell}\right)\left(\frac{r}{\ell}\right) + \left(\frac{r_+}{\ell}\right)^2 + \left(\frac{r_-}{\ell}\right)^2 + \left(\frac{r_+}{\ell}\right)\left(\frac{r_-}{\ell}\right), \tag{4.35}$$

where M is the mass and Q is the charge of the black hole. There are two Killing horizons located at $r = r_+$ and $r = r_-$ $(0 < r_- < r_+)$. We call $r = r_+$ and $r = r_-$ outer and inner horizons, respectively. The black hole is the region given by $r < r_+$. Hereafter, we will consider the evolution of the scalar field in the region $r_+ < r$.

The equation of motion for the scalar field is given by Eq. (4.9) with the 1-form of the gauge field given by

$$A_\mu dx^\mu = -\left(\frac{Q}{r} + \phi_0\right)dt, \tag{4.36}$$

where $\phi_0 \in \mathbb{R}$ is an integration constant. Since the spacetime is static and spherically symmetric, we can expand Ψ in terms of spherical harmonics $Y_{lm}(\theta, \phi)$ as

$$\Psi(t, r, \theta, \phi) = \sum_{l,m} \frac{u_{lm}(r)}{r} Y_{lm}(\theta, \phi)\, e^{-i\omega_{lm}t}, \tag{4.37}$$

where $\omega_{lm} \in \mathbb{R}$ is the frequency. Note that the above sign convention is naturally consistent with that for the gauge covariant derivative. Hereafter,

we focus on a single set of (l, m) and just write $u_{lm}(r)$ and ω_{lm} as $u(r)$ and ω, respectively.

Since we discuss the dynamical properties of a scalar field in Eq. (4.33) in terms of quasinormal modes, we now assume $\omega \in \mathbb{C}$. Redefining the radial part by $\psi(r) = u(r)/r$, Eq. (4.9) can be written in the form

$$\left[\frac{d}{dr}\left(\triangle\frac{d}{dr}\right) + \frac{r^4}{\triangle}\left(\tilde{\omega} - \frac{eQ}{r}\right)^2 - l(l+1) - \mu^2 r^2\right]\psi(r) = 0, \tag{4.38}$$

where $\tilde{\omega} := \omega - e\phi_0$.

Introducing the tortoise coordinate x by

$$dx = \frac{r^2}{\triangle}dr, \ x \in (-\infty, +\infty), \tag{4.39}$$

in the limit $x \to -\infty$ or to the outer horizon, Eq. (4.38) becomes

$$\left[\frac{d^2}{dx^2} + \left(\tilde{\omega} - \frac{eQ}{r_+}\right)^2\right]\psi(x) \simeq 0, \tag{4.40}$$

and the general solution of Eq. (4.40) behaves as

$$\psi(x) \sim B_{\rm in}e^{-i\left(\tilde{\omega}-\frac{eQ}{r_+}\right)x} + B_{\rm out}e^{i\left(\tilde{\omega}-\frac{eQ}{r_+}\right)x}, \ B_{\rm in}, B_{\rm out} \in \mathbb{C}. \tag{4.41}$$

Here the subscripts "in" and "out" denote the ingoing and outgoing modes at the outer horizon, respectively. We demand that $B_{\rm out} = 0$ so that the ingoing-wave condition at the outer horizon can be satisfied.

As for the boundary condition at the conformal infinity, we expect that the classification of Theorem 1 does not change even in the presence of a black hole because that classification is based on the asymptotic behavior of the field near the conformal infinity, although the critical values κ_c and $\tilde{\kappa}_c$ could change because the regularity condition at the origin is replaced with the ingoing-wave condition at the black hole horizon. If both the scalar field and the black hole are charged, there can also appear electromagnetic superradiant instability. The electromagnetic superradiance in the asymptotically flat charged black hole will be briefly reviewed in Section 4.6.1. It should also be noted that the equation of motion for the charged scalar field cannot be written in the Schrödinger form as in Eq. (4.12). Hence, Theorem 1 does not apply for the charged scalar field.

We simultaneously demand the ingoing-wave condition $B_{\rm out} = 0$ at the horizon and the Robin boundary condition (4.26) with the asymptotic form (4.25) at the conformal infinity. In general, this can be met only a discrete

set of complex frequencies. These are called QNFs. Here it is useful to see what symmetry this system has. Eq. (4.38) trivially admits symmetry $(\omega, eQ, \psi) \to (-\omega, -eQ, \psi)$, while we can find other symmetries $(\omega, eQ, \psi) \to (\omega^*, eQ, \psi^*)$ and $(\omega, eQ, \psi) \to (-\omega^*, -eQ, \psi^*)$. Since $\kappa \in \mathbb{R}$ and the asymptotic form (4.25) does not depend on $\tilde{\omega}$, if the Robin boundary condition is satisfied by ψ, it is also by ψ^*. Therefore, all these three transformations are consistent with the Robin boundary condition at the conformal infinity. However, only the transformation $(\omega, eQ, \psi) \to (-\omega^*, -eQ, \psi^*)$ among the three can satisfy the ingoing-wave condition at the outer horizon. Therefore, only this transformation remains as the symmetry of the system, which necessarily involves charge conjugation. In other words, $\omega \to -\omega^*$ is no longer the symmetry of the system for the charged scalar field if we fix eQ.

4.3.2 Matched asymptotic expansion for small AdS black holes

To treat Eq. (4.38) analytically, we apply the matched asymptotic expansion method. The strategy is as follows. We first assume $-9/4 < \mu^2\ell^2 < -5/4$, for which the Robin boundary condition applies. We also assume that the black hole radius is much smaller than the AdS length scale: $r_+ \ll \ell$. Then, we consider two spatial regions outside the black hole. We call the regions given by $r_+ < r \ll \ell$ and $r_+ \ll r$ near and far regions, respectively. Then, we obtain an approximate analytic solution which satisfies the imposed boundary condition in each region. We will show that the two regions have an overlapping region satisfying $r_+ \ll r \ll \ell$, where the both approximate solutions are valid. Then, we match the two solutions there and the matching condition gives an eigenvalue equation for the frequency. Thus, we obtain QNFs and the approximate analytic solution which satisfies the boundary conditions both at the horizon and at the conformal infinity.

Near region: $r_+ < r \ll \ell$

In the near region, since $\triangle \simeq (r - r_+)(r - r_-)$, the metric is approximated by the Reissner-Nordström metric. Now we introduce a new coordinate,

$$z = \frac{r - r_+}{r - r_-}, \tag{4.42}$$

and a function $f(z)$ such that

$$\psi(z) = z^{i\sigma}(1 - z)^{l+1} f(z), \tag{4.43}$$

where

$$\sigma = \frac{\left(\tilde{\omega} - \frac{eQ}{r_+}\right) {r_+}^2}{r_+ - r_-}. \tag{4.44}$$

Then Eq. (4.38) is reduced to

$$z(1-z)\frac{d^2}{dz^2}f(z) + \{c - (a+b+1)z\}\frac{d}{dz}f(z) - (ab + \mathcal{E}_1(r))\, f(z) = 0 \tag{4.45}$$

with

$$a = 2i\sigma + l + 1, b = l + 1, c = 2i\sigma + 1, \tag{4.46}$$

and

$$\mathcal{E}_1(r) := \mu^2 r^2 \left(\frac{r - r_-}{r_+ - r_-}\right) + \frac{1}{(r_+ - r_-)(r - r_+)} \left\{ {r_+}^4 \left(\tilde{\omega} - \frac{eQ}{r_+}\right)^2 - r^4 \left(\tilde{\omega} - \frac{eQ}{r}\right)^2 \right\}. \tag{4.47}$$

In Appendix B.2, it is shown that $\mathcal{E}_1(r) \ll 1$ in the near region.

The two independent solutions of Eq. (4.45) in the region $1 < x \leq x_0$ can be written in terms of the Gaussian hypergeometric functions $F(\ ,\ ;\ ;z)$ as

$$f(z) = F(a, b; c; z)\ ,\ z^{1-c}F(1 - c + a, 1 - c + b; 2 - c; z). \tag{4.48}$$

We thus obtain the general solution of Eq. (4.38) in the region $x \leq x_0$,

$$\psi(z) = Az^{i\sigma}(1-z)^{l+1}F(a, b; c; z) + Bz^{-i\sigma}(1-z)^{l+1}F(1 - c + a, 1 - c + b; 2 - c; z), \tag{4.49}$$

where A and B are arbitrary constants. The first and second terms on the right-hand side are the outgoing and ingoing modes, respectively. Now we impose the ingoing-wave condition on Eq. (4.49), so that the first term should vanish. Thus, we obtain the following approximate analytic solution in the region $x \leq x_0$:

$$\psi(z) = Bz^{-i\sigma}(1-z)^{l+1}F(1 - c + a, 1 - c + b; 2 - c; z). \tag{4.50}$$

Far region: $r_+ \ll r$

In the far region, since $\triangle \simeq r^2\,(1 + r^2/\ell^2)$, the metric is approximated by the AdS metric. Using a new variable

$$y = 1 + \frac{r^2}{\ell^2}, \tag{4.51}$$

which is equivalent to Eq. (4.19), and Eq. (4.20) with the replacement of ω with $\tilde{\omega}$, Eq. (4.38) is reduced to the equation for $g(y)$ given by

$$y(1-y)\frac{d^2}{dy^2}g(y)+\{\gamma-(\alpha+\beta+1)y\}\frac{d}{dy}g(y)-(\alpha\beta+\mathcal{E}_2(r))\,g(y)=0, \quad (4.52)$$

where α, β, and γ are defined by Eq. (4.22) with the replacement of ω with $\tilde{\omega}$ and

$$\mathcal{E}_2(r) := \frac{1}{4}(eQ)\left(\frac{r}{\ell}\right)^{-1}\left(1+\frac{r^2}{\ell^2}\right)^{-1}\left\{2(\tilde{\omega}\ell)-(eQ)\left(\frac{r}{\ell}\right)^{-1}\right\}. \quad (4.53)$$

In Appendix B.2, it is shown that $|\mathcal{E}_2(r)| \ll 1$ in the far region.

Near the conformal infinity, the scalar field behaves as

$$\psi(r) \sim C\left(\frac{r}{\ell}\right)^{-\frac{3}{2}-\frac{1}{2}\sqrt{9+4\mu^2\ell^2}} + D\left(\frac{r}{\ell}\right)^{-\frac{3}{2}+\frac{1}{2}\sqrt{9+4\mu^2\ell^2}}, \quad (4.54)$$

where C and D are arbitrary constants. Since we have assumed $-9/4 < \mu^2\ell^2 < -5/4$, we impose the Robin boundary condition Eq. (4.26). Thus, we find Eq. (4.27) with the replacement of ω by $\tilde{\omega}$ as an approximate solution in the far region.

Matching in the overlapping region

Next we match the near-region and far-region approximate solutions, given by Eqs. (4.50) and (4.27), respectively, in the overlapping region. In Appendix B.2, we show that there really exists an overlapping region, where both the near-region and far-region approximate solutions are valid, if $\tilde{\omega}\ell = O(1)$ and $eQ = o(\epsilon^{1/3+\delta})$ with $\epsilon = r_+/\ell$ and $0 < \delta < 2/3$. We consider the asymptotic behavior of them there. First, we see the asymptotic behavior of the near-region solution (4.50) at $z \sim 1$. As shown in Appendix B.3, in the limit of $z \to 1$, Eq. (4.50) behaves as

$$\psi(z) \sim B\Gamma(1-2i\sigma)\left[B_1(\tilde{\omega},\sigma)r^{-l-1}+B_2(\tilde{\omega},\sigma)r^l\right], \quad (4.55)$$

where

$$B_1(\tilde{\omega},\sigma) = \frac{\Gamma(-2l-1)(r_+-r_-)^{l+1}}{\Gamma(-2i\sigma-l)\Gamma(-l)}\ ,\ B_2(\tilde{\omega},\sigma) = \frac{\Gamma(2l+1)(r_+-r_-)^{-l}}{\Gamma(-2i\sigma+l+1)\Gamma(l+1)}. \quad (4.56)$$

Note that the functions $B_1(\tilde{\omega},\sigma)$ and $B_2(\tilde{\omega},\sigma)$ satisfy the relation $B_1(\tilde{\omega},\sigma) = B_1^*(-\tilde{\omega}^*,-\sigma^*)$ and $B_2(\tilde{\omega},\sigma) = B_2^*(-\tilde{\omega}^*,-\sigma^*)$, respectively.

Next, as derived in Appendix B.3, in the limit of $y \to 1$, the asymptotic form of the far-region solution (4.27) is given by Eq. (4.28). Using $r = 1/\tan\chi$, we find that Eq. (4.28) has the same form as Eq. (4.55).

Since both $y \sim 1$ and $z \sim 1$ are satisfied for $x_1 < x < x_0$, we can match Eq. (4.55) and Eq. (4.28) and obtain

$$\frac{B_1(\tilde{\omega},\sigma)}{B_2(\tilde{\omega},\sigma)} = \ell^{2l+1}\frac{D_1(\tilde{\omega},\kappa)}{D_2(\tilde{\omega},\kappa)}, \tag{4.57}$$

where $D_1(\tilde{\omega},\kappa)$ and $D_2(\tilde{\omega},\kappa)$ are defined by Eq. (4.29). The above gives the relation between κ and $\tilde{\omega}$. It is shown in Appendix B.4 that the above equation is consistent with the symmetry $(\omega, eQ) \to (-\omega^*, -eQ)$.

4.4 Analytic results

We analytically solve the matching condition (4.57) under assumption $|\mathrm{Im}[\tilde{\omega}\ell]| \ll 1$ and discuss stability in terms of the obtained QNFs. We explain here our results without explicit calculations, and complement them in Appendix B.5.

4.4.1 Approximate forms of the matching condition under $|\mathrm{Im}[\tilde{\omega}\ell]| \ll 1$

We shall derive approximate forms of the matching condition (4.57) under the assumption $|\mathrm{Im}[\tilde{\omega}\ell]| \ll 1$. The real and imaginary parts of Eq. (4.57) are

$$\mathrm{Re}\,[D_1]\,\mathrm{Re}\,[D_2] + \mathrm{Im}\,[D_1]\,\mathrm{Im}\,[D_2] = \left(\mathrm{Re}\,[D_2]^2 + \mathrm{Im}\,[D_2]^2\right)\mathrm{Re}\left[\frac{B_1}{B_2}\right], \tag{4.58}$$

and

$$\mathrm{Im}\,[D_1]\,\mathrm{Re}\,[D_2] - \mathrm{Re}\,[D_1]\,\mathrm{Im}\,[D_2] = \left(\mathrm{Re}\,[D_2]^2 + \mathrm{Im}\,[D_2]^2\right)\mathrm{Im}\left[\frac{B_1}{B_2}\right], \tag{4.59}$$

respectively. By solving these for $\mathrm{Re}[D_1]$ and $\mathrm{Im}[D_1]$ simultaneously, we obtain

$$\mathrm{Re}\,[D_1] = \mathrm{Re}\,[D_2]\,\mathrm{Re}\left[\frac{B_1}{B_2}\right] - \mathrm{Im}\,[D_2]\,\mathrm{Im}\left[\frac{B_1}{B_2}\right], \tag{4.60}$$

and

$$\mathrm{Im}\,[D_1] = \mathrm{Im}\,[D_2]\,\mathrm{Re}\left[\frac{B_1}{B_2}\right] + \mathrm{Re}\,[D_2]\,\mathrm{Im}\left[\frac{B_1}{B_2}\right]. \tag{4.61}$$

As will be shown later, under $|\mathrm{Im}[\tilde{\omega}\ell]| \ll 1$, $D_1(\tilde{\omega},\kappa)$ and $D_2(\tilde{\omega},\kappa)$ are written in the form

$$D_1\left(\tilde{\omega},\kappa\right) = \Sigma_{1,R} - i\frac{\Sigma_{1,I}}{2}\mathrm{Im}\left[\tilde{\omega}\ell\right] + \mathcal{O}\left(\left(\mathrm{Im}\left[\tilde{\omega}\ell\right]\right)^2\right), \tag{4.62}$$

and

$$D_2\left(\tilde{\omega},\kappa\right) = \frac{2^{2l+1}\left(-1\right)^{l+1}}{(2l+1)!!\,(2l-1)!!}\left[\Sigma_{2,R} - i\frac{\Sigma_{2,I}}{2}\mathrm{Im}\left[\tilde{\omega}\ell\right]\right] + \mathcal{O}\left(\left(\mathrm{Im}\left[\tilde{\omega}\ell\right]\right)^2\right), \tag{4.63}$$

where $\Sigma_{1,R}$, $\Sigma_{1,I}$, $\Sigma_{2,R}$, and $\Sigma_{2,I}$ are real functions, and depend on $l, \mu^2\ell^2$, and $\mathrm{Re}[\tilde{\omega}\ell]$ but not r_+, r_-, eQ, and $\mathrm{Im}[\tilde{\omega}\ell]$. The explicit forms of them are given in Eqs. (B.20), (B.21), (B.26), and (B.27), respectively. Using Eqs. (4.62) and (4.63), Eqs. (4.60) and (4.61) are rewritten as

$$\begin{aligned}\Sigma_{1,R} =& \frac{2^{2l+1}\left(-1\right)^{l+1}}{(2l+1)!!(2l-1)!!}\left(\Sigma_{2,R}\mathrm{Re}\left[\frac{B_1}{B_2}\right] + \frac{\mathrm{Im}\left[\tilde{\omega}\ell\right]}{2}\Sigma_{2,I}\mathrm{Im}\left[\frac{B_1}{B_2}\right]\right)\ell^{-2l-1} \\ &+ \mathcal{O}\left(\left(\mathrm{Im}\left[\tilde{\omega}\ell\right]\right)^2\right),\end{aligned} \tag{4.64}$$

and

$$\begin{aligned}-\frac{\mathrm{Im}\left[\tilde{\omega}\ell\right]}{2}\Sigma_{1,I} =& \frac{2^{2l+1}\left(-1\right)^{l+1}}{(2l+1)!!(2l-1)!!}\left(\Sigma_{2,R}\mathrm{Im}\left[\frac{B_1}{B_2}\right] - \frac{\mathrm{Im}\left[\tilde{\omega}\ell\right]}{2}\Sigma_{2,I}\mathrm{Re}\left[\frac{B_1}{B_2}\right]\right)\ell^{-2l-1} \\ &+ \mathcal{O}\left(\left(\mathrm{Im}\left[\tilde{\omega}\ell\right]\right)^2\right).\end{aligned} \tag{4.65}$$

We note here that $\mathrm{Re}[B_1/B_2] = \mathcal{O}(\mathrm{Im}[\tilde{\omega}\ell])$ and $\mathrm{Im}[B_1/B_2] = \mathcal{O}((\mathrm{Im}[\tilde{\omega}\ell])^0)$ as seen in Eqs. (B.33) and (B.34). Hence, the second term in the bracket of the right-hand side in Eq. (4.65) is $\mathcal{O}((\mathrm{Im}[\tilde{\omega}\ell])^2)$. Thus, Eq. (4.65) is

$$-\frac{\mathrm{Im}\left[\tilde{\omega}\ell\right]}{2}\Sigma_{1,I} = \frac{2^{2l+1}\left(-1\right)^{l+1}}{(2l+1)!!(2l-1)!!}\Sigma_{2,R}\mathrm{Im}\left[\frac{B_1}{B_2}\right]\ell^{-2l-1} + \mathcal{O}\left(\left(\mathrm{Im}\left[\tilde{\omega}\ell\right]\right)^2\right). \tag{4.66}$$

We thus obtain the approximate forms of the matching condition (4.57) for $|\mathrm{Im}[\tilde{\omega}\ell]| \ll 1$, i.e., Eqs. (4.64) and (4.66).

4.4.2 Real part of QNFs

We first discuss $\mathrm{Re}[\tilde{\omega}\ell]$. We note that $\mathrm{Re}[B_1/B_2]\ell^{-2l-1} = \mathcal{O}((r_+/\ell)^{2(l+1)})$ and $\mathrm{Im}[B_1/B_2]\ell^{-2l-1} = \mathcal{O}((r_+/\ell)^{2(l+1)})$ as seen in Eqs. (B.33) and (B.34). Then,

it can be seen from Eqs. (4.64) and (4.66) that

$$\Sigma_{1,R} = \mathcal{O}\left(\left(\frac{r_+}{\ell}\right)^{2(l+1)}\right), \tag{4.67}$$

and

$$\Sigma_{1,I} = \mathcal{O}\left(\left(\frac{r_+}{\ell}\right)^{2(l+1)}\right), \tag{4.68}$$

because $\Sigma_{2,R}$ and $\Sigma_{2,I}$ are independent of r_+. In the limit of $r_+ \to 0$, these equations are reduced to the equation determining the QNF of the mode, which satisfies the regularity condition at the origin, in the pure AdS spacetime, i.e., Eq. (4.30). Hence, Eqs. (4.67) and (4.68) imply

$$\mathrm{Re}\left[\tilde{\omega}\right] = \mathrm{Re}\left[\omega_{\mathrm{AdS}}\right] + \mathcal{O}\left(\left(\frac{r_+}{\ell}\right)^{2(l+1)}\right), \tag{4.69}$$

where $\mathrm{Re}\left[\omega_{\mathrm{AdS}}\right]$ is the real part of the QNF in the AdS spacetime. The relation between the QNFs in the AdS spacetime and the boundary condition parameter $\zeta = \mathrm{ArcTan}[1/\kappa]$ is given in Figures 4.1(a) and 4.1(b). Thus, the real part of the QNFs in the present spacetime coincides with that in the pure AdS spacetime within $\mathcal{O}((r_+/\ell)^{2(l+1)})$.

4.4.3 Imaginary part of QNFs

We next discuss $\mathrm{Im}[\tilde{\omega}\ell]$. Using the explicit form of $\mathrm{Im}[B_1/B_2]$, which is given by Eq. (B.34), Eq. (4.66) is

$$\mathrm{Im}\left[\tilde{\omega}\right] = -\frac{\mathcal{A}\left(\mathrm{Re}\left[\omega_{\mathrm{AdS}}\right] - \frac{eQ}{r_+}\right)}{\mathrm{Re}\left[\omega_{\mathrm{AdS}}\ell\right]} h_{\mu^2\ell^2,l} + \mathcal{O}\left(\left(\mathrm{Im}\left[\tilde{\omega}\ell\right]\right)^2\right), \tag{4.70}$$

and

$$\mathcal{A} = 2^{2l+3}\left(\frac{r_+}{\ell}\right)^2\left(\frac{r_+}{\ell} - \frac{r_-}{\ell}\right)^{2l} \frac{(l!)^2}{(2l)!\,(2l+1)!(2l+1)!!(2l-1)!!} \prod_{k=1}^{l}\left(k^2 + 4\sigma^2\right), \tag{4.71}$$

and

$$h_{\mu^2\ell^2,l} = (-1)^{l+1}\,\mathrm{Re}\left[\tilde{\omega}\ell\right]\frac{\Sigma_{2,R}}{\Sigma_{1,I}}. \tag{4.72}$$

It follows from Eq. (4.70) that $\mathrm{Im}[\tilde{\omega}\ell]$ vanishes if $\mathrm{Re}[\tilde{\omega}] = eQ/r_+$. Hence, there exists a purely oscillating mode if $\mathrm{Re}[\tilde{\omega}] = eQ/r_+$ for the charged

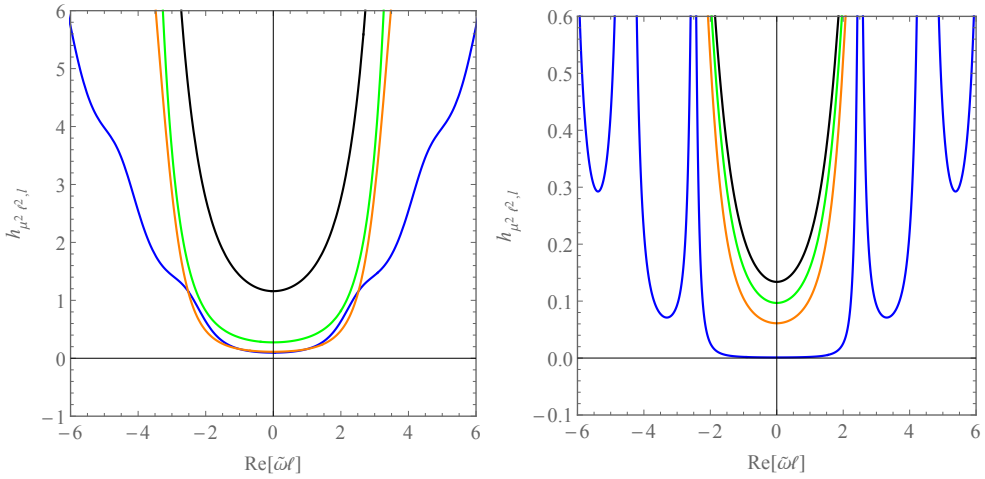

(a) $\mu^2\ell^2 = -2$ (b) $l = 0$

Figure 4.3: Left panel: the relation between $\mathrm{Re}[\tilde{\omega}\ell]$ and $h_{\mu^2\ell^2,l}$ for $\mu^2\ell^2 = -2$ and $l = 0, 1, 2, 3$, which are denoted by the blue, orange, green, and black lines, respectively. Right panel: the relation between $\mathrm{Re}[\tilde{\omega}\ell]$ and $h_{\mu^2\ell^2,l}$ for $l = 0$ and $\mu^2\ell^2 = -1.26, -1.75, -2.00, -2.24$, which are denoted by the blue, orange, green, and red lines, respectively. Note that although the curves get out of the plotted region for some range of $\mathrm{Re}[\tilde{\omega}\ell]$, we confirm that the values of $h_{\mu^2\ell^2,l}$ are positive and finite.

scalar field. For the neutral field, $\mathrm{Re}[\omega] = 0$ does not necessarily imply the existence of a static mode because $h_{\mu^2\ell^2,l}$ in Eq. (4.72) is a finite positive value at $\mathrm{Re}[\omega] = 0$ as will be seen in Figures 4.3(a) and 4.3(b).

In order to determine the sign of $\mathrm{Im}[\tilde{\omega}\ell]$ in Eq. (4.70), we have to discuss that of $h_{\mu^2\ell^2,l}$ in Eq. (4.72). With Eq. (4.67), the boundary condition parameter κ is written in the form of a function of $\mathrm{Re}[\tilde{\omega}\ell]$, $\mu^2\ell^2$, and l. Using that, the leading term of $h_{\mu^2\ell^2,l}$ are expressed by $\mathrm{Re}[\tilde{\omega}\ell]$, $\mu^2\ell^2$, and l. In Figures 4.3(a) and 4.3(b), we numerically show that $h_{\mu^2\ell^2,l}$ is positive. The vertical and horizontal axes denote the value of $h_{\mu^2\ell^2,l}$, respectively. In Figure 4.3(a), we fix $\mu^2\ell^2 = -2$ but $l = 0, 1, 2, 3$ which are denoted by the blue, orange, green, and black lines, respectively, while in Figure 4.3(b), we fix $l = 0$ but $\mu^2\ell^2 = -1.26, -1.75, -2.00, -2.24$ which are denoted by the blue, orange, green, and black lines, respectively. We note that the blue line in Figure 4.3(b) is in $h_{\mu^2\ell^2,l} > 0$. Outside the plotted region as well, the qualitative properties do not change, i.e., $h_{\mu^2\ell^2,l}$ increases with oscillation as $|\mathrm{Re}[\tilde{\omega}\ell]|$ is increased. We can also see $(-1)^{l+1}\,\Sigma_{2,R}/\Sigma_{1,I} \to -\,(-1)^{l+1}\,\Sigma_{2,R}/\Sigma_{1,I}$ under $\mathrm{Re}[\tilde{\omega}] \to -\mathrm{Re}[\tilde{\omega}]$. We will explicitly show it in Appendix B.5.

Thus, Eq. (4.70) shows that for the charged scalar field, the growing modes appear if for $eQ > 0$,

$$0 < \mathrm{Re}[\tilde{\omega}] < \frac{eQ}{r_+}, \tag{4.73}$$

or for $eQ < 0$,

$$\frac{eQ}{r_+} < \mathrm{Re}[\tilde{\omega}] < 0, \tag{4.74}$$

are satisfied, while other modes are stable. These are conditions for electromagnetic supperadiace to occur. Hence, we interpret that this is superradiant instability in the present system. We will straightforwardly derive Eqs. (4.73) and (4.74) from Eq. (4.38) and discuss the physical interpretation in Section 4.6. As for the neutral field, all of the modes decay. We further can see the symmetry $(\tilde{\omega}, eQ) \to (-\tilde{\omega}^*, -eQ)$ in Eq. (4.70).

4.5 Numerical results

We numerically solve Eq. (4.57) by the Newton-Raphson method. We present the result in this section. Hereafter, we fix the mass parameter $\mu^2\ell^2 = -2$ except for subsection 4.5.3 and focus the s-wave, i.e., $l = 0$. Our numerical results are consistent with the analytic results in the previous section.

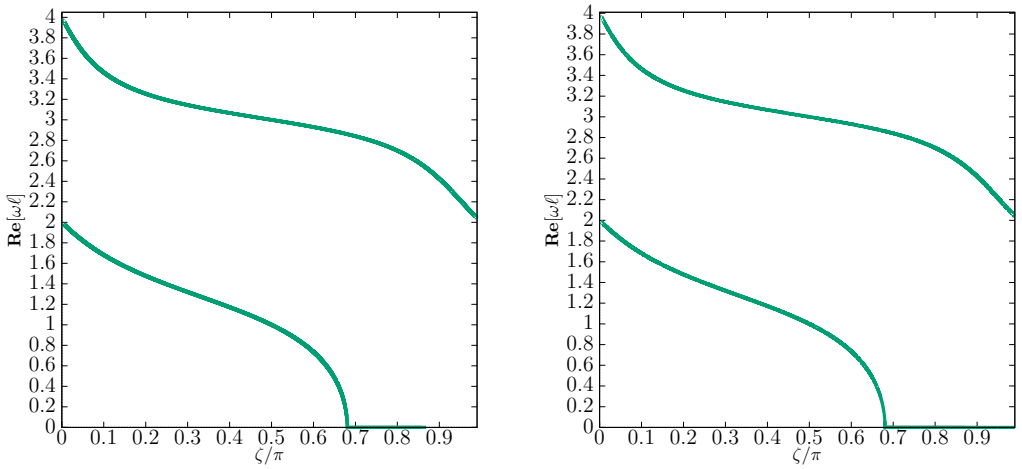

(a) AdS black hole (b) AdS spacetime

Figure 4.4: The relation between ζ and $\mathrm{Re}[\omega\ell] \geq 0$ for the neutral field in the AdS black hole with $(r_+, r_-) = (0.01\ell, 0.001\ell)$ and the AdS spacetime.

4.5.1 Real part of QNFs

Figures 4.4(a) and 4.4(b) give the relation between ζ and $\mathrm{Re}[\omega] \geq 0$ for the neutral field in the AdS black hole with $(r_+, r_-) = (0.01\ell, 0.001\ell)$ and the AdS spacetime, respectively. The vertical and horizontal axes denote $\mathrm{Re}[\omega\ell]$ and the normalized parameter ζ/π, respectively. The symmetry $\omega \to -\omega$ implies that the whole graph has reflectional symmetry with respect to the line $\mathrm{Re}[\omega\ell] = 0$.

We note that only the result for the neutral field is plotted since the results for the neutral and charged fields are indistinguishable in this plot with this parameter set. We call the modes with the smallest and second smallest real parts of frequency first and second fundamental modes, respectively. On the first fundamental mode of the AdS black hole, we stop the numerical calculation at $\zeta = 0.88\pi$, above which the numerical error becomes large. The results for the second fundamental mode are plotted in the whole region $0 \leq \zeta \leq \pi$ for both cases. Figures 4.4(a) and 4.4(b) show that the real part of the QNF of the neutral field in the AdS black hole has the same behavior as in the AdS spacetime qualitatively. Namely, $|\mathrm{Re}[\omega]|$ of the second fundamental mode decreases as ζ increases, and moreover $|\mathrm{Re}[\omega]|$ of the first fundamental mode decreases as ζ increases for $\zeta \leq \zeta_0 \simeq 0.68\pi$ but becomes zero for $\zeta_c \leq \zeta$. The detailed result of the first fundamental mode near $\zeta = 0.68\pi$ is shown in Figures 4.5(a) and 4.5(b). Hereafter we focus on the first fundamental mode because it is most relevant to the stability of the

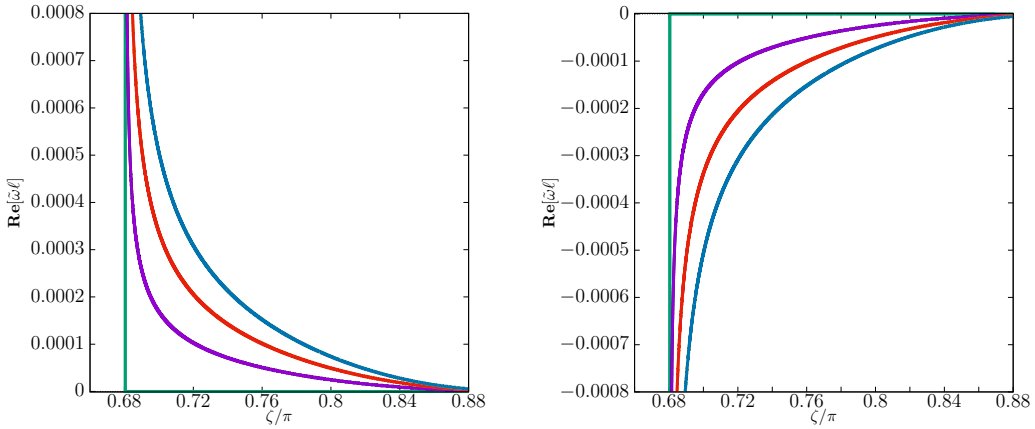

(a) $\mathrm{Re}(\omega) \geq 0$ (b) $\mathrm{Re}(\omega) \leq 0$

Figure 4.5: Same as Figure 4.4(a) but magnified near $\zeta = 0.68\pi$ for the neutral and charged fields in the AdS black hole with $(r_+, r_-) = (0.01\ell, 0.001\ell)$. The green, purple, red, and blue lines correspond to the result with $eQ = 0, 0.01, 0.02$, and 0.03 , respectively.

system. Figures 4.5(a) and 4.5(b) show the relation between ζ and $\mathrm{Re}[\tilde{\omega}\ell]$ for the charged fields in the AdS black hole with $(r_+, r_-) = (0.01\ell, 0.001\ell)$. The green, purple, red, and blue lines denote the result with $eQ = 0, 0.01, 0.02$, and 0.03, respectively. We stress that they are not the reflection of each other with respect to the line $\mathrm{Re}[\omega] = 0$ because the symmetry of the system is deformed to $(\tilde{\omega}, eQ) \to (-\tilde{\omega}^*, -eQ)$ as stated in Section 4.3.1. However, since the result for the negative eQ is not distinguishable from that for the positive eQ of the same absolute value in this plot, we plot the result only for the positive eQ. As we will see later, they can be distinguishable for a larger black hole. We can also see that the neutral field has a critical value $\zeta_0 \simeq 0.68\pi$ at which $\mathrm{Re}[\omega]$ becomes zero within the numerical error, while the charged field does not. For this reason, we define the critical value ζ_0 only for the neutral field, while the charged field does not have such a critical value.

4.5.2 Stability of the scalar field

We judge stability of the scalar field by the sign of the imaginary part of the QNF. If the imaginary part is positive, the mode is unstable.

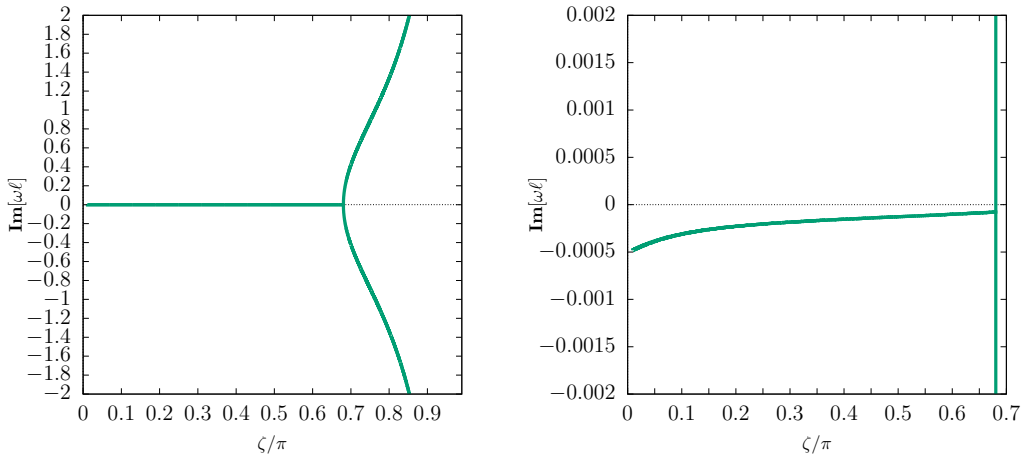

(a) The relation between ζ and $\mathrm{Im}(\omega\ell)$.

(b) The enlarged figure of Figure 4.6(a).

Figure 4.6: The relation between ζ and $\mathrm{Im}[\omega\ell]$ for the neutral field in the AdS black hole with $(r_+, r_-) = (0.01\ell, 0.001\ell)$.

Neutral field

Figures 4.6(a) and 4.6(b) give the relation between ζ and $\mathrm{Im}[\omega]$ for the neutral field in the AdS black hole with $(r_+, r_-) = (0.01\ell, 0.001\ell)$. The imaginary parts of the both modes with positive and negative real parts give the same value because of the symmetry $\omega \to -\omega^*$ as stated in Section 4.3.1. Figure 4.6(a) shows that the positive $\mathrm{Im}[\omega]$ appears for $\zeta_c < \zeta$, where ζ_c is defined as the critical value at which there appears a mode with $\mathrm{Im}[\omega] > 0$. It can be seen that $\mathrm{Im}[\omega] < 0$ of the mode for $\zeta < \zeta_c$ and $\mathrm{Im}[\omega] > 0$ for $\zeta > \zeta_c$. Furthermore, as we will see that $\zeta_0 < \zeta_c$ is satisfied. Figure 4.6(a) demonstrates that $\mathrm{Im}[\omega]$ of the unstable mode increases as ζ increases. This instability is not due to superradiance but purely of boundary origin. Figure 4.6(b) is the enlarged figure of 4.6(a) in the range of $\zeta/\pi \in [0, 0.7]$, and $\mathrm{Im}[\omega\ell] \in [-0.002, 0.002]$. This figure shows that the mode splits into two at $\zeta \simeq \zeta_0$. We have checked that this numerical result for $\zeta \lesssim \zeta_0$ is in good agreement with the analytic result in Eq. (4.70).

Charged field

Figures 4.7(a) and 4.7(b) give the relation between ζ and $\mathrm{Im}[\tilde{\omega}]$ for the mode with $\mathrm{Re}[\tilde{\omega}] > 0$ for the charged field in the AdS black hole with $(r_+, r_-) = (0.01\ell, 0.001\ell)$. The yellow and blue lines denote the results with $eQ = 0.01$ and -0.01, respectively. If we also plot curves for other positive values of eQ, they cannot be distinguished from that for $eQ = 0.01$ in this scale, and

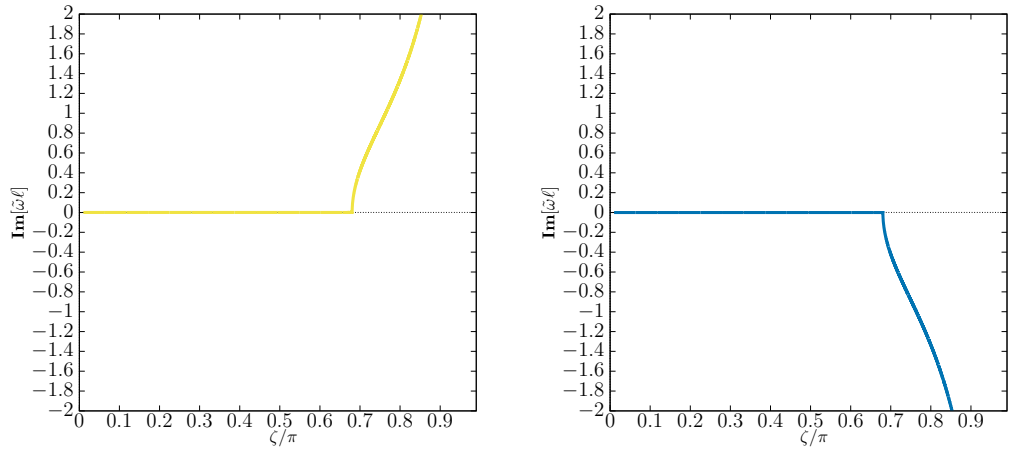

(a) $eQ = 0.01$ (b) $eQ = -0.01$

Figure 4.7: Same as Figure 4.6(a) for the mode with $\mathrm{Re}[\tilde{\omega}] > 0$ for the charged field in the AdS black hole with $(r_+, r_-) = (0.01\ell, 0.001\ell)$. The yellow and blue lines denote $eQ = 0.01$ and -0.01, respectively.

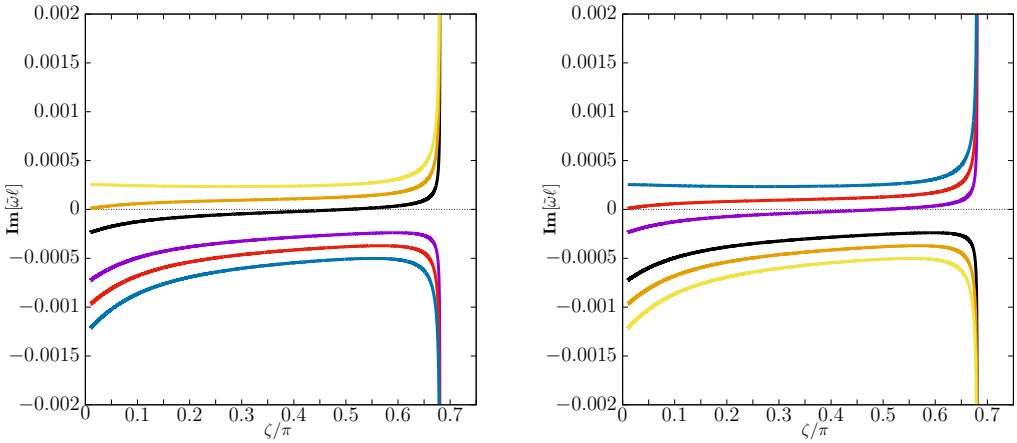

(a) $\mathrm{Re}(\tilde{\omega}) > 0$ (b) $\mathrm{Re}(\tilde{\omega}) < 0$

Figure 4.8: Same as Figure 4.6(b) but for the charged field in the AdS black hole with $(r_+, r_-) = (0.01\ell, 0.001\ell)$. The purple, black, red, orange, blue and yellow lines denote $eQ = -0.01, 0.01, -0.02, 0.02, -0.03$, and 0.03, respectively.

this is also the case for the negative values of eQ. Therefore, we plot only for the mode with $eQ = -0.01$ and 0.01. Figures 4.7(a) and 4.7(b) show that if $eQ > 0$, there appears an unstable mode with $\mathrm{Re}[\tilde{\omega}] > 0$ for $\zeta_c < \zeta$, where ζ_c is defined as the onset of instability also for the charged field. On the other hand, if $eQ < 0$, there appears an unstable mode with $\mathrm{Re}[\tilde{\omega}] < 0$ for $\zeta_c < \zeta$. Note that the symmetry of the system is given by $(\tilde{\omega}, eQ) \to (-\tilde{\omega}^*, -eQ)$. We have checked that all of the unstable modes satisfy the superradiance condition Eq. (4.73) or (4.74), while none of the stable modes does. Hence, this instability comes from superradiance.

The detailed feature of the charged field for $\zeta \simeq \zeta_c$ is shown in Figures 4.8(a) and 4.8(b). They present the relation between ζ and $\mathrm{Im}[\tilde{\omega}]$ for the charged field in the AdS black hole with $(r_+, r_-) = (0.01\ell, 0.001\ell)$. The results with $eQ = -0.01, 0.01, -0.02, 0.02, -0.03$, and 0.03 are denoted by the purple, black, red, orange, blue, and yellow lines, respectively. We can see that the mode with $\mathrm{Re}[\tilde{\omega}\ell] > 0$ can be unstable for $eQ > 0$ even for $\zeta \leq \zeta_0$, while the mode with $\mathrm{Re}[\tilde{\omega}\ell] < 0$ can be unstable for $eQ < 0$. As stated above, we have checked for any ζ we investigated that all of the unstable modes satisfy the superradiance condition Eq. (4.73) or (4.74), while none of the stable modes does. For this reason, we interpret that this instability arises from superradiance. Also, since the time scale of the instability for $\zeta_0 < \zeta$ can be much shorter than that for $\zeta \leq \zeta_0$, superradiant instability can be enhanced by the boundary condition. We have checked that this numerical result for $\zeta \lesssim \zeta_0$ is in good agreement with the analytic result in Eq. (4.70).

4.5.3 Other mass squared cases

We investigate QNFs for other mass squared cases in the range of $-9/4 < \mu^2\ell^2 < -5/4$. Figure 4.9(a) gives the relation between ζ and $\mathrm{Re}[\tilde{\omega}\ell]$ with $(r_+, r_-, eQ) = (0.01\ell, 0.001\ell, 0.01)$ and $\mu^2\ell^2 = -1.26, -1.50, -1.75, -2.00, -2.24$, which are denoted by the yellow, blue, red, black, and purple lines, respectively. The vertical and horizontal axes denote $\mathrm{Re}[\tilde{\omega}\ell]$ and ζ, respectively. We note that Figure 4.9(a) is indistinguishable from Figure 4.2 in this parameter set. Namely, $\mathrm{Re}[\tilde{\omega}\ell]$ in the present system coincides with that of the neutral field in the AdS spacetime in the limit of $r_+/\ell \to 0$. At $\zeta = 0$, $\mathrm{Re}[\tilde{\omega}\ell]$ is larger as $\mu^2\ell^2$ is increased. As ζ is increased from 0, $\mathrm{Re}[\tilde{\omega}\ell]$ decreases for all $\mu^2\ell^2$ we have investigated. We have checked that for the neutral field, as in the pure AdS spacetime case, $\mathrm{Re}[\omega\ell]$ becomes zero at a certain value of ζ, which is denoted by ζ_0. In particular, ζ_0 becomes larger in the order $\mu^2\ell^2 = -2.24, -2.00, -1.75$, while it takes smaller values in the order $\mu^2\ell^2 = -1.75, -1.50, -1.26$. We have also checked that as $\mu^2\ell^2$ is further increased for $-1.26 < \mu^2\ell^2 < -5/4$, ζ_0 approaches π. For the charged field,

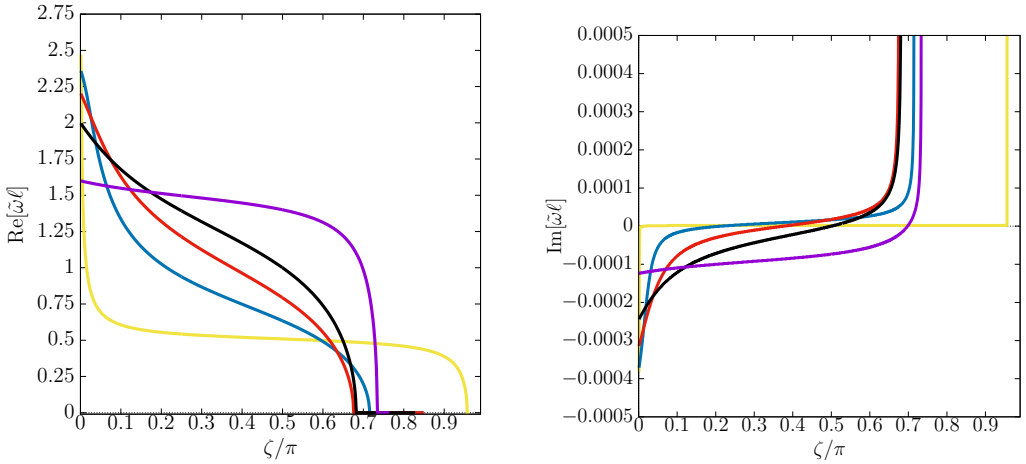

(a) The real part

(b) The imaginary part

Figure 4.9: The relation between ζ and the QNFs with $(r_+, r_-, eQ) = (0.01\ell, 0.001\ell, 0.01)$ and $\mu^2\ell^2 = -1.26, -1.50, -1.75, -2.00, -2.24$, which are denoted by the yellow, blue, red, black, and purple lines, respectively.

on the other hand, Re$[\tilde{\omega}\ell]$ rapidly decreases and approaches zero but does not vanish near $\zeta = \zeta_0$ for the neutral field with the same $\mu^2\ell^2$.

Figure 4.9(b) gives the relation between ζ and Im$[\tilde{\omega}\ell]$ with the same parameters as that in Figure 4.9(a). The vertical and horizontal axes denote Im$[\tilde{\omega}\ell]$ and ζ, respectively. We note that the yellow line is positive in $\zeta/\pi \gtrsim 0.012$. At $\zeta = 0$, Im$[\tilde{\omega}\ell]$ is negative for all $\mu^2\ell^2$ we have investigated and the absolute value is larger as $\mu^2\ell^2$ is increased. For all $\mu^2\ell^2$, as ζ is increased from 0, Im$[\tilde{\omega}\ell]$ increases, vanishes at $\zeta = \zeta_c$, and for $\zeta > \zeta_c$ it becomes a positive value and further increases. The value of ζ_c differs depending on $\mu^2\ell^2$, and in particular, it takes smaller values as $\mu^2\ell^2$ is increased for this parameter set ($eQ\ell/r_+ = 1.00$). However, this will not necessarily also be the case for other eQ, e.g, for $eQ\ell/r_+ = 0.25$, ζ_c is larger in the order $\mu^2\ell^2 = -1.26, -2.24, -1.50, -2.00, -1.75$. This can be understood from the fact that ζ_c is determined by the intersection of each curved line of Re$[\tilde{\omega}\ell](\zeta)$ and the horizontal line Re$[\tilde{\omega}\ell] = eQ\ell/r_+ =$ const. in Figure 4.2. The growing modes satisfy the superradiace conditions (4.73) or (4.74), while the decaying modes do not. Hence, this is superradiant instability in the present system.

4.5.4 Larger black hole

We investigate a black hole larger than the previous one. We fix $\mu^2\ell^2 = -2$. For this purpose, let us consider an AdS black hole with $(r_+, r_-) =$

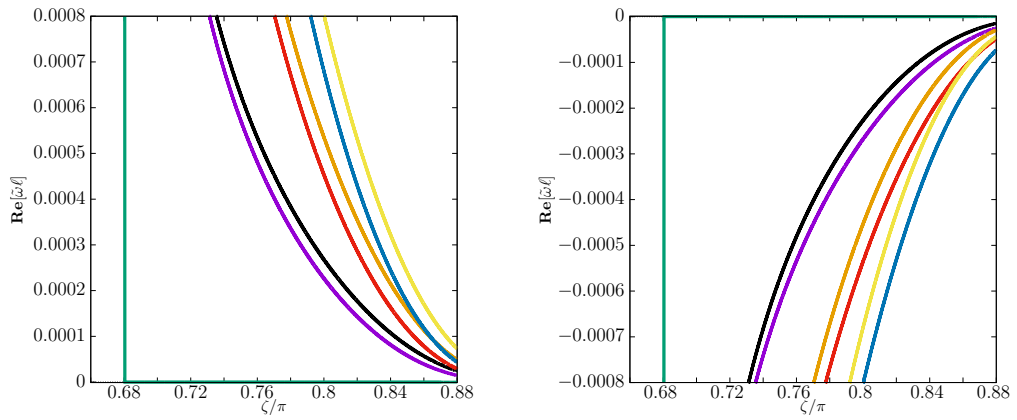

(a) $\mathrm{Re}(\tilde{\omega}) \geq 0$ (b) $\mathrm{Re}(\tilde{\omega}) \leq 0$

Figure 4.10: Same as Figures 4.5(a) and 4.5(b) but in the larger AdS black hole with $(r_+, r_-) = (0.1\ell, 0.001\ell)$. The green, purple, black, red, orange, blue, and yellow lines denote the results with $eQ = 0, -0.01, 0.01, -0.02, 0.02, -0.03$, and 0.03, respectively.

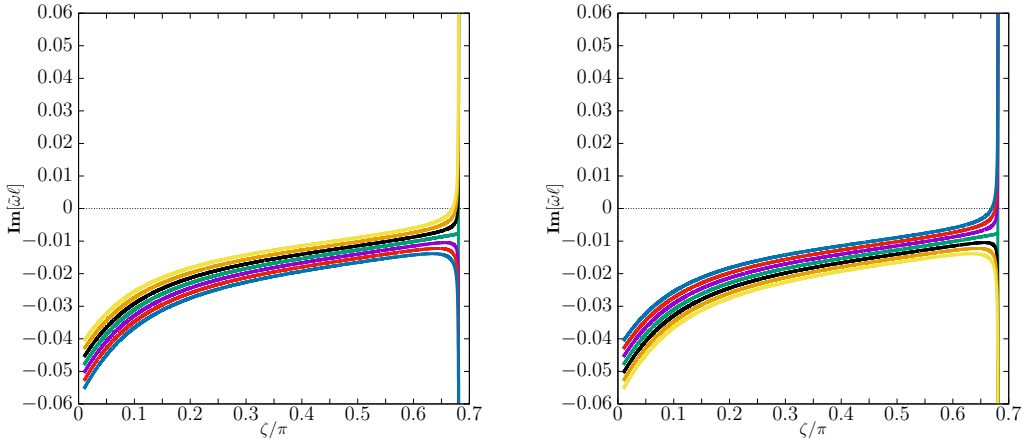

(a) $\mathrm{Re}(\tilde{\omega}) \geq 0$ (b) $\mathrm{Re}(\tilde{\omega}) \leq 0$

Figure 4.11: Same as Figure 4.6(b) but for the charged field in the larger AdS black hole with $(r_+, r_-) = (0.1\ell, 0.001\ell)$. The green, purple, black, red, orange, blue, and yellow lines denote the results with $eQ = 0, -0.01, 0.01, -0.02, 0.02, -0.03$ and 0.03, respectively.

$(0.1\ell, 0.001\ell)$. Although it is not clear how much the condition Eq. (B.5) is met, we would still continue to apply the matched asymptotic expansion method.

The relation between ζ and $\mathrm{Re}[\tilde{\omega}]$ for the neutral and charged fields in the AdS black hole with $(r_+, r_-) = (0.1\ell, 0.001\ell)$ looks similar to Figures 4.5(a) and 4.5(b). However, there is a remarkable difference if it is magnified. Comparing Figures 4.10(a) and 4.10(b) with Figures 4.5(a) and 4.5(b), we can clearly see that the system does not have symmetry $(\omega, eQ) \to (-\omega^*, eQ)$ but $(\omega, eQ) \to (-\omega^*, -eQ)$.

Figures 4.11(a) and 4.11(b) give the relation between ζ and $\mathrm{Im}[\tilde{\omega}]$ for the charged field in the AdS black hole with $(r_+, r_-) = (0.1\ell, 0.001\ell)$. The vertical and horizontal axes denote $\mathrm{Im}[\tilde{\omega}\ell]$ and $\zeta/\pi \in [0, 0.7]$, respectively. Figures 4.11(a) and 4.11(b) show the similar behavior to that seen in the smaller black hole with $(r_+, r_-) = (0.01\ell, 0.001\ell)$. Comparing these figures with Figures 4.6(b), 4.8(a), and 4.8(b), we can see that $|\mathrm{Im}[\tilde{\omega}\ell]|$ of the stable mode for $\zeta \leq \zeta_0$ for the AdS black hole with $(r_+, r_-) = (0.1\ell, 0.001\ell)$ are generally larger than those for the smaller black hole with $(r_+, r_-) = (0.01\ell, 0.001\ell)$ if we fix the values of ζ and eQ.

4.5.5 Fine structure

Neutral field

Here we shall discuss how the results for the neutral field in the AdS black hole are different from that in the AdS spacetime. Figure 4.12(a) gives the relation between ζ and $\omega\ell$ for the neutral field in the AdS black hole with $(r_+, r_-) = (0.1\ell, 0.001\ell)$ as in Figure 4.1(a). Figure 4.12(b) is the enlarged figure of Figure 4.12(a) in the range of $\zeta/\pi \in [0.68042, 0.68048]$ and $\mathrm{Im}[\omega\ell] \in [-0.03, 0.03]$. Comparing these figures with Figures 4.1(a) and 4.1(b), we can see that the symmetries $\omega \to -\omega$ and $\omega \to \omega^*$ for the AdS spacetime are broken for the neutral field in the AdS black hole spacetime. Here we point out that the symmetry for the real part $\omega \to -\omega^*$ remains. Thus, a black hole breaks the symmetry. Physically, the negative imaginary part of the QNF for $\zeta \leq \zeta_c$ comes from the dissipation of the scalar field into the black hole.

Figure 4.12(b) shows that $\zeta_0 < \zeta_c$ is actually satisfied. It is also shown that at $\zeta = \zeta_0$ within the numerical error, the imaginary part splits into two different values. Hence, there are two QNFs which have a vanishing real part but different negative imaginary parts for $\zeta_0 < \zeta < \zeta_c$. Moreover, the two pure imaginary QNFs have one positive and one negative imaginary parts for $\zeta_c < \zeta$. Thus, we can see that there exists a static mode of the neutral

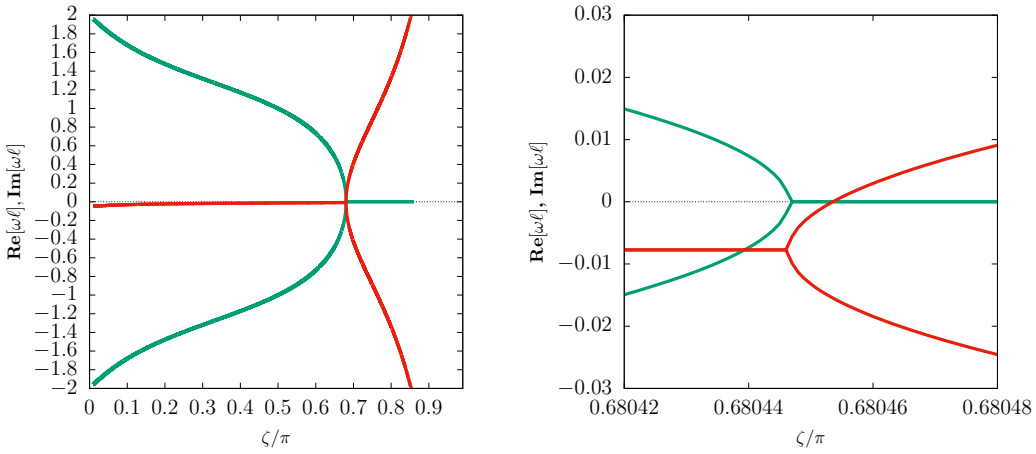

(a) The relation between ζ and ω (b) The enlarged figure of Figure 4.12(a).

Figure 4.12: Same as Figures 4.1(a) and 4.1(b) but for the neutral field in the AdS black hole with $(r_+, r_-) = (0.1\ell, 0.001\ell)$.

field perturbation on the charged AdS black hole for $\zeta = \zeta_c$. This can be most clearly seen in Figure 4.14(a).

Charged field

Figure 4.13(a) gives the relation between ζ and $\tilde{\omega}$ for the charged field with $eQ = 0.01$ in the AdS black hole with $(r_+, r_-) = (0.1\ell, 0.001\ell)$. Figure 4.13(b) is the enlarged figure of Figure 4.13(a) in the range of $\zeta/\pi \in [0.678, 0.682]$ and $\mathrm{Im}[\tilde{\omega}\ell] \in [-0.06, 0.06]$. We note that the result for $eQ = -0.01$ gives the same graph. Figure 4.13(b) shows the existence of the boundary condition at the onset of instability $\zeta = \zeta_c$ such that $\mathrm{Im}[\tilde{\omega}\ell] = 0$ but $\mathrm{Re}[\tilde{\omega}\ell] \neq 0$. This mode is purely oscillative. This suggests a branch to nonlinearly oscillating solutions or charged oscillating black holes dubbed "black resonators" [61, 113] in the AdS spacetime.

Flow of QNFs with respect to ζ

Figures 4.14(a) and 4.14(b) show the flow of the QNFs in the complex plane for the neutral and charged fields, respectively, in the AdS black hole with $(r_+, r_-) = (0.1\ell, 0.001\ell)$. The green, red, and blue lines denote trajectories which the QNFs with $eQ = 0, -0.01, 0.01$ draw when we continuously change ζ. The arrows indicate the direction in which the QNF flows as ζ increases. In Figure 4.14(a), we can see that for the neutral field, the QNF for $\zeta < \zeta_0$ has a non-zero real part and a negative imaginary part. At $\zeta = \zeta_0$, the

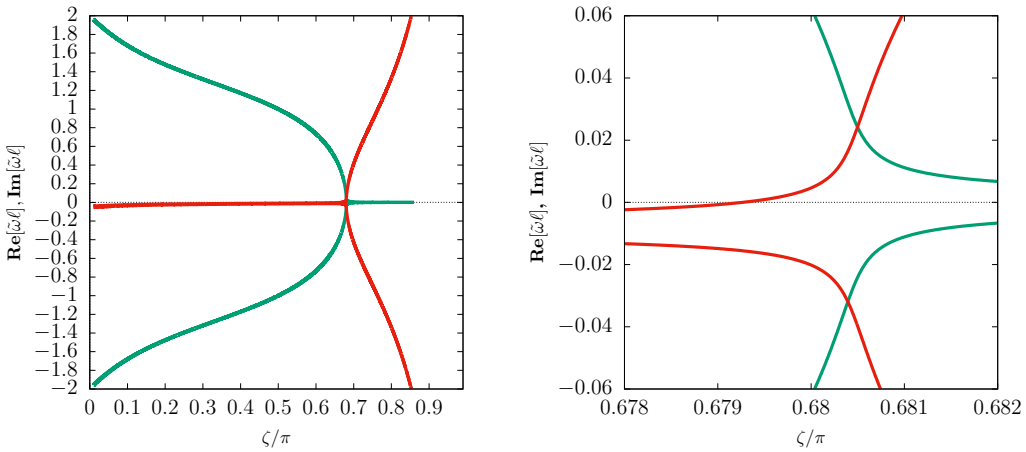

(a) The relation between ζ and $\tilde{\omega}$ (b) The enlarged figure of Figure 4.13(a).

Figure 4.13: Same as Figures 4.1(a) and 4.1(b) but for the charged field with $eQ = 0.01$ in the AdS black hole with $(r_+, r_-) = (0.1\ell, 0.001\ell)$.

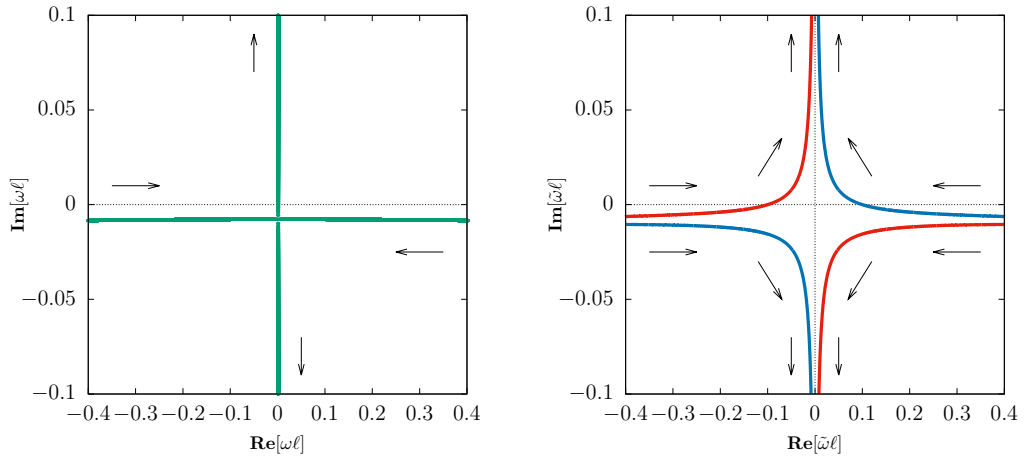

(a) Neutral field (b) Charged field

Figure 4.14: The flow of QNFs in the AdS black hole with $(r_+, r_-) = (0.1\ell, 0.001\ell)$. The $\tilde{\omega}$ moves as ζ is increased continuously. The green, red, and blue lines denote $eQ = 0, -0.01$, and 0.01, respectively.

real part of these QNFs vanishes. Then, the QNFs for $\zeta_0 < \zeta \leq \zeta_c$ are pure imaginary and both move along the arrow on the imaginary axis as ζ increases, the one goes up and the other down in the lower half plane. After that, the imaginary part of the QNF which is going up becomes zero at $\zeta = \zeta_c$, implying the onset of instability. The flow described above is consistent with the symmetry $\omega \to -\omega^*$.

Figure 4.14(b) shows the flow for the charged field. The QNFs approach the imaginary axis as ζ increases. The one mode goes up and the other down along the axis as ζ increases. For $eQ > 0$, the QNF with $\mathrm{Re}[\tilde{\omega}] > 0$ goes up, while that with $\mathrm{Re}[\tilde{\omega}] < 0$ goes down. For $eQ < 0$, the result is opposite. This is a feature quite different from the neutral field. The mode which goes up eventually causes superradiant instability at $\zeta = \zeta_c$. We can see that the flow is consistent with the symmetry $(\tilde{\omega}, eQ) \to (-\tilde{\omega}^*, -eQ)$.

4.6 Physical interpretation

4.6.1 Electromagnetic superradiance

From Eq. (4.9) and Eq. (C.6), we obtain the radial equation,

$$\left[-\frac{d^2}{dx^2} + V(x)\right] u(x) = \left(\tilde{\omega} - \frac{eQ}{r}\right)^2 u(x), \tag{4.75}$$

where

$$V(x) = \frac{\triangle}{r^2}\left[\frac{1}{r}\frac{d}{dr}\left(\frac{\triangle}{r^2}\right) + \frac{1}{r^2}\left\{l(l+1) + \mu^2 r^2\right\}\right]. \tag{4.76}$$

We assume $\omega \in \mathbb{R}$. The effective potential of the charged scalar field in the charged black hole can be negative near the outer horizon depending upon the charge of the field. The region, where the effective potential is negative, is called the generalized ergoregion [87].

Here, we first discuss electromagnetic superradiance for a massless charged scalar field in the charged black hole spacetime with $\mu^2 = \Lambda = 0$, which gives an important background for the physical interpretation of the electromagnetic superradiance in the AdS system. In the limit of $x \to \infty$, Eq. (4.75) is reduced to

$$\left[\frac{d^2}{dx^2} + \tilde{\omega}^2\right] u(x) \simeq 0, \tag{4.77}$$

and we obtain the general solution of Eq. (4.77) as

$$u(x) \sim A_{\mathrm{in}} e^{-i\tilde{\omega}x} + A_{\mathrm{out}} e^{i\tilde{\omega}x},\ A_{\mathrm{in}}, A_{\mathrm{out}} \in \mathbb{C}. \tag{4.78}$$

The subscripts "in" and "out" denote the ingoing and outgoing modes at the conformal infinity, respectively.

Noting the conservation of the number current given by Eq. (4.10), we find

$$\tilde{\omega}(|A_{\rm in}|^2 - |A_{\rm out}|^2) = \left(\tilde{\omega} - \frac{eQ}{r_+}\right)|B_{\rm in}|^2 r_+^2, \tag{4.79}$$

where we have used the asymptotic solutions (4.41) with $B_{\rm out} = 0$ and Eq. (4.78). Thus, we can observe that the amplitude of the reflected wave is larger than that of the incident wave, i.e.

$$|A_{\rm out}|^2 > |A_{\rm in}|^2, \tag{4.80}$$

if the mode with $eQ > 0$ satisfies

$$0 < \tilde{\omega} < \frac{eQ}{r_+}, \tag{4.81}$$

or if the mode with $eQ < 0$ satisfies

$$\frac{eQ}{r_+} < \tilde{\omega} < 0. \tag{4.82}$$

There conditions for $\tilde{\omega}$ are equivalent to Eqs. (4.73) and (4.74), respectively. This amplification of the wave is called electromagnetic superradiance.

Using Eq. (4.78), the conservation of j^a and $j^a_{(e)}$ are integrated to give

$$j^r(t, r, \theta, \phi) = 2\tilde{\omega}(|A_{\rm out}|^2 - |A_{\rm in}|^2)\frac{|Y_{lm}(\theta, \phi)|^2}{r^2}, \tag{4.83}$$

and

$$j^r_{(e)}(t, r, \theta, \phi) = 2e\tilde{\omega}(|A_{\rm out}|^2 - |A_{\rm in}|^2)\frac{|Y_{lm}(\theta, \phi)|^2}{r^2}, \tag{4.84}$$

respectively, for $r_+ \leq r < \infty$. Therefore, there are a net positive (negative) outgoing number current and therefore net positive (negative) outgoing electric current for $\tilde{\omega} > (<)0$. We can conclude that a net positive (negative) particle number and net positive (negative) charge are extracted from the system for $\tilde{\omega} > (< 0)$ and they must be extracted from the black hole. We will see that this is really the case in Section 4.6.2.

Here we see the energetics of the system. The outgoing energy current of the scalar field in the asymptotic region can be calculated to

$$J^r_{(m)} \simeq 2\tilde{\omega}^2(|A_{\rm out}|^2 - |A_{\rm in}|^2)\frac{|Y_{lm}(\theta, \phi)|^2}{r^2} \quad \text{as} \quad r \to \infty, \tag{4.85}$$

while the energy current by the electromagnetic field vanishes there. Therefore, positive energy is extracted from the system in the superradiance. However, it does not necessarily mean that this positive energy must be extracted from the black hole because $J^a_{(m)}$ is not a conserved current as $\nabla_a J^a_{(m)} = -\nabla_a J^a_{(em)}$. In general, since $\nabla^a T_{(em)ab} = j^a_{(e)} F_{ab}$, we obtain $\nabla_a J^a_{(em)} = -j^a_{(e)} \xi^b F_{ab}$. In the present system, this implies

$$\nabla_a J^a_{(em)} = -j^r_{(e)} F_{rt}. \tag{4.86}$$

This shows that the electromagnetic field loses energy due to the work on the electric current exerted by the electric field. On the other hand, this implies

$$\nabla_a J^a_{(m)} = j^r_{(e)} F_{rt} \tag{4.87}$$

Thus, the scalar field receives energy through the work on the electric current exerted by the electric field. We can easily integrate Eq. (4.87) putting Eq. (4.84) in the source term and fix the function of integration using Eq. (4.85). Thus, we obtain

$$J^r_{(m)} = 2\tilde{\omega} \left(\tilde{\omega} - \frac{eQ}{r} \right) (|A_{\rm out}|^2 - |A_{\rm in}|^2) \frac{|Y_{lm}|^2}{r^2} \tag{4.88}$$

for $r_+ \leq r < \infty$. We can see that under the condition for the superradiance, $J^r_{(m)}$ is necessarily negative at $r = r_+$. Therefore, there is a net ingoing energy current at the horizon. $J^r_{(m)}$ changes its sign at $r = r_S = eQ/\tilde{\omega}$. There is a net ingoing energy current for $r_+ \leq r < r_S$, while a net outgoing energy current for $r > r_S$. The radius r_S thus characterizes the energy injection from the electric field into the scalar field. In particle picture, we can interpret it as the pair creation of particles of charge e and antipartcles of charge $-e$ at $r = r_S$. The former runs outwardly away and extracts energy and charge from the system, while the latter runs inwardly into the horizon of the black hole and gives energy to and discharge the horizon.

Now we argue that the superradiance decreases M, the mass of the whole system. Assuming that the superradiance proceeds in a quasi-static manner, Eqs. (4.84) and (4.85) imply that the ratio of δQ and δM, increments of Q and M, is given by

$$\frac{\delta Q}{\delta M} = \frac{e}{\tilde{\omega}} \tag{4.89}$$

From $r_+ = M + \sqrt{M^2 - Q^2}$ and $A = 4\pi r_+^2$, δA, increment of the area of the horizon in a quasistatic process, is calculated to

$$\delta A = 8\pi r_+ \frac{r_+ \delta M - Q \delta Q}{\sqrt{M^2 - Q^2}} \tag{4.90}$$

where κ is the surface gravity given by

$$\kappa = \frac{\sqrt{M^2 - Q^2}}{r_+^2}. \tag{4.91}$$

Using Eq. (4.89), this gives

$$\delta A = \frac{8\pi}{\kappa}\left(1 - \frac{eQ}{\tilde{\omega} r_+}\right)\delta M, \tag{4.92}$$

Noting the superradiance condition, Eq. (4.81) or (4.82), the area law $\delta A > 0$ implies $\delta M < 0$. Thus, the superradiance extracts energy from the whole system. Alternatively, Eq. (4.85) together with Eq. (4.80) directly implies $\delta M < 0$ and thus guarantees the area law through the superradiance condition Eq. (4.81) or (4.82). However, since the energy current for $r < r_S$ falls inwardly, the black hole horizon gains net positive energy. The superradiance extracts energy not from the black hole horizon but from its ambient electric field.

In the AdS charged black hole, we can show that all of $\sqrt{-g}j^r$, $\sqrt{-g}j^r_{(e)}$, and $\sqrt{-g}J^r$ vanish at the conformal infinity by using the asymptotic behavior (4.54) under the Robin boundary condition (4.26). Therefore, the outgoing and ingoing waves must cancel out each other there. This means that the Robin boundary condition makes the conformal boundary perfectly reflective. Since we can regard the overlapping region between the near and far regions as the asymptotically flat region both from the black hole and from the conformal infinity, we can interpret the superradiant instability in the present system as follows. The ingoing wave in the overlapping region is reflected and amplified by electromagnetic superradiance near the black hole. This amplified outgoing wave goes through the overlapping region and perfectly reflected by the AdS boundary under the Robin boundary. This reflected ingoing wave goes through the asymptotic region and becomes the incident wave to the black hole again. A series of these successive processes results in the superradiance instability. The scalar field takes charge from the black hole and energy from its ambient electric field and gives energy to the black hole. The black hole takes energy from and gives charge to the scalar field.

4.6.2 Thermodynamical insight

Here we discuss a thermodynamical argument. We explicitly calculate the energy current and electric current ingoing into the horizon, $J_a n^a|_{\mathcal{H}_+}$ and $j_{(e)a} n^a|_{\mathcal{H}_+}$, respectively, where $n^a = -\xi^a$ at the outer horizon for the static

black hole. To avoid the coordinate singularity at the outer horizon, we use the ingoing Eddington-Finkelstein coordinates

$$ds^2 = -\frac{\triangle}{r^2}dv^2 + 2dvdr + r^2(d\theta^2 + \sin^2\theta d\phi^2), \tag{4.93}$$

where $v = t + x + \text{const}$ and the gauge field takes the form

$$A_\mu dx^\mu = -\left(\frac{Q}{r} + \phi_0\right)dv + \frac{r^2}{\triangle}\left(\frac{Q}{r} + \phi_0\right)dr. \tag{4.94}$$

Near the outer horizon, the scalar field satisfying the ingoing-wave condition behaves as

$$\Psi \sim e^{-i\omega v + i\left(\frac{eQ}{r_+} + e\phi_0\right)x} Y_{lm}(\theta, \phi). \tag{4.95}$$

Assuming that $\tilde{\omega} = \tilde{\omega}_R + i\tilde{\omega}_I$ is complex, we obtain the following result:

$$\begin{aligned} J_{(m)a}n^a|_{\mathcal{H}_+} &= 2\left|\tilde{\omega} - \frac{eQ}{r_+}\right|^2 |\Psi|^2, & (4.96)\\ J_{(em)a}n^a|_{\mathcal{H}_+} &= 0, & (4.97)\\ j_{(e)a}n^a|_{\mathcal{H}_+} &= 2e\left(\tilde{\omega}_R - \frac{eQ}{r_+}\right)|\Psi|^2. & (4.98) \end{aligned}$$

The Misner-Sharp quasi-local energy associated with the energy current J^a is given by

$$E_{\rm MS} := \frac{1}{2}r\left(1 - \nabla_a r \nabla^a r\right) = M - \frac{Q^2}{2r} \tag{4.99}$$

in the Reissner-Nordström spacetime. Eq. (4.96) implies that no energy can be extracted from the black hole irrespective of the value of $\tilde{\omega}$.

Assuming a quasistatic change, we can also find

$$\delta Q = \frac{e\left(\tilde{\omega}_R - \frac{eQ}{r_+}\right)}{\left|\tilde{\omega} - \frac{eQ}{r_+}\right|^2}\delta E_H \tag{4.100}$$

with $\delta E_H \geq 0$, where δE_H stands for the change of the Misner-Sharp energy $M_{\rm MS}$ at $r = r_+$.

From Eq. (4.100), we can see that if the superradiance condition is satisfied in terms of $\tilde{\omega}_R$, we can conclude that $\delta|Q| < 0$, that is, the black hole is discharged by the scalar field. This is because if $eQ > 0$, Eqs. (4.81) and (4.98) imply $e\delta Q < 0$, whereas if $eQ < 0$, Eqs. (4.82) and (4.98) imply $e\delta Q > 0$.

We can approximate the black hole geometry near the horizon by the Reissner-Nordtröm spacetime. Using $E_H = M - Q^2/(2r_+)$ and Eq. (4.90), we find

$$\delta A = \frac{2A}{M}\delta E_H. \tag{4.101}$$

Therefore we conclude that the area of the black hole never decreases.

From Eqs. (4.90) and (4.100), we can derive the following relation between δM and δA:

$$\frac{\delta M}{M} = \frac{-\left[\left(\frac{r_+}{M}-1\right)\tilde{\omega}_R + \left(2-\frac{r_+}{M}\right)\frac{eQ}{r_+}\right]\left(\frac{eQ}{r_+}-\tilde{\omega}_R\right) + \left(\frac{r_+}{M}-1\right)\tilde{\omega}_I^2}{\left|\tilde{\omega}-\frac{eQ}{r_+}\right|^2}\frac{\delta A}{2A}. \tag{4.102}$$

From $M < r_+ < 2M$, the superradiance condition, and $\delta A \geq 0$, we can conclude that $\delta M \leq 0$ if $\tilde{\omega}_I^2$ is sufficiently small. Therefore, the weak superradiance decreases both M and $|Q|$ but increases A. This can be understood as follows. Note that M and E_H stand for the total energy and the quasi-local energy within the horizon, respectively, while the difference $Q^2/(2r_+)$ between the two corresponds to the energy of the electromagnetic field outside the horizon. Since

$$M = E_H + \frac{Q^2}{2r_+}, \tag{4.103}$$

even if E_H increases, the decrease in $Q^2/(2r_+)$ can overcompensate it. This is the case for the weak superradiance and the total energy will decrease in the quasi-static process. In the asymptotically flat case, the difference in the total energy will be radiated away to infinity, while in the asymptotically AdS case in the reflective boundary, it will be converted to the energy of the ambient scalar field.

Since the null energy condition is satisfied in the present system and the boundary condition at the conformal infinity uniquely determines the time development of the scalar field, we can expect that the area law of the AdS black hole holds in an appropriate formulation [122]. We can see that the superradiance conditions given by Eqs. (4.81) and (4.82) in terms of $\tilde{\omega}_R$ imply $\delta A \geq 0$ for $eQ > 0$ and $eQ < 0$, respectively. Therefore, from a thermodynamical point of view, we conclude that the black hole may remain the (approximate) Reissner-Nordström solution with decreasing its mass and the absolute value of its charge, while increasing its area in a quasistatic manner during the superradiance instability, as long as the black hole is much smaller than the AdS length.

4.7 Summary of this chapter

In this chapter, we have extended the result of [63] for a neutral massive scalar field in the AdS spacetime to charged and neutral massive scalar fields in a charged AdS black hole. In Section 4.3, we have clarified the parameter range for which the matched asymptotic expansion method applies for charged massive scalar fields and derived an equation which determines QNFs. In Section 4.4, we have analytically shown that the quasinormal mode of the small charged AdS black hole becomes superradiantly unstable if its frequency in the pure AdS spacetime satisfies the superradiance condition. In Section 4.5, we have numerically obtained the relation between the parameter of the boundary condition at the conformal infinity, $\zeta \in [0, \pi]$, and the QNFs of the scalar field in the AdS black holes with $(r_+, r_-) = (0.01\ell, 0.001\ell)$ and $(r_+, r_-) = (0.1\ell, 0.001\ell)$.

We have shown that the first fundamental mode of the neutral scalar field in the AdS black hole has a critical value ζ_0 beyond which the real part of the QNF vanishes and the imaginary part splits into two different values. We note that such a critical value does not exist for the second fundamental mode. We have also shown that there exists a critical value ζ_c, corresponding to the onset of instability. Furthermore, we find $\zeta_0 < \zeta_c$ and the imaginary parts are negative for $\zeta_0 < \zeta < \zeta_c$. For $\zeta_c < \zeta$, there are two QNFs that have vanishing real part but positive and negative values for the imaginary part. This result indicates instability for $\zeta_c < \zeta$. Since the field is neutral, there is no superradiance. Hence, this instability arises from the boundary condition. The time scale of the instability becomes shorter as ζ increases. At $\zeta = \zeta_c$, there exists a static neutral perturbation in the charged AdS black hole. For $\zeta < \zeta_c$, the evolution is stable and the time scale of the decay becomes longer as ζ increases. Moreover, we analytically and numerically establish that although the system of the neutral field in the pure AdS spacetime has both symmetries $\omega \to -\omega$ and $\omega \to \omega^*$, the existence of the black hole horizon breaks them. Instead, a symmetry $\omega \to -\omega^*$ remains for the neutral field on the AdS black hole spacetime.

The charged scalar field has no critical value at which the real part of the QNF becomes zero. The results we have shown imply that the evolution of the charged field can be unstable by superradiance whether the charge is negative or positive. If $e|Q|\ell/r_+ > (3+\sqrt{9+4\mu^2\ell^2})/2$, the system is superradiantly unstable irrespectively of ζ, while if $e|Q|\ell/r_+ \leq (3+\sqrt{9+4\mu^2\ell^2})/2$, the superradiant stability depends on ζ. The instability can be caused by the charged scalar field even for $\zeta \leq \zeta_0$, where ζ_0 is the critical value at which $\mathrm{Re}[\omega] = 0$ for *the neutral field*. This is remarkably different from the neutral field. Furthermore, the evolution is unstable for $\zeta_c < \zeta$. The time scale of the

instability for $\zeta_0 < \zeta$ can be much shorter than that for $\zeta \leq \zeta_0$. In this sense, the superradiant instability can be enhanced by the boundary condition. We point out that the symmetry $\tilde{\omega} \to -\tilde{\omega}^*$, which exists for the neutral field, is broken. Actually, the symmetry is deformed to $(\tilde{\omega}, eQ) \to (-\tilde{\omega}^*, -eQ)$. We also show that the weak superradiance in this system extracts energy not from the black hole but from its ambient electric field and that it extracts charge from the black hole and thus weakens its ambient electric field. This can be interpreted as a classical scalar-field counterpart of discharging a black hole by the Schwinger effect. The black hole increases its energy within the horizon, decreases the absolute value of its charge, increases its area, but decreases its mass parameter, as long as the black hole is much smaller than the AdS length.

With the symmetry of the QNFs, the superradiant instability in this system is independent of the sign of eQ in contrast to the claim in [106]. Furthermore, we expect that this symmetry gives some explanation on instability shown in [116]. They showed that charged scalar fields in the Reissner-Nordström-AdS black holes can cause instability irrespectively of the sign of eQ. They, however, claim that this has nothing to do with superradiance because the QNMs with $eQ < 0$ cannot satisfy the superradiance condition. Although they do not assume $\mathrm{Re}[\tilde{\omega}] > 0$ in the analysis, they seem to assume it when they interpret the result. Our result implies that the instability they find comes from the superradiance because the symmetry shows that the superradiance *can* occur even in the case of $eQ < 0$ if we admit $\mathrm{Re}[\tilde{\omega}] < 0$.

Chapter 5

Revisiting the Aretakis constants and instability in two-dimensional anti-de Sitter spacetimes

The content in this chapter was originally published as:
T. Katagiri and M. Kimura, "Revisiting the Aretakis constants and instability in two-dimensional anti-de Sitter spacetimes," Phys. Rev. D, 103(6):064011, (2021)

As introduced in section 3.4, the extremal Ressner-Nordström spacetime suffers from horizon-instability called the Aretakis instability against linear massless scalar field perturbations. As seen in section 2.4, extremal black holes admit a highly symmetric structure in the vicinities, which is called the near-horizon geometry. It is expected that the study of scalar fields in the near-horizon geometry brings us insight into the fundamental properties of the Aretakis instability and related conserved quantities called the Aretakis constants. As shown in Appendix C, certain massive scalar fields in arbitrary static and spherically symmetric extremal black hole spacetimes can be reduced to massive scalar fields with specific mass squared in two-dimensional anti-de Sitter spacetimes (AdS_2). In this chapter, we focus on the massive scalar field in AdS_2, and discuss the Aretakis constants and instability in AdS_2.

The Aretakis instability of massive scalar fields in AdS_2 has already been discussed [123, 124, 125, 126, 127, 128, 71]. It has been argued that the higher-order radial derivatives of the scalar field show the polynomial growth on the future Poincaré horizon. In their study (in fact, also in the original

study by Aretakis), the divergent behavior of the higher-order derivatives has been shown in specific coordinate systems. Thus, it is not trivial whether this divergent behavior is just a coordinate effect or not. In the case of the extremal Reissner-Nordström black holes, there is a unique timelike Killing vector V which is the generator of the event horizon. In the Eddington-Finkelstein coordinates (v, r) where the timelike Killing vector V is a coordinate basis, the radial derivative operator ∂_r satisfies $\mathcal{L}_V \partial_r = 0$. Then, the growth of some components of a tensor in the Eddington-Finkelstein coordinates is not a coordinate effect. Because the Aretakis instability, i.e., the growth of $\partial_r^n \Phi$ with an integer n, implies that $\nabla_r \nabla_r \cdots \nabla_r \Phi = \partial_r^n \Phi + \text{lower derivatives}$ is divergent, this is not a coordinate effect. However, in the case of AdS_2, there are many possible timelike Killing vectors, and there is no unique way to choose one of them. Actually, if we choose a coordinate system where one of the coordinate bases is the global timelike Killing vector, we can show that the higher-order derivatives do not blow up. Thus, one may think that the Aretakis instability in AdS_2 is due to the choice of the coordinate systems [123, 128].[1] In this chapter, to make this point clear, we revisit to study the Aretakis constants and instability in AdS_2. We find out the geometrical meaning of the Aretakis instability in the parallelly propagated (parallel-transported) null geodesics frame on the horizon, i.e., some components of the higher-order covariant derivatives of the field in the parallelly propagated frame blow up at the late time. In general relativity, parallelly propagated frames are used for studying the singular behavior of tensors in a coordinate independent way. For example, if the components of the Riemann tensor in the parallelly propagated frame are divergent at some point, we regard the point as a curvature singularity even if all scalar quantities constructed from the Riemann tensor, e.g., the Ricci scalar or the Kretschmann invariant, are finite [84]. Thus, our result implies the divergent behavior of the covariant derivatives of the fields at the late time. In the study of the Aretakis instability, the conserved quantities on the horizon, called the Aretakis constants, make the analysis easier [66, 67, 68, 123, 129, 130, 131]. In this chapter, we also show that Aretakis constants in AdS_2 become some components of the higher-order covariant derivatives of the field in the parallelly propagated frame.

Because AdS_2 is maximally symmetric, any null hypersurfaces have the same geometrical properties. If we prepare the parallelly propagated null

[1] In Ref. [128], there is an argument that the Aretakis instability in $\mathrm{AdS}_2 \times S^2$ is not a coordinate effect if we consider $\mathrm{AdS}_2 \times S^2$ as a near-horizon geometry of extremal black holes. This is because the AdS structure in the near horizon geometry appears in the Poincaré chart and the generator of the Poincaré horizon can be regarded as the horizon generator of the original black hole spacetime.

geodesic frame along any null hypersurfaces, the above discussion holds not only on the future Poincaré horizon but also on any null hypersurfaces. This implies that the Aretakis instability is the result of singular behaviors of the higher-order covariant derivatives of the fields on the whole AdS infinity, rather than a blowup on a specific null hypersurface. Also, by focusing on the maximal symmetry of AdS_2, we can construct scalar quantities that are constant not only on the future Poincaré horizon but also on any null hypersurfaces, and reduce to the Aretakis constants on the future Poincaré horizon. In this chapter, we call these scalar quantities the generalized Aretakis constants. Reference [132] shows that the ladder operators constructed from the spacetime conformal symmetry of AdS_2 lead to conserved quantities on any null hypersurfaces, and checked that they coincide with the generalized Aretakis constants for special mass squared cases. In this chapter, we explicitly show the relation with the generalized Aretakis constants for general cases. We also discuss that the generalized Aretakis constants and instability in AdS_2 are related to the conformal Killing tensors.

This chapter is organized as follows. In Section 5.1, we briefly review the Aretakis constants and instability in AdS_2 based on Ref. [123]. In Section 5.2, we introduce the parallelly propagated null geodesics frame and discuss the Aretakis constants and instability in that frame. We also generalize them to the case for any null hypersurfaces by using parallelly propagated frames on them. In Section 5.3, we discuss a relation between the generalization of the Aretakis constants and the spacetime conformal symmetry in AdS_2. In the final section, we summarize this chapter. In Appendix D.1, we review the mass ladder operators in AdS_2 [132, 133]. Appendix D.2 gives the proof of Proposition 3 introduced in Section 5.3.2.

5.1 The Aretakis constants and instability in AdS_2

We briefly review the Aretakis constants and instability in AdS_2 [66, 67, 68, 123, 124, 125, 126, 127, 128, 71]. In the ingoing Eddington-Finkelstein coordinates (v, r), AdS_2 is described by

$$ds^2 = -r^2 dv^2 + 2dvdr, \tag{5.1}$$

where the future Poincaré horizon is located at $r = 0$. We consider massive scalar fields $\Phi(v, r)$ in AdS_2. The fields obey the massive Klein-Gordon equation

$$2\partial_v\partial_r\Phi + \partial_r\left(r^2\partial_r\Phi\right) - m^2\Phi = 0. \tag{5.2}$$

For mass squared $m^2 = \ell(\ell+1)$ ($\ell = 0, 1, 2, \cdots$), acting the ℓth- order derivative operator ∂_r^ℓ on Eq. (C.7) and evaluating it at $r = 0$ show

$$\partial_v \partial_r^{\ell+1} \Phi\big|_{r=0} = 0. \tag{5.3}$$

This shows that $\mathcal{H}_\ell$ defined by

$$\mathcal{H}_\ell := \partial_r^{\ell+1} \Phi\big|_{r=0} \tag{5.4}$$

are independent of v. Hence, $\mathcal{H}_\ell$ are conserved quantities along the future Poincaré horizon and then called *the Aretakis constants* in AdS_2. For other mass squared, such conserved quantities on the future Poincaré horizon cannot be found. Differentiating Eq. (C.7) $(\ell+1)$ times with respect to r, we obtain

$$\partial_v \partial_r^{\ell+2} \Phi\big|_{r=0} = -(\ell+1)\mathcal{H}_\ell. \tag{5.5}$$

This implies

$$\partial_r^{\ell+2} \Phi|_{r=0} = -(\ell+1)\mathcal{H}_\ell v + \text{const.} \tag{5.6}$$

We see that $(\ell+2)$th-order derivative of the field on the future Poincaré horizon will blow up at the late time if $\mathcal{H}_\ell \neq 0$. This divergent behavior is called *the Aretakis instability* in AdS_2. We note that the $(\ell+3)$th- or higher-order derivatives are polynomially divergent at the late time.

For general mass squared cases with $m^2 \geq m_{\mathrm{BF}}^2 = -1/4$, where m_{BF}^2 is the Breitenlohner-Freedman bound [134, 135] in AdS_2, Ref. [123] shows that the late-time behavior of the nth- derivatives of the fields with respect to r at the future Poincaré horizon $r = 0$ becomes[2]

$$\partial_r^n \Phi\big|_{r=0} \sim v^{n-\Delta_m}, \tag{5.7}$$

where n is a nonnegative integer and

$$\Delta_m := \frac{1}{2} + \sqrt{m^2 + \frac{1}{4}}. \tag{5.8}$$

Hence, using the notation,

$$n_m := \lfloor \Delta_m \rfloor + 1, \tag{5.9}$$

where $\lfloor \Delta_m \rfloor$ denotes the integer part of Δ_m, the n_mth- order derivative of the field at $r = 0$ will blow up at the late time. This is also called the Aretakis instability in AdS_2. We note that the (n_m+1)th- or higher-order derivatives are also unbounded.

[2]Note that we focus on the normalizable modes.

5.2 The Aretakis constants and instability in the parallelly propagated null geodesics frame

In this section, we discuss the geometrical meaning of the Aretakis constants and instability in the parallelly propagated null geodesic frame. We shall show that some components of the higher-order covariant derivatives of the field in the parallelly propagated frame are constant or unbounded, and they correspond to the Aretakis constants and instability, respectively.

5.2.1 On the future Poincaré horizon

We first discuss the late-time divergent behavior in Eq. (5.7). We introduce vector fields on the future Poincaré horizon $r = 0$,

$$e^a_{(0)} = (\partial/\partial v)^a \,,\ e^a_{(1)} = -\,(\partial/\partial r)^a \,, \tag{5.10}$$

where these satisfy

$$\begin{aligned} &e^a_{(0)}\nabla_a e^b_{(0)} = 0,\ e^a_{(0)}\nabla_a e^b_{(1)} = 0, \\ &e^a_{(0)}e_{(0)a} = 0,\ e^a_{(1)}e_{(1)a} = 0,\ e^a_{(0)}e_{(1)a} = -1, \end{aligned} \tag{5.11}$$

at $r = 0$. Hence, $e^a_{(1)}$ is parallelly transported along the null geodesic $e^a_{(0)}$ on the future Poincaré horizon. The frame formed by $(e^a_{(0)}, e^a_{(1)})$ is called *the parallelly propagated null geodesic frame* on the future Poincaré horizon.

For the massive scalar $\Phi(v, r)$ satisfying Eq. (C.7) with general mass squared and positive integer n, the following relation holds:

$$(-1)^n\, e^{a_1}_{(1)} e^{a_2}_{(1)} \cdots e^{a_n}_{(1)} \nabla_{a_1}\nabla_{a_2}\cdots\nabla_{a_n}\Phi\Big|_{r=0} = \partial_r^n \Phi|_{r=0} \,. \tag{5.12}$$

Using the notation n_m is defined in Eq. (5.9), the divergent behavior of $\partial_r^{n_m}\Phi$ at $r = 0$ implies that the n_mth- order covariant derivative is also divergent in the parallelly propagated null geodesic frame. We note that for $n \leq n_m$, the components of $\nabla_{a_1}\cdots\nabla_{a_n}\Phi$ in the parallelly propagated null geodesic frame are bounded except for the $e^{a_1}_{(1)}e^{a_2}_{(1)}\cdots e^{a_n}_{(1)}$ component with $n = n_m$ from Eq. (5.7).[3]

[3]For positive integers n and q, the following relation holds:

$$(-1)^n\, e^{a_1}_{(0)}\cdots e^{a_q}_{(0)} e^{b_1}_{(1)}\cdots e^{b_n}_{(1)} \nabla_{a_1}\cdots\nabla_{a_q}\nabla_{b_1}\cdots\nabla_{b_n}\Phi\Big|_{r=0} = \partial_v^q\partial_r^n\Phi|_{r=0} \,. \tag{5.13}$$

Other components of the covariant derivatives in the parallelly propagated frame can be written by Eq. (5.13) and the lower-order derivatives using the commutation relation for the covariant derivatives.

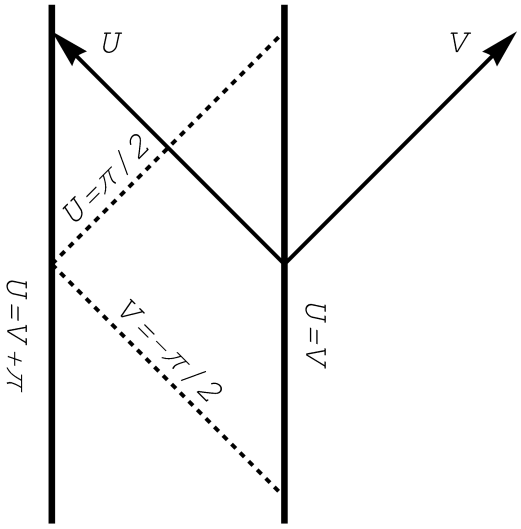

Figure 5.1: The Penrose diagram for AdS_2. The left and right AdS boundaries are located at $U = V + \pi$ and $U = V$, respectively. The future and past Poincaré horizons are located at $U = \pi/2$ and $V = -\pi/2$, respectively.

For the mass squared $m^2 = \ell(\ell+1)$ $(\ell = 0, 1, 2, \cdots)$, we obtain

$$(-1)^{\ell+1}\, e^{a_1}_{(1)} e^{a_2}_{(1)} \cdots e^{a_{\ell+1}}_{(1)} \nabla_{a_1} \nabla_{a_2} \cdots \nabla_{a_{\ell+1}} \Phi \Big|_{r=0} = \partial_r^{\ell+1} \Phi \big|_{r=0} \,. \tag{5.14}$$

We find that the $e^{a_1}_{(1)} e^{a_2}_{(1)} \cdots e^{a_{\ell+1}}_{(1)}$ component of the $(\ell+1)$th-order covariant derivative of the field on the future Poincaré horizon is the Aretakis constant $\mathcal{H}_\ell$ in Eq. (5.4):

$$(-1)^{\ell+1}\, e^{a_1}_{(1)} e^{a_2}_{(1)} \cdots e^{a_{\ell+1}}_{(1)} \nabla_{a_1} \nabla_{a_2} \cdots \nabla_{a_{\ell+1}} \Phi \Big|_{r=0} = \mathcal{H}_\ell. \tag{5.15}$$

5.2.2 On any null hypersurfaces

Because AdS_2 is maximally symmetric, the discussion in the previous subsection should also hold for any other null hypersurfaces. This implies that the Aretakis instability is the result of singular behaviors of the higher-order covariant derivatives of the fields on the whole *AdS* infinity, rather than a blowup on a specific null hypersurface. In this subsection, we explicitly show that for $m^2 = \ell(\ell+1)$ $(\ell = 0, 1, 2, \cdots)$ cases.

Massive scalar fields in the global chart (U, V)

For later convenience, we discuss the massive scalar fields in the global chart [132]. In the double null global chart (U, V) defined by

$$\tan U = v + \frac{2}{r}, \ \ \tan V = v, \tag{5.16}$$

the line element in Eq. (5.1), which describes AdS_2, is rewritten as

$$ds^2 = -\frac{4}{H(U,V)} dU dV, \tag{5.17}$$

where

$$H(U,V) = \sin^2(U - V). \tag{5.18}$$

The coordinate range is $-\infty < U < \infty, -\infty < V < \infty$ with $0 < U - V < \pi$, and the AdS boundary is located at $V = U$ or $V = U + \pi$ where $H(U, V) = 0$. The future and past Poincaré horizons are $U = \pi/2$ and $V = -\pi/2$, respectively. The Penrose diagram of AdS_2 is shown in Fig. 5.1.

In the present coordinates, the massive Klein-Gordon equation (C.7) is rewritten as

$$\left[-H(U,V)\partial_V \partial_U - m^2\right] \Phi(U,V) = 0, \tag{5.19}$$

where $H(U, V)$ is given by Eq. (5.18). We notice that for the massless scalar, this equation shows $\partial_V \partial_U \Phi = 0$, and hence $\partial_U \Phi$ is constant along any null hypersurfaces $U =$ const. At the future Poincaré horizon $U = \pi/2$, it coincides with the Aretakis constant $\mathcal{H}_0$ in Eq. (5.4). In this sense, we interpreted $\partial_U \Phi$ as the generalization of the Aretakis constant $\mathcal{H}_0$. According to Ref. [132], for the mass squared $m^2 = \ell(\ell + 1)$, there exists the generalization of the Aretakis constants $\mathcal{H}_\ell$ in Eq. (5.4) for general ℓ,[4]

$$\mathcal{A}_\ell := \left(\frac{\cos^2 V}{H(U,V)}\right)^{\ell+1} \left[\frac{H(U,V)}{\cos^2 V}\partial_U\right]^{\ell+1} \Phi, \tag{5.20}$$

and they satisfy

$$\partial_v \mathcal{A}_\ell = 0. \tag{5.21}$$

We call $\mathcal{A}_\ell$ *the generalized Aretakis constants*. It is easy to check that $\mathcal{A}_\ell = \mathcal{H}_\ell$ at the future Poincaré horizon $U = \pi/2$. For other mass squared cases, conserved quantities on a null hypersurface cannot be found.

[4] If we exchange U and V in Eq. (5.20), we can construct conserved quantities on $V =$ const. surfaces.

Parallelly propagated null geodesic frame in AdS_2

Now, we introduce null vector fields

$$\mathfrak{e}^a_{(0)} = \frac{f(U)H(U,V)}{4}\left(\partial/\partial V\right)^a, \ \mathfrak{e}^a_{(1)} = \frac{2}{f(U)}\left(\partial/\partial U\right)^a, \tag{5.22}$$

where $f(U)$ is an arbitrary finite function. These satisfy the relations

$$\begin{aligned} &\mathfrak{e}^a_{(0)}\nabla_a\mathfrak{e}^b_{(0)} = 0, \ \mathfrak{e}^a_{(0)}\nabla_a\mathfrak{e}^b_{(1)} = 0, \\ &\mathfrak{e}^a_{(0)}\mathfrak{e}_{(0)a} = 0, \ \mathfrak{e}^a_{(1)}\mathfrak{e}_{(1)a} = 0, \ \mathfrak{e}^a_{(0)}\mathfrak{e}_{(1)a} = -1. \end{aligned} \tag{5.23}$$

Therefore, $(\mathfrak{e}^a_{(0)}, \mathfrak{e}^a_{(1)})$ form the parallelly propagated null geodesic frame for each null hypersurface $U = \text{const}$. We should note that $\mathfrak{e}^a_{(0)}$ and $\mathfrak{e}^a_{(1)}$ are vector fields defined in the whole AdS_2 spacetime, while $e^a_{(0)}$ and $e^a_{(1)}$ in Eq. (5.11) are defined only on $r = 0$ surface. Hereafter, we set $f(U) = 2$. We note that this specific choice of $f(U)$ does not change the conclusion in the following discussions.

Massless scalar cases

General solutions of the massless Klein-Gordon equation (5.19) are

$$\Phi(U,V) = F(U) + G(V). \tag{5.24}$$

Then, the generalized Aretakis constant in Eq. (5.20) is $\mathcal{A}_0 = \partial_U F(U)$. Now, we can see

$$\mathfrak{e}^a_{(1)}\nabla_a\Phi = \mathcal{A}_0, \tag{5.25}$$

$$\mathfrak{e}^a_{(1)}\mathfrak{e}^b_{(1)}\nabla_a\nabla_b\Phi = \mathcal{A}_0\frac{\partial_U H(U,V)}{H(U,V)} + \partial_U^2 F(U). \tag{5.26}$$

Equation (5.25) shows that the geometrical meaning of $\mathcal{A}_0$ at each null hypersurface $U = \text{const.}$ is the same as the Aretakis constant $\mathcal{H}_0$ at $r = 0$; i.e., a component of the covariant derivative in the parallelly propagated frame is constant at each null hypersurface. Because $\partial_U H/H = 2/\tan(U-V)$, $\mathfrak{e}^a_{(1)}\mathfrak{e}^b_{(1)}\nabla_a\nabla_b\Phi$ in Eq. (5.26) is divergent linearly in $(U-V)^{-1}$ at the AdS boundary if $\mathcal{A}_0 \neq 0$.[5] Near the AdS boundary, we further show

$$\mathfrak{e}^{a_1}_{(1)}\mathfrak{e}^{a_2}_{(1)}\cdots\mathfrak{e}^{a_{n+2}}_{(1)}\nabla_{a_1}\nabla_{a_2}\cdots\nabla_{a_{n+2}}\Phi = \mathcal{A}_0\mathcal{O}\left((U-V)^{-n-1}\right), \tag{5.27}$$

[5]If we consider the "normalizable" mode $\Phi \sim (U-V)^{\Delta_m}$ with $\Delta_m = 1$, where Δ_m is defined by Eq. (5.8), for the massless case at the AdS boundary $U = V$, then the function $G(V)$ becomes $G(V) = -F(V)$. We note that the Aretakis instability occurs even in that case.

where $n \geq 1$. Eqs. (5.26) and (5.27) show that the second- and higher-order covariant derivatives of the field *on any null hypersurfaces* have singular behaviors at the AdS boundary if $\mathcal{A}_0 \neq 0$.[6] We comment that other components are bounded,

$$\mathfrak{e}^a_{(0)} \nabla_a \Phi = \frac{H(U,V)}{2} \partial_V G(V), \tag{5.28}$$

$$\mathfrak{e}^a_{(0)} \mathfrak{e}^b_{(0)} \nabla_a \nabla_b \Phi = \frac{H(U,V)}{4} \partial_V \left(H(U,V) \partial_V G(V) \right), \tag{5.29}$$

$$\mathfrak{e}^a_{(0)} \mathfrak{e}^b_{(1)} \nabla_a \nabla_b \Phi = \mathfrak{e}^a_{(1)} \mathfrak{e}^b_{(0)} \nabla_a \nabla_b \Phi = 0. \tag{5.30}$$

Massive scalar cases with $m^2 = \ell(\ell+1)$

For the cases $m^2 = \ell(\ell+1)$ ($\ell = 1, 2, \cdots$), we can also explicitly see the divergent behavior at the AdS boundary. For the $\ell = 1$ case, the general normalizable Klein-Gordon fields, which are derived in Appendix D.1, take the form of

$$\Phi(U,V) = \frac{2\cos U \cos V}{\sin(U-V)} \left(F(U) - F(V) \right) - \cos^2 U \partial_U F(U) - \cos^2 V \partial_V F(V), \tag{5.31}$$

with an arbitrary function F.[7] We obtain

$$\mathfrak{e}^{a_1}_{(1)} \mathfrak{e}^{a_2}_{(1)} \nabla_{a_1} \nabla_{a_2} \Phi = \mathcal{A}_1, \tag{5.32}$$

where $\mathcal{A}_1 = 2(-1+2\cos(2U))\partial_U F(U) + \cos U \left(6 \sin U \partial_U^2 F(U) - \cos U \partial_U^3 F(U) \right)$ is the generalized Aretakis constant (5.20) and

$$\mathfrak{e}^{a_1}_{(1)} \mathfrak{e}^{a_2}_{(1)} \mathfrak{e}^{a_3}_{(1)} \nabla_{a_1} \nabla_{a_2} \nabla_{a_3} \Phi = 2\mathcal{A}_1 \frac{\partial_U H(U,V)}{H(U,V)} + \partial_U \mathcal{A}_1. \tag{5.33}$$

Because $\partial_U H / H = 2/\tan(U-V)$, Eq. (5.33) shows that the third-order covariant derivative of the field on any null hypersurfaces has the linear growth of $(U-V)^{-1}$ at the AdS boundary if $\mathcal{A}_1 \neq 0$. We comment that other components are bounded.

For $\ell \geq 2$, acting the mass ladder operators, which are given by Eq. (D.17), we can easily obtain the explicit form of the general normalizable

[6] If $\mathcal{A}_0 = 0$ and $\partial_U^2 F(U) \neq 0$, the third-order derivative $\mathfrak{e}^{a_1}_{(1)} \mathfrak{e}^{a_2}_{(1)} \mathfrak{e}^{a_3}_{(1)} \nabla_{a_1} \nabla_{a_2} \nabla_{a_3} \Phi$ is divergent (see Proposition 1 in Section 5.2.3).

[7] Note that $\Phi(U,V)$ satisfies the normalizable boundary condition, i.e., $\Phi \sim (U-V)^{\Delta_m}$ with $\Delta_m = \ell + 1$, at $V = U$. If we also impose this condition at $V = U + \pi$, F should satisfy $F(U) = F(U+\pi)$.

Klein-Gordon field, which is Eq. (D.18) with $G(V) = -F(V)$. We can show that $(\ell+1)$th- and $(\ell+2)$th- order covariant derivatives are, respectively, constant along each null hypersurface and divergent at the AdS boundary,

$$\mathfrak{e}_{(1)}^{a_1}\mathfrak{e}_{(1)}^{a_2}\cdots\mathfrak{e}_{(1)}^{a_{\ell+1}}\nabla_{a_1}\nabla_{a_2}\cdots\nabla_{a_{\ell+1}}\Phi = \mathcal{A}_\ell, \tag{5.34}$$

where $\mathcal{A}_\ell$ is the generalized Aretakis constant in Eq. (5.20) and

$$\mathfrak{e}_{(1)}^{a_1}\mathfrak{e}_{(1)}^{a_2}\cdots\mathfrak{e}_{(1)}^{a_{\ell+2}}\nabla_{a_1}\nabla_{a_2}\cdots\nabla_{a_{\ell+2}}\Phi = (\ell+1)\mathcal{A}_\ell\frac{\partial_U H(U,V)}{H(U,V)} + \partial_U\mathcal{A}_\ell. \tag{5.35}$$

5.2.3 Relation between the conserved quantities on the null hypersurface and divergent behavior

We have observed that, for a solution of the massive Klein-Gordon equation (5.19) with the mass squared $m^2 = \ell(\ell+1)$ $(\ell = 0, 1, 2, \cdots)$ in AdS_2, in the parallelly propagated null geodesic frame, the $(\ell+1)$th- covariant derivative of the field gives a constant along each null hypersurface and the $(\ell+2)$th-covariant derivative has a linear divergent behavior along the null hypersurface. We can generalize this relation, i.e., the relation between a conserved quantity on a null hypersurface and the divergent behavior, as follows:

Proposition 1 *If the relation*

$$\mathfrak{e}_{(1)}^{a_n}\mathfrak{e}_{(1)}^{a_{n-1}}\cdots\mathfrak{e}_{(1)}^{a_1}\nabla_{a_n}\nabla_{a_{n-1}}\cdots\nabla_{a_1}\Psi = A(U), \tag{5.36}$$

holds for some scalar field $\Psi(U,V)$ in AdS_2, a positive integer n, and a regular function $A(U)(\not\equiv 0)$, then $\mathfrak{e}_{(1)}^{a_{n+1}}\mathfrak{e}_{(1)}^{a_n}\cdots\mathfrak{e}_{(1)}^{a_1}\nabla_{a_{n+1}}\nabla_{a_n}\cdots\nabla_{a_1}\Psi$ is divergent at the AdS boundary.

Proof. Acting an operator $\mathfrak{e}_{(1)}^{a_{n+1}}\nabla_{a_{n+1}}$ to Eq. (5.36), we obtain

$$\begin{aligned}
&\mathfrak{e}_{(1)}^{a_{n+1}}\mathfrak{e}_{(1)}^{a_n}\cdots\mathfrak{e}_{(1)}^{a_1}\nabla_{a_{n+1}}\nabla_{a_n}\cdots\nabla_{a_1}\Psi \qquad (5.37)\\
&= \partial_U A(U) - \mathfrak{e}_{(1)}^{a_{n+1}}\nabla_{a_{n+1}}\left(\mathfrak{e}_{(1)}^{a_n}\cdots\mathfrak{e}_{(1)}^{a_1}\right)\nabla_{a_n}\cdots\nabla_{a_1}\Psi\\
&= \partial_U A(U) + nA(U)\frac{\partial_U H(U,V)}{H(U,V)}, \qquad (5.38)
\end{aligned}$$

where we have used the relation

$$\mathfrak{e}_{(1)}^{a}\nabla_a\mathfrak{e}_{(1)}^{b} = -\frac{\partial_U H(U,V)}{H(U,V)}\mathfrak{e}_{(1)}^{b}. \tag{5.39}$$

In the right-hand side of Eq. (5.38), the first term is finite but the second term is divergent at the AdS boundary $V = U$ (or $V = U + \pi$) because $\partial_U H/H = 2/\tan(U - V)$. □

If $\Psi(U, V)$ is the massive Klein-Gordon field with the mass squared $m^2 = \ell(\ell + 1)$, the above proposition leads to the relation between the generalized Aretakis constant and the divergent behavior at the AdS boundary.

As another application of the above proposition with $n = 1$, for the massive Klein-Gordon fields $\Phi(U, V)$ with the mass squared $m^2 = \ell(\ell + 1)$ in AdS_2, if we choose the function $\Psi(U, V)$ as

$$\Psi = D_{i_1,1} D_{i_2,2} \cdots D_{i_\ell,\ell} \Phi, \tag{5.40}$$

where $D_{i,\ell}$ are the mass ladder operators in Eq. (D.17), then $\Psi(U, V)$ satisfies the massless Klein-Gordon equation (5.19). Then, $\mathfrak{e}^a_{(1)} \nabla_a \Psi \propto \partial_U \Psi$ is a constant along each null hypersurface, which corresponds to the generalized Aretakis constant $\mathcal{A}_\ell$ in Eq. (5.20) as will be shown in Section 5.3, and $\mathfrak{e}^a_{(1)} \mathfrak{e}^b_{(1)} \nabla_a \nabla_b \Psi$ is linearly divergent along the null hypersurface.

We can also show the following proposition.

Proposition 2 *If the relation*

$$\mathfrak{e}^{a_n}_{(1)} \mathfrak{e}^{a_{n-1}}_{(1)} \cdots \mathfrak{e}^{a_1}_{(1)} \nabla_{a_n} \nabla_{a_{n-1}} \cdots \nabla_{a_1} \Psi = A_0 + A_1(V)(U - U_0) + \mathcal{O}((U - U_0)^2), \tag{5.41}$$

holds for some scalar field $\Psi(U, V)$ in AdS_2, a positive integer n, a constant A_0 ($\neq 0$), and a bounded function $A_1(V)$, then $\mathfrak{e}^{a_{n+1}}_{(1)} \mathfrak{e}^{a_n}_{(1)} \cdots \mathfrak{e}^{a_1}_{(1)} \nabla_{a_{n+1}} \nabla_{a_n} \cdots \nabla_{a_1} \Psi$ is divergent at the AdS boundary along $U = U_0$.

Proof. If we set $A = A_0 + A_1(V)(U - U_0) + \mathcal{O}((U - U_0)^2)$, Eq. (5.38) still holds. Because A_1 is a bounded function, $\mathfrak{e}^{a_{n+1}}_{(1)} \mathfrak{e}^{a_n}_{(1)} \cdots \mathfrak{e}^{a_1}_{(1)} \nabla_{a_{n+1}} \nabla_{a_n} \cdots \nabla_{a_1} \Psi$ is divergent at the AdS boundary along $U = U_0$. □

We note that scalar fields $\Psi(U, V)$ in the above propositions are not necessarily the massive Klein-Gordon fields. Proposition 2 shows that the existence of a constant along a null hypersurface leads to the divergent behavior of the higher derivative. Finally, we comment that Proposition 2 holds if A_0 is a function of V and has a nonvanishing limiting value $\lim_{V\to\infty} A_0 \neq 0$.

5.2.4 Relation among the conformal Killing tensors, the Aretakis constants and instability

For positive integers n, rank-n tensors

$$K^{a_1a_2\cdots a_n} := \mathfrak{e}_{(1)}^{a_1}\mathfrak{e}_{(1)}^{a_2}\cdots\mathfrak{e}_{(1)}^{a_n}, \tag{5.42}$$

are conformal Killing tensors in AdS_2, and the only nontrivial components are $K^{UU\cdots U} = 1$.[8] For the scalar fields $\Phi(U,V)$ with the mass squared $m^2 = \ell(\ell+1)$ ($\ell = 0,1,2,\cdots$), Eq. (5.34) shows that the generalized Aretakis constants $\mathcal{A}_\ell$ in Eq. (5.20) relate with the rank-$(\ell+1)$ conformal Killing tensor [132],

$$K^{a_1a_2\cdots a_{n_{\ell+1}}}\nabla_{a_1}\nabla_{a_2}\cdots\nabla_{a_{\ell+1}}\Phi = \mathcal{A}_\ell. \tag{5.43}$$

Equation (5.35) implies near the AdS boundary $V \simeq U$,

$$K^{a_1a_2\cdots a_{n_{\ell+2}}}\nabla_{a_1}\nabla_{a_2}\cdots\nabla_{a_{\ell+2}}\Phi = 2(\ell+1)\frac{\mathcal{A}_\ell}{U-V} + \mathcal{O}\left((U-V)^0\right). \tag{5.44}$$

Hence, the contraction with the rank-$(\ell+2)$ conformal Killing tensor and the $(\ell+2)$th-order covariant derivative will blow up linearly in $(U-V)^{-1}$ at the AdS boundary if $\mathcal{A}_\ell \neq 0$.

For the general mass squared $m^2 \geq m^2_{\rm BF} = -1/4$, where the Aretakis constants do not necessarily exist, we have the relation

$$K^{a_1a_2\cdots a_{n_m}}\nabla_{a_1}\nabla_{a_2}\cdots\nabla_{a_{n_m}}\Phi = \mathfrak{e}_{(1)}^{a_1}\mathfrak{e}_{(1)}^{a_2}\cdots\mathfrak{e}_{(1)}^{a_{n_m}}\nabla_{a_1}\nabla_{a_2}\cdots\nabla_{a_{n_m}}\Phi, \tag{5.45}$$

where the notation n_m is defined in Eq. (5.9). As discussed in Sections 5.2.1 and 5.2.2, the right-hand side is divergent at the AdS boundary. Thus, the Aretakis instability can also be regarded as that the contraction with the conformal Killing tensor $K^{a_1a_2\cdots a_{n_m}}$ and the n_mth-order covariant derivative of the Klein-Gordon field is divergent at the AdS boundary.

5.3 The Aretakis constants from the spacetime conformal symmetry

In this section, we discuss the relation between the generalized Aretakis constants in AdS_2 in Eq. (5.20) and the ladder operators constructed from the spacetime conformal symmetry [132, 133] for massive Klein-Gordon fields

[8] We note that $K^{a_1a_2\cdots a_n}$ is parallelly propagated along $\mathfrak{e}^a_{(0)}$, i.e., $\mathfrak{e}^b_{(0)}\nabla_b K^{a_1a_2\cdots a_n} = 0$, and satisfies $\mathcal{L}_\xi K^{a_1a_2\cdots a_n} = 0$ with the Killing vector $\xi = \partial_V + \partial_U$.

with the mass squared $m^2 = \ell(\ell+1)$ ($\ell = 0, 1, 2, \cdots$). First, we construct conserved quantities at each null hypersurface $U =$ const. following Ref. [132]. Next, we show that they coincide with the generalized Aretakis constants up to constant factors. Note that cases for $\ell = 1, 2$ have been discussed [132].

5.3.1 Conserved quantities at each null hypersurface from the mass ladder operators

We discuss the scalar fields $\Phi(U, V)$ obeying the massive Klein-Gordon equation (5.19) with the mass squared $m^2 = \ell(\ell + 1)$. First, let us consider the massless case $\ell = 0$. The massless Klein-Gordon equation (5.19) shows

$$\partial_V \partial_U \Phi = 0. \tag{5.46}$$

We can see that $\partial_U \Phi$ is a conserved quantity at each null hypersurface $U =$ const., and this quantity is the generalized Aretakis constant $\mathcal{A}_0$ in Eq. (5.20).

Next, we consider $\ell \geq 1$ cases. Using the mass ladder operators [132, 133] (see Appendix D.1 for a brief review), the massive Klein-Gordon fields can be mapped into the massless Klein-Gordon fields. Following Ref. [132], we can construct conserved quantities at each null hypersurface $U =$ const. similar to the massless case. The explicit calculation is shown below. From the relation (D.16) with $k = s = \ell$ on the scalar field Φ, we obtain

$$\begin{aligned} &D_{i_\ell,-1} D_{i_{\ell-1},0} \cdots D_{i_1,\ell-2} \left[-H(U,V) \partial_V \partial_U - \ell(\ell+1) \right] \Phi \\ &= -H(U,V) \partial_V \partial_U D_{i_\ell,1} D_{i_{\ell-1},2} \cdots D_{i_1,\ell} \Phi, \end{aligned} \tag{5.47}$$

where the mass ladder operators $D_{i,k}$ are given by Eq. (D.17) and $H(U, V)$ is given by Eq. (5.18). Since the left-hand side vanishes due to the Klein-Gordon equation for Φ, Eq. (5.47) leads to

$$-H(U,V) \partial_V \partial_U D_{i_\ell,1} D_{i_{\ell-1},2} \cdots D_{i_1,\ell} \Phi = 0. \tag{5.48}$$

Thus, solutions of the massive Klein-Gordon equation with the mass squared $m^2 = \ell(\ell+1)$ in AdS_2 can be mapped into that of the massless Klein-Gordon equation. We note that massive fields with other mass squared cannot be mapped into massless fields. As in the case $\ell = 0$, Eq. (5.48) shows

$$\partial_V \mathcal{Q}_\ell = 0, \tag{5.49}$$

where

$$\mathcal{Q}_\ell := W(U) \partial_U D_{i_\ell,1} D_{i_{\ell-1},2} \cdots D_{i_1,\ell} \Phi. \tag{5.50}$$

For later convenience, using $\partial_V W(U) = 0$, we have added an arbitrary function $W(U)$ as a factor. Eq. (5.49) shows that $\mathcal{Q}_\ell$ are conserved quantities at each null hypersurface $U = \text{const}$. As will be discussed below, the quantity $\mathcal{Q}_\ell$ relates to the generalized Aretakis constant $\mathcal{A}_\ell$.

5.3.2 Relation with the Aretakis constants on the future Poincaré horizon

We shall show that $\mathcal{Q}_\ell$ coincide with the Aretakis constants $\mathcal{H}_\ell$ in Eq. (5.4) on the future Poincaré horizon $U = \pi/2$ by choosing $W(U)$ appropriately. It is convenient to use the ingoing Eddington-Finkelstein coordinates (v, r). Using $\partial_U = -(2 + 2vr + (1/2 + v^2/2)r^2)\partial_r$, Eq. (5.50) is written as

$$\mathcal{Q}_\ell = -W(U)\left(2 + 2vr + \frac{1+v^2}{2}r^2\right)\partial_r D_{i_\ell,1} D_{i_{\ell-1},2} \cdots D_{i_1,\ell}\Phi. \tag{5.51}$$

Because $\tan U = v + 2/r$ in Eq. (5.16), we can regard W as a function of $v + 2/r$. Hereafter, we consider $W = -2^{-1}C_W(v/2 + 1/r)^q$ cases, where C_W and q are constants. Then, we can evaluate the leading term of $\mathcal{Q}_\ell$ as

$$\mathcal{Q}_\ell = C_W r^{-q}\partial_r D_{i_\ell,1} D_{i_{\ell-1},2} \cdots D_{i_1,\ell}\Phi\left(1 + \mathcal{O}\left(r\right)\right). \tag{5.52}$$

By choosing C_W and q appropriately, we can show that $\mathcal{Q}_\ell$ coincide with the Aretakis constants on the future Poincaré horizon, $\mathcal{H}_\ell$ in Eq. (5.4). For this purpose, we introduce the following proposition.

Proposition 3 *For analytic solutions of the massive Klein-Gordon equation with the mass squared $\ell(\ell+1)$, $(\ell = 0, 1, 2, \cdots)$ in AdS_2,*

$$\left[2\partial_v\partial_r + 2r\partial_r + r^2\partial_r^2 - \ell(\ell+1)\right]\Phi(v, r) = 0, \tag{5.53}$$

the relation

$$2^{-n_1+n_{-1}} r^{-2n_{-1}-n_0}\partial_r D_{i_\ell,1} D_{i_{\ell-1},2} \cdots D_{i_1,\ell}\Phi = \partial_r^{\ell+1}\Phi + \mathcal{O}(r), \tag{5.54}$$

holds, where n_{-1}, n_0, n_1 are the numbers of times we have acted on the mass ladder operators made from $\zeta_{-1}, \zeta_0, \zeta_1$, respectively. The numbers n_{-1}, n_0, n_1 satisfy $n_{-1} + n_0 + n_1 = \ell$.

The proof is given in Appendix D.2. Because $\mathcal{H}_\ell = \partial_r^{\ell+1}\Phi|_{r=0}$, the above proposition and Eq. (5.52) show $\mathcal{Q}_\ell|_{r=0} = \mathcal{H}_\ell$ if $C_W = 2^{-n_1+n_{-1}}$ and $q = 2n_{-1} + n_0$. We should note that regardless of the choice of the closed conformal Killing vectors $\zeta_{-1}, \zeta_0, \zeta_1$, $\mathcal{Q}_\ell|_{r=0}$ relate with the same conserved quantities $\mathcal{H}_\ell$.

5.3.3 Relation with the generalized Aretakis constants

We shall discuss the relation between $\mathcal{Q}_\ell$ in Eq. (5.50) and the generalized Aretakis constants $\mathcal{A}_\ell$ in Eq. (5.20) on any null hypersurfaces. For convenience, in the construction of $\mathcal{Q}_\ell$ in Eq. (5.50), we use the general mass ladder operators in Eq. (D.14) instead of the mass ladder operators $D_{i,k}$. The quantities $\mathcal{Q}_\ell$ are still independent of V. After some calculations, we can see that $\mathcal{Q}_\ell$ are functions proportional to the generalized Aretakis constants $\mathcal{A}_\ell$. Let those coefficient functions be $C(U)$ such that $(C(U)/W(U))\mathcal{Q}_\ell = \mathcal{A}_\ell$, where $W(U)$ is in Eq. (5.50). Choosing $W(U)$ so that $W(U) = C(U)$, $\mathcal{Q}_\ell$ coincide with the generalized Aretakis constants $\mathcal{A}_\ell$ up to the factor.

We comment on the behavior of $\mathcal{Q}_\ell$ constructed above at the Poicaré horizon $U = \pi/2$. If $\mathcal{Q}_\ell$ is constructed without ξ_1, its coefficient function $C(U)$ is singular at the future Poincaré horizon $U = \pi/2$. On the other hand, if $\mathcal{Q}_\ell$ is constructed only by ξ_1, $C(U)$ is a constant at $U = \pi/2$. This is consistent with discussion for the Aretakis constants $\mathcal{H}_\ell$ at the Poincaré horizon as already seen in the previous subsection.

5.4 Summary of this chapter

In this chapter, we have studied the geometrical meaning of the Aretakis constants and instability for massive scalar fields in AdS_2. We have shown that the Aretakis constants and instability in AdS_2 can be understood as some components of the higher-order covariant derivatives of the scalar fields in the parallelly propagated null geodesic frame being constant or unbounded at the future Poincaré horizon. Because of the maximal symmetry of AdS_2, the same discussion holds not only on the future Poincaré horizon but also on any null hypersurfaces. We have clarified that the generalization of the Aretakis constants [132] called the generalized Aretakis constants have the same geometrical meaning as that in the future Poincaré horizon; i.e., some components of the higher-order covariant derivatives in the parallelly propagated null geodesic frame are constant at each null hypersurface. Also, we have seen that the higher-order covariant derivatives of the scalar fields have singular behaviors at the whole AdS boundary, and that causes the Aretakis instability in AdS_2. If we consider cases for the mass squared with $m^2_{\mathrm{BF}} < m^2 < 0$, where $m^2_{\mathrm{BF}} = -1/4$ is the Breitenlohner-Freedman bound [134, 135], the first order covariant derivatives of the scalar fields are divergent at the AdS boundary. This implies that some physical quantities such as components of the energy-momentum tensor also have divergent behaviors at the AdS boundary for $m^2_{\mathrm{BF}} < m^2 < 0$.

We have also discussed the relation with the spacetime conformal symmetry. For the fields with the mass squared $m^2 = \ell(\ell+1)$ ($\ell = 0, 1, 2, \cdots$), the contraction with the rank-$(\ell+2)$ conformal Killing tensor and the $(\ell+2)$th-order covariant derivatives of the field is divergent at the whole AdS boundary if the generalized Aretakis constant exists. If we see this divergent behavior on a null hypersurface, it corresponds to the Aretakis instability. We note that the generalized Aretakis constants can be expressed as the contraction with the rank-$(\ell+1)$ conformal Killing tensor and the $(\ell+1)$th-order covariant derivatives [132]. We have demonstrated that the generalized Aretakis constants can be derived from the mass ladder operators constructed from the closed conformal Killing vectors [132].

Chapter 6

Conclusions

In this thesis, we have studied the black hole perturbation theory to spherically symmetric black holes. In chapter 2, we have reviewed the basic properties of maximally symmetric spacetimes, spherically symmetric spacetimes, the Schwarzschild spacetimes, and the Reissner-Nordström spacetime. In chapter 3, we have explored dynamics of linear perturbations in spherically symmetric black holes.

In chapter 4, we have analytically and numerically studied quasinormal mode frequencies of neutral and charged scalar field perturbations in the small charged AdS black holes with the Robin boundary condition parametrized by ζ and discussed the stability. In the case of the neutral field, we have shown that there exists a critical value ζ_c beyond which there are two quasinormal mode frequencies that have vanishing real part but positive and negative values for the imaginary part. This result indicates instability which arises from the boundary condition. At $\zeta = \zeta_c$, there exists a static neutral perturbation in the charged AdS black hole. As for the charged scalar field, we have found a criterion in that the black hole is superradiantly unstable irrespectively of ζ. On the other hand, if the criterion is not satisfied, the stability crucially depends on ζ. There appears a purely oscillating mode at the onset of the instability. We have further demonstrated that the superradiant instability can be enhanced by the boundary condition. We have shown that the superradiance in this system extracts energy not from the black hole but from its ambient electric field and that it extracts charge from the black hole and thus weakens its ambient electric field. This can be interpreted as a classical scalar-field counterpart of discharging a black hole by the Schwinger effect. The black hole increases its energy within the horizon, decreases the absolute value of its charge, increases its area, but decreases its mass parameter, as long as the black hole is much smaller than the AdS length.

In the context of AdS/CFT correspondence, the instabilities of the AdS black hole are expected to imply the phase transition of dual theories. Our result suggests the new dynamics of the dual quantum field theory. Also, we would like to know the final fate of the instabilities. The hairy black hole solution with the nontrivial ambient scalar field could be a candidate for the final fate of the instabilities we have shown. For the charged scalar field case, both the black hole and the charged field have charges of the same sign. The construction of the hairy black hole solution remain for our outlook .

In chapter 5, we have studied the geometrical meaning of the Aretakis constants and instability of extremal black holes in terms of massive scalar fields in AdS_2. We have shown that the Aretakis constants and instability in AdS_2 can be understood as some components of the higher-order covariant derivatives of the scalar fields in the parallelly propagated null geodesic frame being constant or unbounded at the future Poincaré horizon. The generalization of the Aretakis constants [132] called the generalized Aretakis constants have also the same geometrical meaning at each null hypersurface as that in the future Poincaré horizon. We have further seen that the higher-order covariant derivatives of the scalar fields have singular behaviors at the whole AdS boundary, and that causes the Aretakis instability in AdS_2. We have also discussed the relation with the spacetime conformal symmetry. For the fields with the mass squared $m^2 = \ell(\ell+1)$ $(\ell = 0, 1, 2, \cdots)$, the contraction with the rank-$(\ell+2)$ conformal Killing tensor and the $(\ell+2)$th-order covariant derivatives of the field is divergent at the whole AdS boundary if the generalized Aretakis constant exists. We have demonstrated that the generalized Aretakis constants can be derived from the mass ladder operators constructed from the closed conformal Killing vectors [132].

Our work implies that the Aretakis instability is universal in extremal black holes. However, we still have some questions: What initial data do exhibit the Aretakis instability? To what extent generic is it? What physical parameters do determine the exponent of that polynomial growth? How does the presence of surface gravity affect it? Part of the answers to these questions is given in our recent work [136].

Appendix A

Spherical harmonic decompositions and the Ragge-Wheeler gauge

We briefly review decompositions of vectors, symmetric tensors, and the Regge-Wheeler gauge used in section 3.2.2.

A.1 Spherical decompositions of vectors and symmetric second rank tensors on the unit two-sphere

We first give two important propositions [63]:

Proposition A.1 *Let $(\mathcal{M}, \gamma_{AB})$ be a compact Reimannian Manifold. Any vector v_A on $\mathcal{M}$ can be uniquely decomposed as*

$$v_A = V_A + D_A S, \tag{A.1}$$

where D_A is the covariant derivative with respect to the metric γ_{AB} and $D^A V_A = 0$. We refer to V_A and S as the vector and scalar components of v_A, respectively.

Proposition A.2 *Let $(\mathcal{M}, \gamma_{AB})$ be a compact Reimannian Einstein space in $(n-2)$ dimensions. Any second rank symmetric tensor t_{AB} on $\mathcal{M}$ can be*

uniquely decomposed as

$$t_{AB} = T_{AB} + \frac{1}{2}\left(D_A V_B + D_B V_A\right) + \left(D_A D_B - \frac{1}{n-2}\gamma_{AB} D^C D_C\right) S + \frac{1}{n-2}\gamma_{AB} t^C{}_C, \tag{A.2}$$

where D_A is the covariant derivative with respect to the metric γ_{AB} and $D^A T_{AB} = 0$, $T^A{}_A = 0$, and $D^A V_A = 0$. We refer to T_{AB}, V_A, and $(S, t^C{}_C)$ as the tensor, vector, and scalar components of t_{AB}, respectively.

A manifold with the metric γ_{AB} is said to be the Einstein space if the metric satisfies $R_{AB} = c\gamma_{AB}$ for a constant c.

We next introduce the notion of spherical harmonic decompositions of scalar and vector fields on the unit two-sphere, S^2. We define the scalar spherical harmonics $Y_{\ell m}(\theta, \varphi)$ as

$$\left(D_A D^A + k_s^2\right) Y_{\ell m} = 0, \tag{A.3}$$

where D_A is the covariant derivative associated with the metric of S^2 and with

$$\int_{S^2} d\Omega \; Y_{\ell m} Y_{\ell' m'} = \delta_{\ell,\ell'} \delta_{m,m'}, \tag{A.4}$$

where $d\Omega = \sin\theta d\theta d\varphi$ and $k_s^2 = \ell(\ell+1)$ for $\ell = 0, 1, 2, \cdots$. Here, $D_A D^A$ is the Laplacian on S^2. An important property of the scalar spherical harmonics is the completeness, i.e., any arbitrary scalar function on S^2, $F(t, r, \theta, \varphi)$, can be expanded as

$$F\left(t, r, \theta, \varphi\right) = \sum_{\ell=0}^{\infty} \sum_{m=-\ell}^{\ell} f_{\ell m}(t, r) Y_{\ell m}, \tag{A.5}$$

where $f_{\ell m}$ is a scalar function of (t, r). Under the parity transformation $\theta \to \pi - \theta$ and $\varphi \to \varphi + \pi$, the scalar spherical harmonics transform as $Y_{\ell m} \to (-1)^\ell Y_{\ell m}$.

We also define the vector spherical harmonics $\mathbb{V}_{\ell m A}$ as

$$\left(D_A D^A + k_v^2\right) \mathbb{V}_{\ell m B} = 0, \quad D^A \mathbb{V}_{\ell m A} = 0, \tag{A.6}$$

with

$$\int_{S^2} d\Omega \; \mathbb{V}_{\ell m A} \mathbb{V}_{\ell' m'}{}^A = \delta_{\ell,\ell'} \delta_{m,m'}, \tag{A.7}$$

where $k_v^2 = \ell(\ell+1) - 1$ for $\ell = 1, 2, \cdots$. The vector spherical harmonics also form a complete set, i.e., a vector V_A on S^2 such that $D^A V_A = 0$ can be expanded as

$$V_A\left(t, r, \theta, \varphi\right) = \sum_{\ell=1}^{\infty} \sum_{m=-\ell}^{\ell} v_{\ell m}(t, r) \mathbb{V}_{\ell m A}, \tag{A.8}$$

where $v_{\ell m}$ is a scalar function of (t, r) on S^2 for rotations. Note that on S^2 the vector spherical harmonics $\mathbb{V}_{\ell mA}$ can be written in terms of the scalar spherical harmonics as

$$\mathbb{V}_{\ell mA} = \epsilon_{AB} D^B Y_{\ell m}, \tag{A.9}$$

where ϵ_{AB} is the Levi-Civita tensor on S^2, which has the nonvanising components $\epsilon_{\theta\varphi} = -\epsilon_{\varphi\theta} = \sin\theta$ in spherical coordinates. Under the parity transformation $\theta \to \pi - \theta$ and $\varphi \to \varphi + \pi$, the vector spherical harmonics transform as $\mathbb{V}_{\ell mA} \to (-1)^{\ell+1}\mathbb{V}_{\ell mA}$. In the case of S^{n-2} for $n \geq 5$, we can further define the tensor spherical harmonics that are trivial in S^2.

Let γ_{AB} be the metric of S^2. The space (S^2, γ_{AB}) is the Einstein space with $R_{AB} = \gamma_{AB}$. Thus, proposition A.1 and also proposition A.2 in S^2 can apply. Our strategy is to project tensor field perturbations into parts that are tangent and orthogonal to S^2, and to decompose vector and tensor fields projected on S^2 into scalar and vector components of them, and to expand each component on S^2 in terms of suitable spherical harmonics. Now, we project tensor field perturbations h_{ab} as

$$\begin{aligned} h_{ab}dx^a dx^b =& h_{tt}dt^2 + 2h_{tr}dtdr + h_{rr}dr^2 \\ &+ 2h_{tA}dtdx^A + 2h_{rA}drdx^A \\ &+ h_{AB}dx^A dx^B, \end{aligned} \tag{A.10}$$

where, now, (A, B) run over $2, 3$. The orthogonal-orthogonal projections to S^2, i.e., h_{tt}, h_{tr}, and h_{rr}, are a scalar with respect to rotations. The orthogonal-tangent projections, i.e., h_{tA} and h_{rA}, are a vector on S^2 and hence can be decomposed into their scalar and vector components by proposition A.1. The tangent-tangent projection h_{AB} is a tensor on S^2 and hence can further be decomposed into their scalar and vector components by proposition A.2. Expanding each component in terms of spherical harmonics, the tensor field perturbations can be expressed by the form

$$h_{ab} = h_{ab}^{polar} + h_{ab}^{axial}, \tag{A.11}$$

where

$$
\begin{aligned}
h_{ab}^{polar} = & \sum_{\ell=0}^{\infty} \sum_{m=-\ell}^{\ell} \left[h_{\ell m}^{tt}(t,r) \left(\boldsymbol{t}_{\ell m}^{tt} \right)_{ab} + h_{\ell m}^{Rt}(t,r) \left(\boldsymbol{t}_{\ell m}^{Rt} \right)_{ab} \right] \\
& + \sum_{\ell=0}^{\infty} \sum_{m=-\ell}^{\ell} \left[h_{\ell m}^{L0}(t,r) \left(\boldsymbol{t}_{\ell m}^{L0} \right)_{ab} + h_{\ell m}^{T0}(t,r) \left(\boldsymbol{t}_{\ell m}^{T0} \right)_{ab} \right] \\
& + \sum_{\ell=1}^{\infty} \sum_{m=-\ell}^{\ell} \left[h_{\ell m}^{Et}(t,r) \left(\boldsymbol{t}_{\ell m}^{Et} \right)_{ab} + h_{\ell m}^{E1}(t,r) \left(\boldsymbol{t}_{\ell m}^{E1} \right)_{ab} \right] \\
& + \sum_{\ell=2}^{\infty} \sum_{m=-\ell}^{\ell} h_{\ell m}^{E2}(t,r) \left(\boldsymbol{t}_{\ell m}^{E2} \right)_{ab},
\end{aligned}
\tag{A.12}
$$

and

$$
\begin{aligned}
h_{ab}^{axial} = & \sum_{\ell=1}^{\infty} \sum_{m=-\ell}^{\ell} \left[h_{\ell m}^{Bt}(t,r) \left(\boldsymbol{t}_{\ell m}^{Bt} \right)_{ab} + h_{\ell m}^{B1}(t,r) \left(\boldsymbol{t}_{\ell m}^{B1} \right)_{ab} \right] \\
& + \sum_{\ell=2}^{\infty} \sum_{m=-\ell}^{\ell} h_{\ell m}^{B2}(t,r) \left(\boldsymbol{t}_{\ell m}^{B2} \right)_{ab},
\end{aligned}
\tag{A.13}
$$

with

$$
\begin{aligned}
\boldsymbol{t}^{tt}_{\ell m} &= \begin{pmatrix} 1 & 0 & 0 & 0 \\ 0 & 0 & 0 & 0 \\ 0 & 0 & 0 & 0 \\ 0 & 0 & 0 & 0 \end{pmatrix} Y_{\ell m}, \quad \boldsymbol{t}^{Rt}_{\ell m} = \begin{pmatrix} 0 & 1 & 0 & 0 \\ 1 & 0 & 0 & 0 \\ 0 & 0 & 0 & 0 \\ 0 & 0 & 0 & 0 \end{pmatrix} Y_{\ell m}, \\
\boldsymbol{t}^{L0}_{\ell m} &= \begin{pmatrix} 0 & 0 & 0 & 0 \\ 0 & 1 & 0 & 0 \\ 0 & 0 & 0 & 0 \\ 0 & 0 & 0 & 0 \end{pmatrix} Y_{\ell m}, \quad \boldsymbol{t}^{T0}_{\ell m} = \begin{pmatrix} 0 & 0 & 0 & 0 \\ 0 & 0 & 0 & 0 \\ 0 & 0 & 1 & 0 \\ 0 & 0 & 0 & \sin^2\theta \end{pmatrix} Y_{\ell m}, \\
\boldsymbol{t}^{Et}_{\ell m} &= \begin{pmatrix} 0 & 0 & \partial_\theta & \partial_\varphi \\ 0 & 0 & 0 & 0 \\ \partial_\theta & 0 & 0 & 0 \\ \partial_\varphi & 0 & 0 & 0 \end{pmatrix} Y_{\ell m}, \quad \boldsymbol{t}^{E1}_{\ell m} = \begin{pmatrix} 0 & 0 & 0 & 0 \\ 0 & 0 & \partial_\theta & \partial_\varphi \\ 0 & \partial_\theta & 0 & 0 \\ 0 & \partial_\varphi & 0 & 0 \end{pmatrix} Y_{\ell m}, \\
\boldsymbol{t}^{Bt}_{\ell m} &= \begin{pmatrix} 0 & 0 & (1/\sin\theta)\partial_\varphi & -\sin\theta\partial_\theta \\ 0 & 0 & 0 & 0 \\ (1/\sin\theta)\partial_\varphi & 0 & 0 & 0 \\ -\sin\theta\partial_\theta & 0 & 0 & 0 \end{pmatrix} Y_{\ell m}, \qquad \text{(A.14)} \\
\boldsymbol{t}^{B1}_{\ell m} &= \begin{pmatrix} 0 & 0 & 0 & 0 \\ 0 & 0 & (1/\sin\theta)\partial_\varphi & -\sin\theta\partial_\theta \\ 0 & (1/\sin\theta)\partial_\varphi & 0 & 0 \\ 0 & -\sin\theta\partial_\theta & 0 & 0 \end{pmatrix} Y_{\ell m}, \\
\boldsymbol{t}^{E2}_{\ell m} &= \begin{pmatrix} 0 & 0 & 0 & 0 \\ 0 & 0 & 0 & 0 \\ 0 & 0 & W & X \\ 0 & 0 & X & -\sin^2\theta W \end{pmatrix} Y_{\ell m}, \\
\boldsymbol{t}^{B2}_{\ell m} &= \begin{pmatrix} 0 & 0 & 0 & 0 \\ 0 & 0 & 0 & 0 \\ 0 & 0 & -(1/\sin\theta)X & \sin\theta W \\ 0 & 0 & \sin\theta W & \sin\theta X \end{pmatrix} Y_{\ell m},
\end{aligned}
$$

where

$$
X = 2\partial_\theta\partial_\varphi - \frac{2}{\tan\theta}\partial_\varphi, \quad W = \partial_\theta^2 - \frac{1}{\tan\theta}\partial_\theta - \frac{1}{\sin^2\theta}\partial_\varphi^2. \qquad \text{(A.15)}
$$

Under the parity transformation $\theta \to \pi - \theta$ and $\varphi \to \varphi + \pi$, h^{polar}_{ab} and h^{axial}_{ab} pick up the factor $(-1)^\ell$ and $(-1)^{\ell+1}$, respectively.

A.2 Tensor field perturbations in the Regge-Wheeler gauge

We consider the gauge freedom to formulate the gauge-invariant perspective. Under an infinitesimal coordinate transformation $x^a \to x^a + \xi^a$, h_{ab} transforms as

$$h_{ab} \to h_{ab} - \left(\nabla^{(0)}_a \xi_b + \nabla^{(0)}_b \xi_a \right), \tag{A.16}$$

where $\nabla^{(0)}_a$ is the covariant derivative associated with the Schwarzschild metric (2.36). To simplify Eqs. (A.12) and (A.13), we exploit this gauge freedom as in the tensor field perturbations in the Minkowski spacetime in section 3.1.

Axial perturbations

First, we consider the gauge transformation generated by an axial vector

$$\xi^{axial}_a = \sum_{\ell=1}^{\infty} \sum_{m=-\ell}^{\ell} \Lambda_{\ell m}(t,r) \left(0, 0, -\frac{\partial_\varphi}{\sin\theta}, \sin\theta \partial_\theta \right) Y_{\ell m}. \tag{A.17}$$

Then, we have

$$\begin{aligned} \nabla^{(0)}_a \xi^{axial}_b + \nabla^{(0)}_b \xi^{axial}_a = &- \sum_{\ell=1}^{\infty} \sum_{m=-\ell}^{\ell} \left(\partial_t \Lambda_{\ell m} \right) \left(\boldsymbol{t}^{Bt}_{\ell m} \right)_{ab} \\ &- \sum_{\ell=1}^{\infty} \sum_{m=-\ell}^{\ell} \left(\partial_r \Lambda_{\ell m} - \frac{2}{r} \Lambda_{\ell m} \right) \left(\boldsymbol{t}^{B1}_{\ell m} \right)_{ab} \\ &+ \sum_{\ell=2}^{\infty} \sum_{m=-\ell}^{\ell} \Lambda_{\ell m} \left(\boldsymbol{t}^{B2}_{\ell m} \right)_{ab}. \end{aligned} \tag{A.18}$$

On the last line of the right-hand side, we have used the result that $\boldsymbol{t}^{B2}_{\ell m}$ vanishes for $\ell = 1$. It follows from Eq. (A.18) that the gauge transformation generated by ξ^{axial}_a does affect only on h^{axial}_{ab} via Eq. (A.16), while leaves h^{polar}_{ab} invariant. In particular, using Eq. (A.18) and comparing Eq. (A.16) with Eq. (A.13), we can see that each component of (t, r) in h^{axial}_{ab} act as

$$\begin{aligned} h^{Bt}_{\ell m} &\to h^{Bt}_{\ell m} + \partial_t \Lambda_{\ell m}, \\ h^{B1}_{\ell m} &\to h^{B1}_{\ell m} + \partial_r \Lambda_{\ell m} - \frac{2\Lambda_{\ell m}}{r}, \\ h^{B2}_{\ell m} &\to h^{B2}_{\ell m} - \Lambda_{\ell m}. \end{aligned} \tag{A.19}$$

under the transformation. We now choose $\Lambda_{\ell m}$ so that $h^{B2}_{\ell m} = 0$ for all $\ell \geq 2$. Besides, the remaining freedom of $\Lambda_{\ell m}$ for $\ell = 1$ is used to set $h^{Bt}_{\ell m} = 0$ for $\ell = 1$. This gauge choice is called the *Regge-Wheeler gauge*. In this gauge fixing, h^{axial}_{ab} takes the form

$$h^{axial}_{ab} = \sum_{\ell=2}^{\infty} \sum_{m=-\ell}^{\ell} h^{Bt}_{\ell m} \left(\boldsymbol{t}^{Bt}_{\ell m}\right)_{ab} + \sum_{\ell=1}^{\infty} \sum_{m=-\ell}^{\ell} h^{B1}_{\ell m} \left(\boldsymbol{t}^{B1}_{\ell m}\right)_{ab}. \tag{A.20}$$

Redefining

$$\begin{aligned} h^{Bt}_{\ell m} &= - h^{(0)}_{\ell m}(t, r), \\ h^{B1}_{\ell m} &= - h^{(1)}_{\ell m}(t, r), \end{aligned} \tag{A.21}$$

Eq. (A.20) yields Eq. (3.22).

We can observe from Eq. (A.19) that there is the gauge-invariant quantity

$$q_{\ell m} \equiv -h^{B1}_{\ell m} - \left(\partial_r - \frac{2}{r}\right) h^{B2}_{\ell m}, \tag{A.22}$$

for $\ell \geq 2$. In particular, in the Regge-Wheeler gauge, we have

$$q_{\ell m} = -h^{B1}_{\ell m}. \tag{A.23}$$

Therefore, with Eq. (A.21), the quantity

$$Q_{\ell m}(t, r) = \frac{1}{r}\left(1 - \frac{2M}{r}\right) h^{(1)}_{\ell m}(t, r), \tag{A.24}$$

also has a gauge-invariant meaning in the Regge-Wheeler gauge.

Polar perturbations

Next, we consider the gauge transformation generated by a polar vector

$$\begin{aligned} \xi^{polar}_a = &\sum_{\ell=0}^{\infty} \sum_{m=-\ell}^{\ell} \left(\Lambda^{(t)}_{\ell m}(t, r), \Lambda^{(R)}_{\ell m}(t, r), 0, 0\right) Y_{\ell m} \\ &+ \sum_{\ell=1}^{\infty} \sum_{m=-\ell}^{\ell} \Lambda^{(E)}_{\ell m}(t, r) \left(0, 0, \partial_\theta, \partial_\varphi\right) Y_{\ell m}. \end{aligned} \tag{A.25}$$

Then, we have[1]

$$
\begin{aligned}
h^{tt}_{\ell m} \to & h^{tt}_{\ell m} - \left[2\partial_t \Lambda^{(t)}_{\ell m} - \frac{2M}{r^2}\left(1-\frac{2M}{r}\right)\Lambda^{(R)}_{\ell m} \right], \\
h^{Rt}_{\ell m} \to & h^{Rt}_{\ell m} - \left[\partial_t \Lambda^{(R)}_{\ell m} + \partial_r \Lambda^{(t)}_{\ell m} - \frac{2M}{r^2}\left(1-\frac{2M}{r}\right)^{-1}\Lambda^{(t)}_{\ell m} \right], \\
h^{L0}_{\ell m} \to & h^{L0}_{\ell m} - \left[2\partial_r \Lambda^{(R)}_{\ell m} + \frac{2M}{r^2}\left(1-\frac{2M}{r}\right)^{-1}\Lambda^{(R)}_{\ell m} \right], \\
h^{T0}_{\ell m} \to & h^{T0}_{\ell m} - \left[2r\left(1-\frac{2M}{r}\right)\Lambda^{(R)}_{\ell m} - \ell(\ell+1)\Lambda^{(E)}_{\ell m} \right], \\
h^{Et}_{\ell m} \to & h^{Et}_{\ell m} - \left[\Lambda^{(t)}_{\ell m} + \partial_t \Lambda^{(E)}_{\ell m} \right], \\
h^{E1}_{\ell m} \to & h^{E1}_{\ell m} - \left[\left(\partial_r - \frac{2}{r}\right)\Lambda^{(E)}_{\ell m} + \Lambda^{(R)}_{\ell m} \right], \\
h^{E2}_{\ell m} \to & h^{E2}_{\ell m} - \Lambda^{(E)}_{\ell m}.
\end{aligned}
\tag{A.26}
$$

First, we choose $\Lambda^{(E)}_{\ell m}$ so that $h^{E2}_{\ell m} = 0$ for all $\ell \geq 2$. We also choose $\Lambda^{(R)}_{\ell m}$ so that $h^{E1}_{\ell m} = 0$ for $\ell \geq 1$ and $\Lambda^{(t)}_{\ell m}$ so that $h^{Et}_{\ell m} = 0$ for $\ell \geq 1$. We still have the freedom $\Lambda^{(E)}_{1m}$, $\Lambda^{(R)}_{00}$ and $\Lambda^{(t)}_{00}$. We use the function $\Lambda^{(E)}_{1m}$ so that $h^{T0}_{\ell m} = 0$ for $\ell = 1$ and further exploit $\Lambda^{(R)}_{00}$ so that $h^{T0}_{\ell m} = 0$ for $\ell = 0$. We finally choose $\Lambda^{(t)}_{00}$ so that $h^{Rt}_{\ell m} = 0$ for $\ell = 0$. We thus have the expression of h^{polar}_{ab} in the Regge-Wheeler gauge,

$$
\begin{aligned}
h^{polar}_{ab} = & \sum_{\ell=0}^{\infty}\sum_{m=-\ell}^{\ell}\left[h^{tt}_{ab}\left(\boldsymbol{t}^{tt}_{\ell m}\right)_{ab} + h^{L0}_{ab}\left(\boldsymbol{t}^{L0}_{\ell m}\right)_{ab} \right] \\
& + \sum_{\ell=1}^{\infty}\sum_{m=-\ell}^{\ell} h^{Rt}_{ab}\left(\boldsymbol{t}^{Rt}_{\ell m}\right)_{ab} + \sum_{\ell=2}^{\infty}\sum_{m=-\ell}^{\ell} h^{T0}_{ab}\left(\boldsymbol{t}^{T0}_{\ell m}\right)_{ab}.
\end{aligned}
\tag{A.27}
$$

[1]Maggiore [137] has a typo in Eq. (12.72): the derivative of $\xi^{(R)}_{\ell m}$ is that with respect to t in [137] but the correct one is that with respect to r as $\partial_r \Lambda^{(R)}_{\ell m}$ in the third line of Eq. (A.26).

Redefining

$$\begin{aligned} h^{tt}_{\ell m} &= \left(1-\frac{2M}{r}\right) H^{(0)}_{\ell m}(t,r), \\ h^{L0}_{\ell m} &= \left(1-\frac{2M}{r}\right)^{-1} H^{(2)}_{\ell m}(t,r), \\ h^{Rt}_{\ell m} &= H^{(1)}_{\ell m}(t,r), \\ h^{T0}_{\ell m} &= r^2 K_{\ell m}(t,r), \end{aligned} \tag{A.28}$$

Eq. (A.27) gives rise to Eq. (3.21).

For $\ell \geq 2$, we have the gauge-invariant quantity

$$\begin{aligned} \tilde{z}_{\ell m}(\omega,r) \equiv & \tilde{h}^{T0}_{\ell m} + \frac{r}{i\omega}\left(1-\frac{2M}{r}\right)\tilde{h}^{RT}_{\ell m} \\ & - \frac{1}{i\omega}\left[r\left(1-\frac{2M}{r}\right)\partial_r - \frac{2M}{r}\right]\tilde{h}^{Et}_{\ell m} - r\left(1-\frac{2M}{r}\right)\tilde{h}^{E1}_{\ell m} + \frac{2}{r}\left(\lambda r + 3M\right)\tilde{h}^{E2}_{\ell m}, \end{aligned} \tag{A.29}$$

where $\lambda \equiv (\ell+2)(\ell-1)/2$ and the functions with tilde denote the Fourier components in the frequency domain with respect to t,

$$\tilde{h}^{k}_{\ell m}(\omega,r) = \int_{-\infty}^{\infty} dt\ e^{i\omega t} h^{k}_{\ell m}(t,r), \tag{A.30}$$

with $k = T0, RT, Et, E1, E2$. In the Regge-Wheeler gauge, we rewrite as

$$\tilde{z}_{\ell m} = \tilde{h}^{T0}_{\ell m} + \frac{r}{i\omega}\left(1-\frac{2M}{r}\right)\tilde{h}^{RT}_{\ell m}. \tag{A.31}$$

With Eq. (A.28), the quantity

$$\tilde{Z}_{\ell m}(\omega,r) = \frac{r^2}{\lambda r + 3M}\tilde{K}_{\ell m} + \frac{r}{i\omega(\lambda r+3M)}\left(1-\frac{2M}{r}\right)\tilde{H}^{(1)}_{\ell m}, \tag{A.32}$$

is also gauge-invariant in the Regge-Wheeler gauge.

Appendix B

Appendix of Chapter 4

B.1 Positive self-adjoint extension of symmetric operators

Here we provide definitions for the mathematical notions used in Section 4.2.

A subset D of $\mathcal{H}$ is said to be *dense* if D satisfies $\mathcal{H} = \bar{D}$, where $\bar{D}$ is the closure of D. A vector $\psi \in \mathcal{H}$ is said to be *normalisable* if and only if $(\psi, \psi) < \infty$. The domain of a linear operator $\mathcal{O}$ is denoted by $D(\mathcal{O})$.

A linear operator $\mathcal{O}$ is said to be *positive* if and only if $(\psi, \mathcal{O}\psi) > 0$ for any nonzero vector $\psi \in D(\mathcal{O})$, where $(\cdot, \cdot)$ stands for the inner product. A linear operator $\mathcal{P}$ is said to be an *adjoint* of $\mathcal{O}$ if and only if $(\psi, \mathcal{O}\phi) = (\Theta, \phi)$ and $\mathcal{P}\psi = \Theta$ for any vectors $\phi \in D(\mathcal{O})$, $\psi \in D(\mathcal{P})$ and $\Theta \in \mathcal{H}$. The adjoint of $\mathcal{O}$ is denoted by $\mathcal{O}^*$. A linear operator $\mathcal{P}$ is said to be an *extension* of $\mathcal{O}$ if and only if $D(\mathcal{O}) \subset D(\mathcal{P})$.

A linear operator $\mathcal{O}$ is said to be *symmetric* if all of the following three conditions are satisfied: (i) $D(\mathcal{O})$ is dense, (ii) $(\psi, \mathcal{O}\phi) = (\mathcal{O}\psi, \phi)$ for any vectors $\psi, \phi \in D(\mathcal{O})$, and (iii) $D(\mathcal{O}) \subset D(\mathcal{O}^*)$. Therefore, the adjoint of a symmetric operator is an extension of the symmetric operator.

A symmetric operator $\mathcal{O}$ is said to be *bounded below if and only if there exists* $\gamma \in \mathbb{R}$ *such that* $(\mathcal{O}\psi, \psi) \geq \gamma(\psi, \psi)$ for any vector $\psi \in D(\mathcal{O})$. A symmetric operator is said to be *unbounded below* if and only if it is not bounded below.

A linear operator $\mathcal{O}$ is said to be *self-adjoint* if and only if all of the following three conditions are satisfied: (i) $D(\mathcal{O})$ is dense, (ii) $(\psi, \mathcal{O}\phi) = (\mathcal{O}\psi, \phi)$ for any vectors $\psi, \phi \in D(\mathcal{O})$, and (iii) $D(\mathcal{O}) = D(\mathcal{O}^*)$. One can obtain a self-adjoint operator by extending a symmetric operator [121, 109]. Thus obtained self-adjoint operator is called *self-adjoint extension*.

B.2 Validity of the matching of the near-region and far-region solutions

We introduce a small parameter $\epsilon = r_+/\ell$ and a nondimensional coordinate $x = r/r_+$. First we focus on the validity of the near-horizon solution. Eq. (4.47) is rewritten in the form

$$\mathcal{E}_1(x) = -\frac{(\epsilon x)^2}{1-\frac{r_-}{r_+}}\left[-\mu^2\ell^2\left(x-\frac{r_-}{r_+}\right)+(\tilde{\omega}\ell)^2(1+x)\left(1+\frac{1}{x^2}\right)\right.$$
$$\left.-2(\tilde{\omega}\ell)\left(\frac{eQ}{\epsilon}\right)\left(1+\frac{1}{x}+\frac{1}{x^2}\right)+\left(\frac{eQ}{\epsilon}\right)^2\left(\frac{1}{x}+\frac{1}{x^2}\right)\right]. \tag{B.1}$$

Because $-(\tilde{\omega}\ell)(eQ) \leq |\tilde{\omega}\ell||eQ|$, we find an inequality $|\mathcal{E}_1(x)| \leq \tilde{\mathcal{E}}_1(x)$, where we have defined

$$\tilde{\mathcal{E}}_1(x) := \frac{(\epsilon x)^2}{1-\frac{r_-}{r_+}}\left[-\mu^2\ell^2\left(x-\frac{r_-}{r_+}\right)+|\tilde{\omega}\ell|^2(1+x)\left(1+\frac{1}{x^2}\right)\right.$$
$$\left.+2|\tilde{\omega}\ell|\left(\frac{|eQ|}{\epsilon}\right)\left(1+\frac{1}{x}+\frac{1}{x^2}\right)+\left(\frac{|eQ|}{\epsilon}\right)^2\left(\frac{1}{x}+\frac{1}{x^2}\right)\right]. \tag{B.2}$$

Here we note that $\tilde{\mathcal{E}}_1(x)$ is an increasing function of x. In the limit of $1 \ll x$, the asymptotic behavior of $\tilde{\mathcal{E}}_1(x)$ can be written as

$$\tilde{\mathcal{E}}_1(x) \simeq x\left[\{|\tilde{\omega}\ell|(\epsilon x)+|eQ|\}^2-\mu^2\ell^2(\epsilon x)^2\right]. \tag{B.3}$$

As for $|ab|$, we have an inequality

$$1 < |ab| = \sqrt{4\sigma^2+(l+1)^2}. \tag{B.4}$$

Hence, $|\mathcal{E}_1(x)| \ll |ab|$ is satisfied in the region given by $1 < x \leq x_0$, if x_0 satisfies $1 \ll x_0 \ll 1/\epsilon$ and

$$\tilde{\mathcal{E}}_1(x_0) \ll 1 \Leftrightarrow \epsilon^2\left\{\left(|\tilde{\omega}\ell|+\frac{|eQ|}{\epsilon}\frac{1}{x_0}\right)^2-\mu^2\ell^2\right\} \ll \frac{1}{{x_0}^3}. \tag{B.5}$$

Assuming $\tilde{\omega}\ell = O(1)$ and $eQ = o(\epsilon^{1/3+\delta})$, we find that if we take $x_0 = c_0\epsilon^{-2/3+\delta}$ with $c_0 = O(1)$ and $0 < \delta < 2/3$, the inequality (B.5) is satisfied.

Next we focus on the validity of the far-region solution. Clearly, Eq. (4.52) is reduced to Eq. (4.21) for the neutral scalar field because of $\mathcal{E}_2(r) = 0$. For the charged field, we can approximate Eq. (4.52) to Eq. (4.21) if $\mathcal{E}_2(r)$ satisfies $h(y)|\mathcal{E}_2(y)| \ll 1$, where we have defined

$$h(y) := \frac{|g(y)|}{|y(1-y)\frac{d^2}{dy^2}g(y)| + |\{\gamma - (\alpha+\beta+1)y\}\frac{d}{dy}g(y)| + |-\alpha\beta g(y)|}. \tag{B.6}$$

Substituting Eq. (4.23) into the above $g(y)$, we notice $\max h(y) = \mathcal{O}(1)$ for $y \lesssim 200$ with $|\tilde{\omega}\ell| = \mathcal{O}(1)$, $l = \mathcal{O}(1)$. Hence, the charged scalar field in the far region can be described by the Gaussian hypergeometric functions if $|\mathcal{E}_2(y)| \ll 1$ is satisfied. We shall discuss whether $|\mathcal{E}_2(y)| \ll 1$ is satisfied. In terms of ϵ and x, $\mathcal{E}_2(y)$ is rewritten as

$$\mathcal{E}_2(x) = \frac{1}{4(\epsilon x)^2}\frac{1}{1+(\epsilon x)^2}\left\{2(\tilde{\omega}\ell)(eQ)(\epsilon x) - (eQ)^2\right\}. \tag{B.7}$$

Noting $-(\tilde{\omega}\ell)(eQ) \leq |\tilde{\omega}\ell||eQ|$, we find

$$|\mathcal{E}_2(x)| \leq \tilde{\mathcal{E}}_2(x), \tag{B.8}$$

where we have defined

$$\tilde{\mathcal{E}}_2(x) := \frac{1}{4(\epsilon x)^2}\frac{1}{1+(\epsilon x)^2}\left\{2|\tilde{\omega}\ell||eQ|(\epsilon x) + |eQ|^2\right\}. \tag{B.9}$$

Note that $\tilde{\mathcal{E}}_2(x)$ is a decreasing function of x and $\tilde{\mathcal{E}}_2(x) \ll 1$ in the limit of $x \to \infty$. Therefore, if we can find x_1 such that $\tilde{\mathcal{E}}_2(x_1) \ll 1$ and $1 \ll x_1 \ll 1/\epsilon$, $|\mathcal{E}_2(x)| \ll 1$ is satisfied for $x_1 \leq x$. Assuming $|eQ| \ll \epsilon x_1$ and $\tilde{\omega}\ell = O(1)$, $|\mathcal{E}_2(y)| \ll 1$ holds for $x_1 \leq x < \infty$.

Finally, we discuss whether there is an overlapping region, where both the near-region and far-region solutions are valid. For the neutral field, we can match them without further discussion. The reason is that the far-region approximate solution (4.27) can describe the field everywhere in the region $1 \ll x$ and the near-region approximate solution (4.50) is valid in $1 \ll x \leq x_0$ such that $1 \ll x_0 \ll 1/\epsilon$ because there exists x_0 such that the inequality (B.5) is satisfied for $eQ = 0$ under the assumption $|\omega\ell| = \mathcal{O}(1)$. For the charged field case, assuming $|eQ| = o(\epsilon^{1/3+\delta})$ and $|\tilde{\omega}\ell| = O(1)$, if we choose $x_0 = c_0\epsilon^{-2/3+\delta}$ and $x_1 = c_1\epsilon^{-2/3+\delta}$ with $0 < c_1 < c_0$ and $0 < \delta < 2/3$, both $\tilde{\mathcal{E}}_1 \ll 1$ and $\tilde{\mathcal{E}}_2 \ll 1$ are satisfied for $x_1 \leq x \leq x_0$. Therefore, we can identify the overlapping region with the interval $x_1 \leq x \leq x_0$.

B.3 Asymptotic behaviors of the near-region and far-region solutions

We are interested in the asymptotic behavior of the far-region solution (4.27) at $y \simeq 1$. Using the transformation formula of the Gaussian hypergeometric functions [138], we obtain

$$\begin{aligned} F\left(\alpha, \alpha-\gamma+1; \alpha-\beta+1; \frac{1}{y}\right) =& y^{\alpha-\gamma+1}(y-1)^{\gamma-\alpha-\beta}\frac{\Gamma(\alpha-\beta+1)\Gamma(\alpha+\beta-\gamma)}{\Gamma(\alpha)\Gamma(\alpha-\gamma+1)} \\ & \times F(1-\alpha, 1-\beta; \gamma-\alpha-\beta; y-1) \\ & + y^{\alpha}\frac{\Gamma(\alpha-\beta+1)\Gamma(\gamma-\alpha-\beta)}{\Gamma(1-\beta)\Gamma(\gamma-\beta)} \\ & \times F(\alpha, \beta; \alpha+\beta-\gamma+1; y-1), \end{aligned} \tag{B.10}$$

and

$$\begin{aligned} F\left(\beta, \beta-\gamma+1; \beta-\alpha+1; \frac{1}{y}\right) =& y^{\beta-\gamma+1}(y-1)^{\gamma-\alpha-\beta}\frac{\Gamma(\beta-\alpha+1)\Gamma(\alpha+\beta-\gamma)}{\Gamma(\beta)\Gamma(\beta-\gamma+1)} \\ & \times F(1-\alpha, 1-\beta; \gamma-\alpha-\beta; y-1) \\ & + y^{\beta}\frac{\Gamma(\beta-\alpha+1)\Gamma(\gamma-\alpha-\beta)}{\Gamma(1-\alpha)\Gamma(\gamma-\alpha)} \\ & \times F(\alpha, \beta; \alpha+\beta-\gamma+1; y-1). \end{aligned} \tag{B.11}$$

Therefore Eq. (4.27) is rewritten in the form

$$\begin{aligned} \psi(y) =& D y^{\frac{\tilde{\omega}\ell}{2}}(y-1)^{\frac{l}{2}} \\ & \times \left[y^{-\gamma+1}(y-1)^{\gamma-\alpha-\beta}\Gamma(\alpha+\beta-\gamma)\left(\frac{\kappa\Gamma(\alpha-\beta+1)}{\Gamma(\alpha)\Gamma(\alpha-\gamma+1)} + \frac{\Gamma(\beta-\alpha+1)}{\Gamma(\beta)\Gamma(\beta-\gamma+1)}\right)\right. \\ & \times F(1-\alpha, 1-\beta; \gamma-\alpha-\beta; y-1) \\ & + \Gamma(\gamma-\alpha-\beta)\left(\frac{\kappa\Gamma(\alpha-\beta+1)}{\Gamma(1-\beta)\Gamma(\gamma-\beta)} + \frac{\Gamma(\beta-\alpha+1)}{\Gamma(1-\alpha)\Gamma(\gamma-\alpha)}\right) \\ & \left. \times F(\alpha, \beta; \alpha+\beta-\gamma+1; y-1)\right]. \end{aligned} \tag{B.12}$$

The above expression gives the asymptotic behavior (4.28).

Next we are interested in the asymptotic behavior of the near-region solution (4.50) at $z \simeq 1$. Using the transformation formula of the Gaussian

hypergeometric functions [138],

$$\begin{aligned}F(1-c+a,1-c+b;2-c;z) =& \frac{\Gamma(2-c)\Gamma(c-a-b)}{\Gamma(1-a)\Gamma(1-b)} \\ & \times F(1-c+a,1-c+b;-c+a+b+1;1-z) \\ & + (1-z)^{c-a-b}\frac{\Gamma(2-c)\Gamma(-c+a+b)}{\Gamma(1-c+a)\Gamma(1-c+b)} \\ & \times F(1-a,1-b;c-a-b+1;1-z).\end{aligned} \tag{B.13}$$

Therefore, the near-region solution (4.50) is rewritten in the form

$$\begin{aligned}\psi(z) = Bz^{-i\sigma}\Gamma(1-2i\sigma)\Bigg[& \frac{\Gamma(-2l-1)}{\Gamma(-2i\sigma-l)\Gamma(-l)}(1-z)^{l+1} \\ & \times F(1-c+a,1-c+b;-c+a+b+1;1-z) \\ & + \frac{\Gamma(2l+1)}{\Gamma(-2i\sigma+l+1)\Gamma(l+1)}(1-z)^{-l} \\ & \times F(1-a,1-b;c-a-b+1;1-z)\Bigg].\end{aligned} \tag{B.14}$$

From the above expression, we obtain the asymptotic form (4.55) with Eq. (4.56).

B.4 Symmetry $(\omega, eQ) \to (-\omega^*, -eQ)$ in the matched asymptotic expansion

Note that σ is transformed to $-\sigma^*$ by this transformation. Then, the left-hand side of Eq. (4.57) is transformed as

$$\frac{B_1(\tilde{\omega},\sigma)}{B_2(\tilde{\omega},\sigma)} \to \frac{B_1(-\tilde{\omega}^*,-\sigma^*)}{B_2(-\tilde{\omega}^*,-\sigma^*)} = \left(\frac{B_1(\tilde{\omega},\sigma)}{B_2(\tilde{\omega},\sigma)}\right)^*, \tag{B.15}$$

because $B_1(\tilde{\omega},\sigma)$ and $B_2(\tilde{\omega},\sigma)$ satisfy the relation $B_1(\tilde{\omega},\sigma) = B_1^*(-\tilde{\omega}^*,-\sigma^*)$ and $B_2(\tilde{\omega},\sigma) = B_2^*(-\tilde{\omega}^*,-\sigma^*)$. Next, the right-hand side of Eq. (4.57) is transformed as

$$\frac{D_1(\tilde{\omega},\kappa)}{D_2(\tilde{\omega},\kappa)} \to \frac{D_1(-\tilde{\omega}^*,\kappa)}{D_2(-\tilde{\omega}^*,\kappa)} = \left(\frac{D_1(\tilde{\omega},\kappa)}{D_2(\tilde{\omega},\kappa)}\right)^*, \tag{B.16}$$

because of $D_1(\tilde{\omega},\kappa) = {D_1}^*(-\tilde{\omega}^*,\kappa)$ and $D_2(\tilde{\omega},\kappa) = {D_2}^*(-\tilde{\omega}^*,\kappa)$ as stated below Eq. (4.30). Hence, this transformation brings Eq. (4.57) to

$$\left(\frac{B_1(\tilde{\omega},\sigma)}{B_2(\tilde{\omega},\sigma)}\right)^* = \ell^{2l+1}\left(\frac{D_1(\tilde{\omega},\kappa)}{D_2(\tilde{\omega},\kappa)}\right)^*. \tag{B.17}$$

Since the above is nothing but the complex conjugate of Eq. (4.57), the solution of the above is the same as the solution obtained before the transformation. Thus, the symmetry for the charged scalar field in the charged black hole is given by $(\tilde{\omega}, eQ) \to (-\tilde{\omega}^*, -eQ)$.

B.5 Explicit calculations

We give the explicit forms of $\Sigma_{1,R}$, $\Sigma_{1,I}$, $\Sigma_{2,R}$, and $\Sigma_{2,I}$ in Eqs. (4.62) and (4.63), and $\mathrm{Re}[B_1/B_2]$, $\mathrm{Im}[B_1/B_2]$ in Eqs. (4.64) and (4.66).

$\Sigma_{1,R}$ and $\Sigma_{1,I}$

$D_1(\tilde{\omega}, \kappa)$ in Eq. (4.57) is explicitly

$$\begin{aligned} D_1(\tilde{\omega}, \kappa) =& \frac{\kappa\Gamma\left(1+\frac{1}{2}\sqrt{9+4\mu^2\ell^2}\right)}{\Gamma\left(\frac{\tilde{\omega}\ell}{2}+\frac{l}{2}+\frac{3}{4}+\frac{1}{4}\sqrt{9+4\mu^2\ell^2}\right)\Gamma\left(-\frac{\tilde{\omega}\ell}{2}+\frac{l}{2}+\frac{3}{4}+\frac{1}{4}\sqrt{9+4\mu^2\ell^2}\right)} \\ &+ \frac{\Gamma\left(1-\frac{1}{2}\sqrt{9+4\mu^2\ell^2}\right)}{\Gamma\left(\frac{\tilde{\omega}\ell}{2}+\frac{l}{2}+\frac{3}{4}-\frac{1}{4}\sqrt{9+4\mu^2\ell^2}\right)\Gamma\left(-\frac{\tilde{\omega}\ell}{2}+\frac{l}{2}+\frac{3}{4}-\frac{1}{4}\sqrt{9+4\mu^2\ell^2}\right)}. \end{aligned} \tag{B.18}$$

Assuming $|\mathrm{Im}[\tilde{\omega}\ell]| \ll 1$, $D_1(\tilde{\omega}, \kappa)$ takes a form

$$D_1(\tilde{\omega}, \kappa) = \Sigma_{1,R} - i\frac{\Sigma_{1,I}}{2}\mathrm{Im}[\tilde{\omega}\ell] + \mathcal{O}\left((\mathrm{Im}[\tilde{\omega}\ell])^2\right), \tag{B.19}$$

where

$$\begin{aligned} \Sigma_{1,R} =& \frac{\kappa\Gamma\left(1+\frac{1}{2}\sqrt{9+4\mu^2\ell^2}\right)}{\Gamma\left(\frac{\mathrm{Re}[\tilde{\omega}\ell]}{2}+\frac{l}{2}+\frac{3}{4}+\frac{1}{4}\sqrt{9+4\mu^2\ell^2}\right)\Gamma\left(-\frac{\mathrm{Re}[\tilde{\omega}\ell]}{2}+\frac{l}{2}+\frac{3}{4}+\frac{1}{4}\sqrt{9+4\mu^2\ell^2}\right)} \\ &+ \frac{\Gamma\left(1-\frac{1}{2}\sqrt{9+4\mu^2\ell^2}\right)}{\Gamma\left(\frac{\mathrm{Re}[\tilde{\omega}\ell]}{2}+\frac{l}{2}+\frac{3}{4}-\frac{1}{4}\sqrt{9+4\mu^2\ell^2}\right)\Gamma\left(-\frac{\mathrm{Re}[\tilde{\omega}\ell]}{2}+\frac{l}{2}+\frac{3}{4}-\frac{1}{4}\sqrt{9+4\mu^2\ell^2}\right)}. \end{aligned} \tag{B.20}$$

and

$$\begin{aligned}\Sigma_{1,I} =&\frac{\kappa\Gamma\left(1+\frac{1}{2}\sqrt{9+4\mu^2\ell^2}\right)}{\Gamma\left(\frac{\mathrm{Re}[\tilde{\omega}\ell]}{2}+\frac{l}{2}+\frac{3}{4}+\frac{1}{4}\sqrt{9+4\mu^2\ell^2}\right)\Gamma\left(-\frac{\mathrm{Re}[\tilde{\omega}\ell]}{2}+\frac{l}{2}+\frac{3}{4}+\frac{1}{4}\sqrt{9+4\mu^2\ell^2}\right)}\\ &\times\left(P\left(\frac{\mathrm{Re}\left[\tilde{\omega}\ell\right]}{2}+\frac{l}{2}+\frac{3}{4}+\frac{1}{4}\sqrt{9+4\mu^2\ell^2}\right)-P\left(-\frac{\mathrm{Re}\left[\tilde{\omega}\ell\right]}{2}+\frac{l}{2}+\frac{3}{4}+\frac{1}{4}\sqrt{9+4\mu^2\ell^2}\right)\right)\\ &+\frac{\Gamma\left(1-\frac{1}{2}\sqrt{9+4\mu^2\ell^2}\right)}{\Gamma\left(\frac{\mathrm{Re}[\tilde{\omega}\ell]}{2}+\frac{l}{2}+\frac{3}{4}-\frac{1}{4}\sqrt{9+4\mu^2\ell^2}\right)\Gamma\left(-\frac{\mathrm{Re}[\tilde{\omega}\ell]}{2}+\frac{l}{2}+\frac{3}{4}-\frac{1}{4}\sqrt{9+4\mu^2\ell^2}\right)}\\ &\times\left(P\left(\frac{\mathrm{Re}\left[\tilde{\omega}\ell\right]}{2}+\frac{l}{2}+\frac{3}{4}-\frac{1}{4}\sqrt{9+4\mu^2\ell^2}\right)-P\left(-\frac{\mathrm{Re}\left[\tilde{\omega}\ell\right]}{2}+\frac{l}{2}+\frac{3}{4}-\frac{1}{4}\sqrt{9+4\mu^2\ell^2}\right)\right).\end{aligned} \tag{B.21}$$

Here, $P(z)$ is the digamma function. Eq. (B.19) is the same as Eq. (4.62).

$\Sigma_{2,R}$ and $\Sigma_{2,I}$

$D_2(\tilde{\omega},\kappa)$ in Eq. (4.57) is explicitly

$$\begin{aligned}D_2\left(\tilde{\omega},\kappa\right) =&\frac{\Gamma\left(-l-\frac{1}{2}\right)}{\Gamma\left(l+\frac{1}{2}\right)}\\ &\times\left(\frac{\kappa\Gamma\left(1+\frac{1}{2}\sqrt{9+4\mu^2\ell^2}\right)}{\Gamma\left(\frac{\tilde{\omega}\ell}{2}-\frac{l}{2}+\frac{1}{4}+\frac{1}{4}\sqrt{9+4\mu^2\ell^2}\right)\Gamma\left(-\frac{\tilde{\omega}\ell}{2}-\frac{l}{2}+\frac{1}{4}+\frac{1}{4}\sqrt{9+4\mu^2\ell^2}\right)}\right.\\ &\left.+\frac{\Gamma\left(1-\frac{1}{2}\sqrt{9+4\mu^2\ell^2}\right)}{\Gamma\left(\frac{\tilde{\omega}\ell}{2}-\frac{l}{2}+\frac{1}{4}-\frac{1}{4}\sqrt{9+4\mu^2\ell^2}\right)\Gamma\left(-\frac{\tilde{\omega}\ell}{2}-\frac{l}{2}+\frac{1}{4}-\frac{1}{4}\sqrt{9+4\mu^2\ell^2}\right)}\right).\end{aligned} \tag{B.22}$$

We have

$$\frac{\Gamma\left(-l-\frac{1}{2}\right)}{\Gamma\left(l+\frac{1}{2}\right)}=\frac{2^{2l+1}\left(-1\right)^{l+1}}{(2l+1)!!\,(2l-1)!!}, \tag{B.23}$$

by using properties of the gamma functions for a non-negative integer m,

$$\begin{aligned}\Gamma\left(-m-\frac{1}{2}\right) =&(-1)^{m+1}2^{m+1}\frac{\pi^{1/2}}{(2m+1)!!},\\ \Gamma\left(m+\frac{1}{2}\right) =&2^{-m}\pi^{1/2}(2m-1)!!.\end{aligned} \tag{B.24}$$

Assuming $|\mathrm{Im}\left[\tilde{\omega}\ell\right]| \ll 1$, $D_2\left(\tilde{\omega},\kappa\right)$ takes a form

$$D_2\left(\tilde{\omega},\kappa\right) = \frac{2^{2l+1}\left(-1\right)^{l+1}}{\left(2l+1\right)!!\left(2l-1\right)!!}\left[\Sigma_{2,R} - -i\frac{\Sigma_{2,I}}{2}\mathrm{Im}\left[\tilde{\omega}\ell\right]\right] + \mathcal{O}\left(\left(\mathrm{Im}\left[\tilde{\omega}\ell\right]\right)^2\right), \tag{B.25}$$

where

$$\begin{aligned}\Sigma_{2,R} =& \frac{\kappa\Gamma\left(1+\frac{1}{2}\sqrt{9+4\mu^2\ell^2}\right)}{\Gamma\left(\frac{\mathrm{Re}[\tilde{\omega}\ell]}{2}-\frac{l}{2}+\frac{1}{4}+\frac{1}{4}\sqrt{9+4\mu^2\ell^2}\right)\Gamma\left(-\frac{\mathrm{Re}[\tilde{\omega}\ell]}{2}-\frac{l}{2}+\frac{1}{4}+\frac{1}{4}\sqrt{9+4\mu^2\ell^2}\right)} \\ &+ \frac{\Gamma\left(1-\frac{1}{2}\sqrt{9+4\mu^2\ell^2}\right)}{\Gamma\left(\frac{\mathrm{Re}[\tilde{\omega}\ell]}{2}-\frac{l}{2}+\frac{1}{4}-\frac{1}{4}\sqrt{9+4\mu^2\ell^2}\right)\Gamma\left(-\frac{\mathrm{Re}[\tilde{\omega}\ell]}{2}-\frac{l}{2}+\frac{1}{4}-\frac{1}{4}\sqrt{9+4\mu^2\ell^2}\right)}\end{aligned} \tag{B.26}$$

and

$$\begin{aligned}\Sigma_{2,I} =& \frac{\kappa\Gamma\left(1+\frac{1}{2}\sqrt{9+4\mu^2\ell^2}\right)}{\Gamma\left(\frac{\mathrm{Re}[\tilde{\omega}\ell]}{2}-\frac{l}{2}+\frac{1}{4}+\frac{1}{4}\sqrt{9+4\mu^2\ell^2}\right)\Gamma\left(-\frac{\mathrm{Re}[\tilde{\omega}\ell]}{2}-\frac{l}{2}+\frac{1}{4}+\frac{1}{4}\sqrt{9+4\mu^2\ell^2}\right)} \\ &\times\left(P\left(\frac{\mathrm{Re}\left[\tilde{\omega}\ell\right]}{2}-\frac{l}{2}+\frac{1}{4}+\frac{1}{4}\sqrt{9+4\mu^2\ell^2}\right)-P\left(-\frac{\mathrm{Re}\left[\tilde{\omega}\ell\right]}{2}-\frac{l}{2}+\frac{1}{4}+\frac{1}{4}\sqrt{9+4\mu^2\ell^2}\right)\right) \\ &+ \frac{\Gamma\left(1-\frac{1}{2}\sqrt{9+4\mu^2\ell^2}\right)}{\Gamma\left(\frac{\mathrm{Re}[\tilde{\omega}\ell]}{2}-\frac{l}{2}+\frac{1}{4}-\frac{1}{4}\sqrt{9+4\mu^2\ell^2}\right)\Gamma\left(-\frac{\mathrm{Re}[\tilde{\omega}\ell]}{2}-\frac{l}{2}+\frac{1}{4}-\frac{1}{4}\sqrt{9+4\mu^2\ell^2}\right)} \\ &\times\left(P\left(\frac{\mathrm{Re}\left[\tilde{\omega}\ell\right]}{2}-\frac{l}{2}+\frac{1}{4}-\frac{1}{4}\sqrt{9+4\mu^2\ell^2}\right)-P\left(-\frac{\mathrm{Re}\left[\tilde{\omega}\ell\right]}{2}-\frac{l}{2}+\frac{1}{4}-\frac{1}{4}\sqrt{9+4\mu^2\ell^2}\right)\right).\end{aligned} \tag{B.27}$$

Here, $P(z)$ is the digamma function. Eq. (B.25) is the same as Eq. (4.63).

$\mathrm{Re}[B_1/B2]$ and $\mathrm{Im}[B_1/B2]$

The left-hand side of Eq. (4.57) is explicitly

$$\frac{B_1(\tilde{\omega},\sigma)}{B_2(\tilde{\omega},\sigma)}\ell^{-2l-1} = \frac{\Gamma\left(l+1\right)\Gamma\left(-2l-1\right)\Gamma\left(-2i\sigma+l+1\right)}{\Gamma\left(2l+1\right)\Gamma\left(-l\right)\Gamma\left(-2i\sigma-l\right)}\left(\frac{r_+}{\ell}-\frac{r_-}{\ell}\right)^{2l+1}. \tag{B.28}$$

This is rewritten as

$$\frac{B_1(\tilde{\omega},\sigma)}{B_2(\tilde{\omega},\sigma)}\ell^{-2l-1} = 2i\left(\tilde{\omega}-\frac{eQ}{r_+}\right)\frac{{r_+}^2}{\ell}\left(\frac{r_+}{\ell}-\frac{r_-}{\ell}\right)^{2l}\frac{\left(l!\right)^2}{\left(2l\right)!\left(2l+1\right)!}\prod_{k=1}^{l}\left(k^2+4\sigma^2\right), \tag{B.29}$$

with the aid of properties and functional relations of the gamma functions,

$$\Gamma(k+z) = (k-1+z)(k-2+z)\cdots(1+z)\Gamma(1+z), \tag{B.30}$$

$$\frac{\Gamma(-2m-1)}{\Gamma(-m)} = (-1)^{m+1}\frac{m!}{(2m+1)!}, \tag{B.31}$$

$$\frac{\Gamma(-2iz+m+1)}{\Gamma(-2iz-m)} = 2iz(-1)^{m+1}\prod_{k=1}^{m}\left(k^2+4z^2\right), \tag{B.32}$$

for a complex number z, and non-negative integers k, m. Then, the real and imaginary parts of Eq. (B.29) are respectively

$$\mathrm{Re}\left[\frac{B_1}{B_2}\right]\ell^{-2l-1} = -2\left(\mathrm{Im}\left[\tilde{\omega}\ell\right]\right)\left(\frac{r_+}{\ell}\right)^2\left(\frac{r_+}{\ell}-\frac{r_-}{\ell}\right)^{2l}\frac{(l!)^2}{(2l)!\,(2l+1)!}\prod_{k=1}^{l}\left(k^2+4\sigma^2\right), \tag{B.33}$$

and

$$\mathrm{Im}\left[\frac{B_1}{B_2}\right]\ell^{-2l-1} = 2\ell\left(\mathrm{Re}\left[\tilde{\omega}\right]-\frac{eQ}{r_+}\right)\left(\frac{r_+}{\ell}\right)^2\left(\frac{r_+}{\ell}-\frac{r_-}{\ell}\right)^{2l}\frac{(l!)^2}{(2l)!\,(2l+1)!}\prod_{k=1}^{l}\left(k^2+4\sigma^2\right). \tag{B.34}$$

We notice here that $\mathrm{Re}[B_1/B_2] = \mathcal{O}(\mathrm{Im}\left[\tilde{\omega}\ell\right], (r_+/\ell)^{2(l+1)})$ and $\mathrm{Im}[B_1/B_2] = \mathcal{O}((\mathrm{Im}\left[\tilde{\omega}\ell\right])^0, (r_+/\ell)^{2(l+1)})$.

$(-1)^{l+1}\,\Sigma_{2,R}/\Sigma_{1,I} \to -\,(-1)^{l+1}\,\Sigma_{2,R}/\Sigma_{1,I}$ **under** $\mathrm{Re}[\tilde{\omega}] \to -\mathrm{Re}[\tilde{\omega}]$

We shall explicitly show that $(-1)^{l+1}\,\Sigma_{2,R}/\Sigma_{1,I}$ changes the sign under $\mathrm{Re}[\tilde{\omega}] \to -\mathrm{Re}[\tilde{\omega}]$. First, we express the boundary condition parameter κ as a function of $\mathrm{Re}[\tilde{\omega}\ell]$, $\mu^2\ell^2$, and l by using Eq. (4.67). Then, we can express the leading term of $\Sigma_{1,I}$ and $\Sigma_{2,R}$ in $r_+/\ell \ll 1$ as a function of them:

$$\begin{aligned}\Sigma_{1,I} =& \frac{\Gamma\left(1-\frac{1}{2}\sqrt{9+4\mu^2\ell^2}\right)}{\Gamma\left(\frac{\mathrm{Re}[\tilde{\omega}\ell]}{2}+\frac{l}{2}+\frac{3}{4}-\frac{1}{4}\sqrt{9+4\mu^2\ell^2}\right)\Gamma\left(-\frac{\mathrm{Re}[\tilde{\omega}\ell]}{2}+\frac{l}{2}+\frac{3}{4}-\frac{1}{4}\sqrt{9+4\mu^2\ell^2}\right)} \\ &\times\left[P\left(\frac{\mathrm{Re}\left[\tilde{\omega}\ell\right]}{2}+\frac{l}{2}+\frac{3}{4}-\frac{1}{4}\sqrt{9+4\mu^2\ell^2}\right)-P\left(-\frac{\mathrm{Re}\left[\tilde{\omega}\ell\right]}{2}+\frac{l}{2}+\frac{3}{4}-\frac{1}{4}\sqrt{9+4\mu^2\ell^2}\right)\right. \\ &\left.-P\left(\frac{\mathrm{Re}\left[\tilde{\omega}\ell\right]}{2}+\frac{l}{2}+\frac{3}{4}+\frac{1}{4}\sqrt{9+4\mu^2\ell^2}\right)+P\left(-\frac{\mathrm{Re}\left[\tilde{\omega}\ell\right]}{2}+\frac{l}{2}+\frac{3}{4}+\frac{1}{4}\sqrt{9+4\mu^2\ell^2}\right)\right] \\ &+\mathcal{O}\left(\left(\frac{r_+}{\ell}\right)^{2(l+1)}\right),\end{aligned} \tag{B.35}$$

and

$$\Sigma_{2,R} = \frac{\Gamma\left(1-\frac{1}{2}\sqrt{9+4\mu^2\ell^2}\right)}{\Gamma\left(\frac{\mathrm{Re}[\tilde{\omega}\ell]}{2}+\frac{l}{2}+\frac{3}{4}-\frac{1}{4}\sqrt{9+4\mu^2\ell^2}\right)\Gamma\left(-\frac{\mathrm{Re}[\tilde{\omega}\ell]}{2}+\frac{l}{2}+\frac{3}{4}-\frac{1}{4}\sqrt{9+4\mu^2\ell^2}\right)}$$
$$\times\left[\frac{\Gamma\left(\frac{\mathrm{Re}[\tilde{\omega}\ell]}{2}+\frac{l}{2}+\frac{3}{4}-\frac{1}{4}\sqrt{9+4\mu^2\ell^2}\right)\Gamma\left(-\frac{\mathrm{Re}[\tilde{\omega}\ell]}{2}+\frac{l}{2}+\frac{3}{4}-\frac{1}{4}\sqrt{9+4\mu^2\ell^2}\right)}{\Gamma\left(\frac{\mathrm{Re}[\tilde{\omega}\ell]}{2}-\frac{l}{2}+\frac{1}{4}-\frac{1}{4}\sqrt{9+4\mu^2\ell^2}\right)\Gamma\left(-\frac{\mathrm{Re}[\tilde{\omega}\ell]}{2}-\frac{l}{2}+\frac{1}{4}-\frac{1}{4}\sqrt{9+4\mu^2\ell^2}\right)}\right.$$
$$\left.-\frac{\Gamma\left(\frac{\mathrm{Re}[\tilde{\omega}\ell]}{2}+\frac{l}{2}+\frac{3}{4}+\frac{1}{4}\sqrt{9+4\mu^2\ell^2}\right)\Gamma\left(-\frac{\mathrm{Re}[\tilde{\omega}\ell]}{2}+\frac{l}{2}+\frac{3}{4}+\frac{1}{4}\sqrt{9+4\mu^2\ell^2}\right)}{\Gamma\left(\frac{\mathrm{Re}[\tilde{\omega}\ell]}{2}-\frac{l}{2}+\frac{1}{4}+\frac{1}{4}\sqrt{9+4\mu^2\ell^2}\right)\Gamma\left(-\frac{\mathrm{Re}[\tilde{\omega}\ell]}{2}-\frac{l}{2}+\frac{1}{4}+\frac{1}{4}\sqrt{9+4\mu^2\ell^2}\right)}\right]$$
$$+\mathcal{O}\left(\left(\frac{r_+}{\ell}\right)^{2(l+1)}\right). \tag{B.36}$$

It follows from the above equations that $\Sigma_{1,I} \to -\Sigma_{1,I}$ under $\mathrm{Re}[\tilde{\omega}] \to -\mathrm{Re}[\tilde{\omega}]$, while $\Sigma_{2,R} \to \Sigma_{2,R}$. Hence, $(-1)^{l+1}\,\Sigma_{2,R}/\Sigma_{1,I}$ changes the sign for $\mathrm{Re}[\tilde{\omega}] \to -\mathrm{Re}[\tilde{\omega}]$. This is consistent with the results in Figures 4.3(a) and 4.3(b).

Appendix C

Reduction of scalar fields in extremal black holes to massive scalar fields in two-dimensional anti-de Sitter spacetimes

We explain the reduction of scalar fields in extremal black hole spacetimes to massive scalar fields in two-dimensional anti-de Sitter spacetimes (AdS_2).

Massless scalar field perturbations in four-dimensional extremal Reissner-Nordström spacetimes

For convenience, we rewrite the extremal Reissner-Nordström metric (2.72) as

$$ds^2 = -\frac{\rho^2}{(r_+ + \rho)^2} dv^2 + 2dvd\rho + (r_+ + \rho)^2 \, d\Omega^2. \tag{C.1}$$

where

$$\rho = r - r_+, \tag{C.2}$$

and $dv = dt + d\rho(r_+ + \rho)^2/\rho^2$. By definition of ρ, the event horizon is located at $\rho = 0$, and the exterior region corresponds to $\rho > 0$. The coordinate transformation

$$v = \frac{\tilde{v}}{\epsilon}, \quad \rho = \epsilon\tilde{\rho}, \tag{C.3}$$

and taking the limit of $\epsilon \to 0$ give rise to the near-horizon geometry of the extremal Reissner-Nordström black hole,

$$ds^2 = -r_+^{-2}\tilde{\rho}^2 d\tilde{\rho}^2 + 2d\tilde{v}d\tilde{\rho} + r_+^2 d\Omega^2. \tag{C.4}$$

We consider a test massless scalar field $\Phi(v, \rho, \theta, \varphi)$ obeying

$$\Box\Phi = 0. \tag{C.5}$$

Expanding the field in the scalar harmonics $Y_{\ell m}(\theta, \varphi)$ as

$$\Phi = \phi_\ell(v, \rho) \sum_{\ell=0}^{\infty} \sum_{m=-\ell}^{\ell} Y_{\ell m}(\theta, \varphi), \tag{C.6}$$

we obtain an equation for ϕ_ℓ,

$$\partial_\rho\left(\rho^2\partial_\rho\phi_\ell\right) + 2(r_+ + \rho)\,\partial_v\partial_\rho\left[(r_+ + \rho)\,\phi_\ell\right] - \ell(\ell+1)\phi_\ell = 0. \tag{C.7}$$

This equation can be rewritten as

$$\left[2\partial_v\partial_\rho + \partial_\rho\left(r_+^{-2}\rho^2\partial_\rho\right) - r_+^{-2}\ell(\ell+1)\right]\phi_\ell = \delta[\phi_\ell], \tag{C.8}$$

where

$$\delta\left[\phi_\ell\right] = -2r_+^{-1}\partial_v\left[2\rho\partial_\rho\phi_\ell + \phi_\ell\right]. \tag{C.9}$$

We note that the first and second terms in the square bracket of the left-hand side of Eq. (C.8) can be written by the d'Alembertian for AdS_2, i.e.,

$$2\partial_v\partial_\rho + \partial_\rho\left(r_+^{-2}\rho^2\partial_\rho\right) =: \Box_{\mathrm{AdS}_2}. \tag{C.10}$$

Performing the coordinate transformation (C.3), Eq. (C.8) takes the form

$$\left[\tilde{\Box}_{\mathrm{AdS}_2} - r_+^{-2}\ell(\ell+1)\right]\phi_\ell = \mathcal{O}(\epsilon), \tag{C.11}$$

where $\tilde{\Box}_{\mathrm{AdS}_2} := 2\partial_{\tilde{v}}\partial_{\tilde{\rho}} + \partial_{\tilde{\rho}}(r_+^{-2}\tilde{\rho}^2\partial_{\tilde{\rho}})$. Thus, in the limit of $\epsilon \to 0$, Eq. (C.11) is reduced to the massive Klein-Gordon equation with mass squared $m^2 = r_+^{-2}\ell(\ell+1)$ $(\ell = 0, 1, 2, \cdots)$ in AdS_2.

Massive scalar field perturbations in any static and spherically symmetric extremal black hole spacetimes

In the same manner, we can reduce massive scalar fields in any static and spherically symmetric black hole into massive scalar fields in AdS_2. As explained in section 2.4, in the Gaussian null coordinates (v, ρ, θ^A), the static and spherical symmetric extremal black holes in n dimensions are described by

$$ds^2 = -\rho^2\left(\lambda_0 + \delta\lambda(\rho)\right)dv^2 + 2dvd\rho + \left(\gamma_0 + \delta\gamma(\rho)\right)d\Omega_{n-2}^2, \tag{C.12}$$

where λ_0, γ_0 are positive constants, $\delta\lambda(\rho)$, $\delta\gamma(\rho)$ are functions with $\delta\lambda(0) = \delta\gamma(0) = 0$, and $d\Omega_{n-2}^2 = \gamma_{AB}d\theta^A d\theta^B$ is the line element of the $(n-2)$-dimensional unit sphere, $A, B = 2, 3, \cdots n-1$.

Massive scalar fields that we consider satisfy

$$\left[\Box - \mu^2\right] \Phi\left(v, \rho, \theta^A\right) = 0. \tag{C.13}$$

Expanding Φ as in Eq. (C.6), we obtain an equation for $\phi_\ell(v, \rho)$. With the transformation (C.3) and the limit $\epsilon \to 0$, that equation is reduced to

$$\left[\tilde{\Box}_{\mathrm{AdS}_2} - \lambda_0\Delta(\Delta - 1)\right] \phi_\ell = 0, \tag{C.14}$$

where

$$\Delta := \frac{1}{2} + \sqrt{\frac{\mu^2}{\lambda_0} + \frac{\ell(\ell + n - 3)}{\lambda_0\gamma_0} + \frac{1}{4}}. \tag{C.15}$$

If a value $N \equiv \Delta - 1$ is an integer, the discussion in chapter 5 can apply to the current system straightforwardly. The value N becomes an integer in three cases: (i) $\mu = 0$ and $\ell = 0$ case, (ii) $\mu^2 = \lambda_0 k(k+1)$ ($k = 0, 1, 2, \cdots$) and $\ell = 0$ case, and (iii) $\mu = 0$ and $\lambda_0\gamma_0 = (n-3)^2$ case. Note that $\lambda_0\gamma_0 = (n-3)^2$ holds for n-dimensional extremal Reissner-Nordström spacetimes. In particular, if N is an integer, the extremal black holes have the Aretakis constants, if not such a conserved quantity cannot be found [136].

Appendix D

Appendix of Chapter 5

D.1 Mass ladder operators in AdS_2

We briefly review the mass ladder operators [132, 133] in AdS_2, which map solutions of the massive Klein-Gordon equation into that with the different mass squared.

Spacetime conformal symmetries and mass ladder operators

It is said that an n-dimensional spacetime $(\mathcal{M}, g_{ab})$ possesses a spacetime conformal symmetry if the metric g_{ab} admits a conformal isometry ϕ defined by $\phi : \mathcal{M} \to \mathcal{M}$ such that $\phi^* g_{ab} = \exp(2Q) g_{ab}$, where Q is a function on $\mathcal{M}$. The transformation of the conformal isometry group is generated by an infinitesimal coordinate transformation $x^a \to \bar{x}^a = x^a - \zeta^a$ along a vector field ζ^a called a *conformal Killing vector*. The conformal Killing vector ζ^a obeys the *conformal Killing equation*

$$\mathcal{L}_\zeta g_{ab} = 2Q g_{ab}, \quad Q = \frac{1}{n} \nabla_a \zeta^a. \tag{D.1}$$

A conformal Killing vector is said to be *closed* if $\nabla_{[a}\zeta_{b]} = 0$ is satisfied. Then, the closed conformal Killing vector satisfies the *closed conformal Killing equation*

$$\nabla_a \zeta_b = Q g_{ab}. \tag{D.2}$$

If the closed conformal Killing vector ζ^a further satisfies

$$R^a{}_b \zeta^b = \lambda \, \zeta^a, \tag{D.3}$$

where λ is a constant, we can define *the mass ladder operator* [132, 133],

$$D_k := \mathcal{L}_\zeta - kQ, \quad k \in \mathbb{R}, \tag{D.4}$$

which maps a solution of the massive Klein-Gordon equation to that with a different mass squared, i.e., for a solution of the massive Klein-Gordon equation,

$$\left[\Box - m^2\right] \Phi = 0, \tag{D.5}$$

with $m^2 = -\lambda k(k+n-1)$, $D_k\Phi$ becomes another solution of the massive Klein-Gordon equation

$$[\Box - (m^2 + \delta m^2)] D_k \Phi = 0, \tag{D.6}$$

with $m^2 + \delta m^2 = -\lambda(k-1)(k+n-2)$. Here, we have used the commutation relations for D_k,

$$[\Box, D_k] = \lambda(2k+n-2)D_k + \frac{2}{n}(\nabla_a \zeta^a)\left[\Box + \lambda k(k+n-1)\right]. \tag{D.7}$$

Note that the condition (D.3) is automatically satisfied for vacuum solutions of the Einstein equations with a cosmological constant, e.g., the anti-de Sitter spacetime. For a given mass squared with $(n-1)^2 - 4m^2/\lambda \geq 0$ ($\lambda \neq 0$), there are two possible $k = k_\pm$ as solutions of $m^2 = -\lambda k(k+n-1)$,

$$k_\pm = \frac{1 - n \pm \sqrt{(n-1)^2 - 4m^2/\lambda}}{2}. \tag{D.8}$$

The mass ladder operators D_k correspond to a mass raising or lowering operator, depending on the sign of λ.

If there exist two or more closed conformal Killing vectors, we can investigate the Lie bracket among them. It is defined by

$$\xi^a{}_{i,j} := [\zeta_i, \zeta_j]^a = \zeta^b{}_i \nabla_b \zeta^a{}_j - \zeta^b{}_j \nabla_b \zeta^a{}_i, \tag{D.9}$$

where the indices "i" and"j" label the different closed conformal Killing vectors. Then, the vectors (D.9) satisfy the Killing equation $\mathcal{L}_\xi g_{ab} = 0$, where we have used Eq. (D.3).

Explicit forms of mass ladder operators in AdS_2

In the AdS_2 cases, i.e., $n = 2$ and $\lambda = -1$, the mass ladder operators exist when $m^2 \geq m^2_{\mathrm{BF}} = -1/4$. Note that this condition corresponds to the non-negativity of the inside of the square root in Eq. (D.8). For the massive Klein-Gordon equation (D.5) in AdS_2, $k_\pm$ in Eq. (D.8) are

$$k_+ = b, \quad k_- = -(b+1), \tag{D.10}$$

where we parametrized the mass squared as $m^2 = b(b+1)$.[1] Note that $k_- = -\Delta_m$ in Eq. (5.8).

Solving the closed conformal Killing equation (D.2) for AdS_2, we obtain three closed conformal Killing vectors,

$$\begin{aligned} \zeta_{-1} &= \partial_v + r^2\partial_r, \\ \zeta_0 &= v\partial_v + \left(r + vr^2\right)\partial_r, \\ \zeta_1 &= v^2\partial_v + \left(2 + 2vr + v^2r^2\right)\partial_r. \end{aligned} \tag{D.11}$$

We note here that ζ^a_{-1} and ζ^a_0 become null on the Poincaré horizon, while ζ^a_1 does not. We comment that the Lie bracket (D.9) among the closed conformal Killing vectors ζ^a_i $(i = -1, 0, 1)$ yields three Killing vectors,

$$\begin{aligned} \xi_{-1}\,(:= \xi_{0,-1}) &= \partial_v, \\ \xi_0\,(:= \xi_{-1,1}) &= v\partial_v - r\partial_r, \\ \xi_1\,(:= \xi_{1,0}) &= v^2\partial_v - 2\,(1+vr)\,\partial_r. \end{aligned} \tag{D.12}$$

Using the closed conformal Killing vectors (D.11), we obtain three mass ladder operators,

$$\begin{aligned} D_{-1,k} =& \partial_v + r^2\partial_r - kr, \\ D_{0,k} =& v\partial_v + r\,(1+vr)\,\partial_r - k\,(1+vr)\,, \\ D_{1,k} =& v^2\partial_v + \left(2 + 2vr + v^2r^2\right)\partial_r - kv\,(2+vr)\,. \end{aligned} \tag{D.13}$$

For the closed conformal Killing vectors ζ^a_i in Eq. (D.11), the mass ladder operators $D_{i,k}$ defined in Eq. (D.13) map a solution of the massive Klein-Gordon equation (D.5) with $m^2 = k(k+1)$ to that with a different mass squared $m^2 + \delta m^2 = (k-1)k$. Note that if we consider the general closed conformal Killing vectors $\zeta = a_{-1}\zeta_{-1} + a_0\zeta_0 + a_1\zeta_1$, where a_{-1}, a_0, a_1 are constants, we can construct the general mass ladder operators in AdS_2 as

$$D_k = a_{-1}D_{-1,k} + a_0 D_{0,k} + a_1 D_{1,k}. \tag{D.14}$$

The commutation relation (D.7) can be written as

$$D_{i,k-2}\left[\Box - k(k+1)\right] = \left[\Box - k(k-1)\right] D_{i,k}. \tag{D.15}$$

Using this, for a positive integer s, we can show

$$\begin{aligned} &D_{i_s,k-s-1}\cdots D_{i_2,k-3}D_{i_1,k-2}\left[\Box - k(k+1)\right] \\ &= \left[\Box - (k-s)(k+s-1)\right] D_{i_s,k-s+1}\cdots D_{i_2,k-1}D_{i_1,k}. \end{aligned} \tag{D.16}$$

[1] In the derivation of Eq. (D.10), we have assumed $b \geq -1/2$. If $b < -1/2$, $k_+ = -(b+1)$ and $k_- = b$. We note that $m^2 = b(b+1)$ with $b \geq -1/2$ corresponds to $m^2 \geq m^2_{\rm BF}$; thus, it is enough to consider $b \geq -1/2$ cases.

Mass ladder operators in the global chart

We introduce here the mass ladder operators in the (U, V) chart in Eq. (5.16),

$$\begin{aligned} D_{-1,k} =& \cos^2 V \partial_V - \cos^2 U \partial_U - k \frac{2 \cos V \cos U}{\sin (U - V)}, \\ D_{0,k} =& \sin V \cos V \partial_V - \sin U \cos U \partial_U - k \frac{\sin (U + V)}{\sin (U - V)}, \\ D_{1,k} =& \sin^2 V \partial_V - \sin^2 U \partial_U - k \frac{2 \sin U \sin V}{\sin (U - V)}. \end{aligned} \tag{D.17}$$

We note that the above mass ladder operators are regular differential operators except at the AdS boundary, and the divergent behavior at the AdS boundary changes the asymptotic behavior of the scalar fields near the AdS boundary from $\Phi(U, V) \sim c_1 (U - V)^{-k} + c_2 (U - V)^{(k+1)}$ to $D_{i,k}\Phi \sim c_1 (U - V)^{-(k-1)} + c_2 (U - V)^k$, where $c_1 = c_1(U)$ and $c_2 = c_2(U)$, and we have assumed the mass squared of the massive Klein-Gordon equation is $m^2 = k(k + 1)(\geq -1/4)$ [132].

We can construct the general solutions of the massive Klein-Gordon equation (5.19) with the mass squared $m^2 = \ell(\ell + 1)$ $(\ell = 1, 2, \cdots)$, from the general solution of the massless Klein-Gordon equation, $\Phi_0(U, V) = F(U) + G(V)$, as follows:

$$\Phi_\ell (U, V) = D_{i_\ell, -\ell} D_{i_{\ell-1}, -(\ell-1)} \cdots D_{i_1, -1} \Phi_0. \tag{D.18}$$

Because the mass ladder operators are surjective (onto) maps as shown in Ref. [132], $\Phi_\ell(U, V)$ becomes the general solution of the massive Klein-Gordon equation. For example, $\Phi_1(U, V)$ with $D_{-1,k}$ becomes

$$\Phi_1 (U, V) = \frac{2 \cos U \cos V}{\sin (U - V)} \left(F(U) + G(V) \right) - \cos^2 U \partial_U F(U) + \cos^2 V \partial_V G(V). \tag{D.19}$$

If we impose the normalizable boundary condition at $U = V$, we obtain Eq. (5.31).

D.2 Proof of Proposition 3

In this proof, for scalar fields with the mass squared $m^2 = \ell(\ell + 1)$ $(\ell = 0, 1, 2, \cdots)$, we write Φ, n_{-1}, n_0, n_1 as $\Phi_\ell, n^\ell_{-1}, n^\ell_0, n^\ell_1$, respectively. We expand $\Phi_\ell(v, r)$ as a Taylor series around $r = 0$,

$$\Phi_\ell (v, r) = \sum_{s=0}^{\infty} C^\ell_s (v) r^s. \tag{D.20}$$

where $C_s^\ell(v)$ is given by $C_s^\ell(v) = (s!)^{-1}\,\partial_r^s \Phi_\ell|_{r=0}$. The massive Klein-Gordon equation (5.53) becomes

$$\sum_{s=1}^{\infty}\left[2s\frac{dC_s^\ell}{dv} + (s+\ell)(s-\ell-1)C_{s-1}^\ell\right] r^s = 0, \tag{D.21}$$

then, we obtain the relation[2]

$$\frac{dC_s^\ell}{dv} = -\frac{(s+\ell)(s-\ell-1)}{2s}C_{s-1}^\ell. \tag{D.22}$$

We would like to show that if the relation (5.54) holds for ℓ, then it also holds for $\ell+1$,

$$2^{-n_1^{\ell+1}+n_0^{\ell+1}} r^{-2n_{-1}^{\ell+1}-n_0^{\ell+1}} \partial_r D_{i_\ell,1} D_{i_{\ell-1},2}\cdots D_{i_1,\ell} D_{i_{\ell+1},\ell+1}\Phi_{\ell+1} = \partial_r^{\ell+2}\Phi_{\ell+1} + \mathcal{O}(r), \tag{D.23}$$

where $n_{-1}^{\ell+1} + n_0^{\ell+1} + n_1^{\ell+1} = \ell+1$. We note that relation (5.54) trivially holds for $\ell = 0$. Substituting Eq. (D.22) into Eq. (D.20), after some straightforward calculations, we can show the relations

$$2r^{-2}\partial_r^{\ell+1} D_{-1,\ell+1}\Phi_{\ell+1} = \partial_r^{\ell+2}\Phi_{\ell+1} + \mathcal{O}(r), \tag{D.24}$$

$$r^{-1}\partial_r^{\ell+1} D_{0,\ell+1}\Phi_{\ell+1} = \partial_r^{\ell+2}\Phi_{\ell+1} + \mathcal{O}(r), \tag{D.25}$$

$$2^{-1}\partial_r^{\ell+1} D_{1,\ell+1}\Phi_{\ell+1} = \partial_r^{\ell+2}\Phi_{\ell+1} + \mathcal{O}(r). \tag{D.26}$$

These relations immediately lead to Eq. (D.23). As an example, we show the $i_{\ell+1} = -1$ case below. Since $D_{i_{\ell+1},\ell+1}\Phi_{\ell+1}$ is a solution of the Klein-Gordon equation with the mass squared $\ell(\ell+1)$, we can set

$$\Phi_\ell = D_{-1,\ell+1}\Phi_{\ell+1}. \tag{D.27}$$

The left-hand side of Eq. (D.23) becomes

$$\begin{aligned}
&2^{-n_1^\ell+n_{-1}^\ell+1} r^{-2(n_{-1}^\ell+1)-n_0^\ell}\partial_r D_{i_\ell,1} D_{i_{\ell-1},2}\cdots D_{i_1,\ell} D_{-1,\ell+1}\Phi_{\ell+1} \\
&= 2^{-n_1^\ell+n_{-1}^\ell+1} r^{-2(n_{-1}^\ell+1)-n_0^\ell}\partial_r D_{i_\ell,1} D_{i_{\ell-1},2}\cdots D_{i_1,\ell}\Phi_\ell \\
&= 2r^{-2}\partial_r^{\ell+1}\Phi_\ell + \mathcal{O}(r) \\
&= 2r^{-2}\partial_r^{\ell+1} D_{-1,\ell+1}\Phi_{\ell+1} + \mathcal{O}(r) \\
&= \partial_r^{\ell+2}\Phi_{\ell+1} + \mathcal{O}(r).
\end{aligned} \tag{D.28}$$

Note that the cases for $i_{\ell+1} = 0, 1$ can be shown in the same way.

[2]Note that the relation Eq. (D.22) implies $dC_{\ell+1}^k/dv = 0$; then, $(\ell+1)!C_{\ell+1}^\ell = \mathcal{H}_\ell =$ const. and $dC_{\ell+2}^\ell/dv = -C_{\ell+1}^\ell(\ell+1)/(\ell+2)$; then, $(\ell+2)!C_{\ell+2}^\ell = \partial_r^{\ell+2}\Phi|_{r=0} = -(\ell+1)\mathcal{H}_\ell v +$ const. These correspond to the Aretakis constants and instability in Eqs. (5.4) and (5.6). We note that the coefficients C_s^ℓ with $s \le \ell$ are decaying functions of v if we choose the normalizable modes.

Bibliography

[1] Albert Einstein. *The Foundation of the General Theory of Relativity.* Annalen Phys., 49(7):769–822, 1916.

[2] B. P. Abbott et al. *Observation of Gravitational Waves from a Binary Black Hole Merger.* Phys. Rev. Lett., 116(6):061102, 2016.

[3] B. P. Abbott et al. *GW151226: Observation of Gravitational Waves from a 22-Solar-Mass Binary Black Hole Coalescence.* Phys. Rev. Lett., 116(24):241103, 2016.

[4] B. P. Abbott et al. *Binary Black Hole Mergers in the first Advanced LIGO Observing Run.* Phys. Rev. X, 6(4):041015, 2016. [Erratum: Phys.Rev.X 8, 039903 (2018)].

[5] Kazunori Akiyama et al. *First M87 Event Horizon Telescope Results. I. The Shadow of the Supermassive Black Hole.* Astrophys. J. Lett., 875:L1, 2019.

[6] Kazunori Akiyama et al. *First M87 Event Horizon Telescope Results. II. Array and Instrumentation.* Astrophys. J. Lett., 875(1):L2, 2019.

[7] Kazunori Akiyama et al. *First M87 Event Horizon Telescope Results. III. Data Processing and Calibration.* Astrophys. J. Lett., 875(1):L3, 2019.

[8] Kazunori Akiyama et al. *First M87 Event Horizon Telescope Results. IV. Imaging the Central Supermassive Black Hole.* Astrophys. J. Lett., 875(1):L4, 2019.

[9] Kazunori Akiyama et al. *First M87 Event Horizon Telescope Results. V. Physical Origin of the Asymmetric Ring.* Astrophys. J. Lett., 875(1):L5, 2019.

[10] Kazunori Akiyama et al. *First M87 Event Horizon Telescope Results. VI. The Shadow and Mass of the Central Black Hole.* Astrophys. J. Lett., 875(1):L6, 2019.

[11] Juan Martin Maldacena. *The Large N limit of superconformal field theories and supergravity.* Adv. Theor. Math. Phys., 2:231–252, 1998.

[12] Sean A. Hartnoll. *Lectures on holographic methods for condensed matter physics.* Class. Quant. Grav., 26:224002, 2009.

[13] Edward Shuryak. *Physics of Strongly coupled Quark-Gluon Plasma.* Prog. Part. Nucl. Phys., 62:48–101, 2009.

[14] Yukinao Akamatsu, Tetsuo Hatsuda, and Tetsufumi Hirano. *Heavy Quark Diffusion with Relativistic Langevin Dynamics in the Quark-Gluon Fluid.* Phys. Rev. C, 79:054907, 2009.

[15] Harvey B. Meyer. *Transport Properties of the Quark-Gluon Plasma: A Lattice QCD Perspective.* Eur. Phys. J. A, 47:86, 2011.

[16] Jorge Casalderrey-Solana, Hong Liu, David Mateos, Krishna Rajagopal, and Urs Achim Wiedemann. *Gauge/String Duality, Hot QCD and Heavy Ion Collisions.* Cambridge University Press, 2014.

[17] Wilke van der Schee, Paul Romatschke, and Scott Pratt. *Fully Dynamical Simulation of Central Nuclear Collisions.* Phys. Rev. Lett., 111(22):222302, 2013.

[18] Justin R. David, Gautam Mandal, and Spenta R. Wadia. *Microscopic formulation of black holes in string theory.* Phys. Rept., 369:549–686, 2002.

[19] Juan Maldacena and Leonard Susskind. *Cool horizons for entangled black holes.* Fortsch. Phys., 61:781–811, 2013.

[20] Samir D. Mathur. *The Information paradox: A Pedagogical introduction.* Class. Quant. Grav., 26:224001, 2009.

[21] Micha Berkooz, Amit Sever, and Assaf Shomer. *'Double trace' deformations, boundary conditions and space-time singularities.* JHEP, 05:034, 2002.

[22] Lukasz Fidkowski, Veronika Hubeny, Matthew Kleban, and Stephen Shenker. *The Black hole singularity in AdS / CFT.* JHEP, 02:014, 2004.

[23] Thomas Faulkner, Monica Guica, Thomas Hartman, Robert C. Myers, and Mark Van Raamsdonk. *Gravitation from Entanglement in Holographic CFTs*. JHEP, 03:051, 2014.

[24] Eran Palti. *The Swampland: Introduction and Review*. Fortsch. Phys., 67(6):1900037, 2019.

[25] B. Carter. *Axisymmetric Black Hole Has Only Two Degrees of Freedom*. Phys. Rev. Lett., 26:331–333, 1971.

[26] Bekenstein, Jacob D. *Nonexistence of Baryon Number for Static Black Holes*. Phys. Rev. D, 5:1239–1246, 1972.

[27] S. W. Hawking. *Black holes in general relativity*. Commun. Math. Phys., 25:152–166, 1972.

[28] D. C. Robinson. *Uniqueness of the Kerr black hole*. Phys. Rev. Lett., 34:905–906, 1975.

[29] Aaron J. Amsel, Gary T. Horowitz, Donald Marolf, and Matthew M. Roberts. *Uniqueness of Extremal Kerr and Kerr-Newman Black Holes*. Phys. Rev. D, 81:024033, 2010.

[30] Roy P. Kerr. *Gravitational field of a spinning mass as an example of algebraically special metrics*. Phys. Rev. Lett., 11:237–238, 1963.

[31] Edward W. Leaver. *Spectral decomposition of the perturbation response of the Schwarzschild geometry*. Phys. Rev. D, 34:384–408, 1986.

[32] Nils Andersson. *Evolving test fields in a black hole geometry*. Phys. Rev. D, 55:468–479, 1997.

[33] Vitor Cardoso and Leonardo Gualtieri. *Testing the black hole 'no-hair' hypothesis*. Class. Quant. Grav., 33(17):174001, 2016.

[34] Hirotaka Yoshino and Hideo Kodama. *Bosenova collapse of axion cloud around a rotating black hole*. Prog. Theor. Phys., 128:153–190, 2012.

[35] Vitor Cardoso, Óscar J. C. Dias, Gavin S. Hartnett, Matthew Middleton, Paolo Pani, and Jorge E. Santos. *Constraining the mass of dark photons and axion-like particles through black-hole superradiance*. JCAP, 03:043, 2018.

[36] Steven Blau and Steven K. *A String-Theory Calculation of Viscosity Could Have Surprising Applications*. Physics Today - PHYS TODAY, 58:23–24, 2005.

[37] Karl Schwarzschild. *On the gravitational field of a sphere of incompressible fluid according to Einstein's theory.* Sitzungsber. Preuss. Akad. Wiss. Berlin (Math. Phys.), 1916:424–434, 1916.

[38] Karl Schwarzschild. *On the gravitational field of a mass point according to Einstein's theory.* Sitzungsber. Preuss. Akad. Wiss. Berlin (Math. Phys.), 1916:189–196, 1916.

[39] D. Christodoulou and S. Klainerman. *The Global nonlinear stability of the Minkowski space.* 1993.

[40] Mihalis Dafermos, Gustav Holzegel, Igor Rodnianski, and Martin Taylor. *The non-linear stability of the Schwarzschild family of black holes.* 4 2021.

[41] R. A. Konoplya and A. Zhidenko. *Quasinormal modes of black holes: From astrophysics to string theory.* Rev. Mod. Phys., 83:793–836, 2011.

[42] Paolo Pani, Vitor Cardoso, Leonardo Gualtieri, Emanuele Berti, and Akihiro Ishibashi. *Black hole bombs and photon mass bounds.* Phys. Rev. Lett., 109:131102, 2012.

[43] Sam R. Dolan. *Superradiant instabilities of rotating black holes in the time domain.* Phys. Rev. D, 87(12):124026, 2013.

[44] Asimina Arvanitaki, Savas Dimopoulos, Sergei Dubovsky, Nemanja Kaloper, and John March-Russell. *String Axiverse.* Phys. Rev. D, 81:123530, 2010.

[45] Asimina Arvanitaki and Sergei Dubovsky. *Exploring the String Axiverse with Precision Black Hole Physics.* Phys. Rev. D, 83:044026, 2011.

[46] Matthew J. Stott and David J. E. Marsh. *Black hole spin constraints on the mass spectrum and number of axionlike fields.* Phys. Rev. D, 98(8):083006, 2018.

[47] Otto A. Hannuksela, Kaze W. K. Wong, Richard Brito, Emanuele Berti, and Tjonnie G. F. Li. *Probing the existence of ultralight bosons with a single gravitational-wave measurement.* Nature Astron., 3(5):447–451, 2019.

[48] Carlos A. R. Herdeiro and Eugen Radu. *Kerr black holes with scalar hair.* Phys. Rev. Lett., 112:221101, 2014.

[49] Oscar J. C. Dias, Pau Figueras, Ricardo Monteiro, Jorge E. Santos, and Roberto Emparan. *Instability and new phases of higher-dimensional rotating black holes.* Phys. Rev. D, 80:111701, 2009.

[50] Roberto Emparan and Harvey S. Reall. *Black Holes in Higher Dimensions.* Living Rev. Rel., 11:6, 2008.

[51] Thomas Hertog and Kengo Maeda. *Stability and thermodynamics of AdS black holes with scalar hair.* Phys. Rev. D, 71:024001, 2005.

[52] Oscar J. C. Dias, Ricardo Monteiro, Harvey S. Reall, and Jorge E. Santos. *A Scalar field condensation instability of rotating anti-de Sitter black holes.* JHEP, 11:036, 2010.

[53] Pablo Bosch, Stephen R. Green, and Luis Lehner. *Nonlinear Evolution and Final Fate of Charged Anti–de Sitter Black Hole Superradiant Instability.* Phys. Rev. Lett., 116(14):141102, 2016.

[54] Hector O. Silva, Jeremy Sakstein, Leonardo Gualtieri, Thomas P. Sotiriou, and Emanuele Berti. *Spontaneous scalarization of black holes and compact stars from a Gauss-Bonnet coupling.* Phys. Rev. Lett., 120(13):131104, 2018.

[55] Daniela D. Doneva and Stoytcho S. Yazadjiev. *New Gauss-Bonnet Black Holes with Curvature-Induced Scalarization in Extended Scalar-Tensor Theories.* Phys. Rev. Lett., 120(13):131103, 2018.

[56] Sean A. Hartnoll, Christopher P. Herzog, and Gary T. Horowitz. *Building a Holographic Superconductor.* Phys. Rev. Lett., 101:031601, 2008.

[57] Sean A. Hartnoll, Christopher P. Herzog, and Gary T. Horowitz. *Holographic Superconductors.* JHEP, 12:015, 2008.

[58] Piotr Bizon and Andrzej Rostworowski. *On weakly turbulent instability of anti-de Sitter space.* Phys. Rev. Lett., 107:031102, 2011.

[59] P. Bizoń and A. Rostworowski. *Gravitational Turbulent Instability of AdS_5.* Acta Phys. Polon. B, 48:1375, 2017.

[60] Óscar J. C. Dias, Jorge E. Santos, and Benson Way. *Black holes with a single Killing vector field: black resonators.* JHEP, 12:171, 2015.

[61] Takaaki Ishii and Keiju Murata. *Black resonators and geons in AdS5.* Class. Quant. Grav., 36(12):125011, 2019.

[62] Stephen R. Green, Stefan Hollands, Akihiro Ishibashi, and Robert M. Wald. *Superradiant instabilities of asymptotically anti-de Sitter black holes*. Class. Quant. Grav., 33(12):125022, 2016.

[63] Akihiro Ishibashi and Robert M. Wald. *Dynamics in nonglobally hyperbolic static space-times. 3. Anti-de Sitter space-time*. Class. Quant. Grav., 21:2981–3014, 2004.

[64] Piotr Bizoń, Dominika Hunik-Kostyra, and Maciej Maliborski. *AdS Robin solitons and their stability*. Class. Quant. Grav., 37(10):105010, 2020.

[65] Roger Penrose. *Gravitational collapse and space-time singularities*. Phys. Rev. Lett., 14:57–59, 1965.

[66] Stefanos Aretakis. *Stability and Instability of Extreme Reissner-Nordström Black Hole Spacetimes for Linear Scalar Perturbations I*. Commun. Math. Phys., 307:17–63, 2011.

[67] Stefanos Aretakis. *Stability and Instability of Extreme Reissner-Nordström Black Hole Spacetimes for Linear Scalar Perturbations II*. Annales Henri Poincare, 12:1491–1538, 2011.

[68] Stefanos Aretakis. *Horizon Instability of Extremal Black Holes*. Adv. Theor. Math. Phys., 19:507–530, 2015.

[69] Stefanos Aretakis. *Nonlinear instability of scalar fields on extremal black holes*. Phys. Rev. D, 87:084052, 2013.

[70] Keiju Murata, Harvey S. Reall, and Norihiro Tanahashi. *What happens at the horizon(s) of an extreme black hole?* Class. Quant. Grav., 30:235007, 2013.

[71] Shahar Hadar. *Near-extremal black holes at late times, backreacted*. JHEP, 01:214, 2019.

[72] Yannis Angelopoulos, Stefanos Aretakis, and Dejan Gajic. *Nonlinear scalar perturbations of extremal Reissner-Nordström spacetimes*. 7 2019.

[73] Yannis Angelopoulos, Stefanos Aretakis, and Dejan Gajic. *Late-time asymptotics for the wave equation on extremal Reissner–Nordström backgrounds*. Adv. Math., 375:107363, 2020.

[74] Marta Volonteri, Piero Madau, Eliot Quataert, and Martin J. Rees. *The Distribution and cosmic evolution of massive black hole spins.* Astrophys. J., 620:69–77, 2005.

[75] Jeffrey E. McClintock, Rebecca Shafee, Ramesh Narayan, Ronald A. Remillard, Shane W. Davis, and Li-Xin Li. *The Spin of the Near-Extreme Kerr Black Hole GRS 1915+105.* Astrophys. J., 652:518–539, 2006.

[76] Laura W. Brenneman and Christopher S. Reynolds. *Constraining Black Hole Spin Via X-ray Spectroscopy.* Astrophys. J., 652:1028–1043, 2006.

[77] Lijun Gou, Jeffrey E. McClintock, Ronald A. Remillard, James F. Steiner, Mark J. Reid, Jerome A. Orosz, Ramesh Narayan, Manfred Hanke, and Javier García. *Confirmation Via the Continuum-Fitting Method that the Spin of the Black Hole in Cygnus X-1 is Extreme.* Astrophys. J., 790(1):29, 2014.

[78] Jeffrey E. McClintock, Ramesh Narayan, and James F. Steiner. *Black Hole Spin via Continuum Fitting and the Role of Spin in Powering Transient Jets.* Space Sci. Rev., 183:295–322, 2014.

[79] Takuya Katagiri and Tomohiro Harada. *Stability of small charged anti-de Sitter black holes in the Robin boundary.* Class. Quant. Grav., 38(13):135026, 2021.

[80] Takuya Katagiri and Masashi Kimura. *Revisiting the Aretakis constants and instability in two-dimensional anti–de Sitter spacetimes.* Phys. Rev. D, 103(6):064011, 2021.

[81] Werner Israel. *Event Horizons in Static Vacuum Space-Times.* Phys. Rev., 164:1776–1779, 1967.

[82] F. R. Tangherlini. *Schwarzschild field in n dimensions and the dimensionality of space problem.* Nuovo Cim., 27:636–651, 1963.

[83] Kottler, Friedrich. *Über die physikalischen Grundlagen der Einsteinschen Gravitationstheorie.* Annalen der Physik, 361(14):401–462, jan 1918.

[84] S. W. Hawking and G. F. R. Ellis. *The Large Scale Structure of Space-Time.* Cambridge Monographs on Mathematical Physics. Cambridge University Press, 2 2011.

[85] H. Reissner. *Über die Eigengravitation des elektrischen Feldes nach der Einsteinschen Theorie.* Annalen der Physik, 355(9):106–120, January 1916.

[86] G. Nordström. *On the Energy of the Gravitation field in Einstein's Theory.* Koninklijke Nederlandse Akademie van Wetenschappen Proceedings Series B Physical Sciences, 20:1238–1245, January 1918.

[87] G. Denardo and R. Ruffini. *On the energetics of Reissner Nordström geometries.* Phys. Lett. B, 45:259–262, 1973.

[88] Hari K. Kunduri and James Lucietti. *Classification of near-horizon geometries of extremal black holes.* Living Rev. Rel., 16:8, 2013.

[89] Tullio Regge and John A. Wheeler. *Stability of a Schwarzschild singularity.* Phys. Rev., 108:1063–1069, 1957.

[90] Frank J. Zerilli. *Effective potential for even parity Regge-Wheeler gravitational perturbation equations.* Phys. Rev. Lett., 24:737–738, 1970.

[91] E. S. C. Ching, P. T. Leung, W. M. Suen, and K. Young. *Late time tail of wave propagation on curved space-time.* Phys. Rev. Lett., 74:2414–2417, 1995.

[92] E. S. C. Ching, P. T. Leung, W. M. Suen, and K. Young. *Wave propagation in gravitational systems: Late time behavior.* Phys. Rev. D, 52:2118–2132, 1995.

[93] Richard H. Price. *Nonspherical perturbations of relativistic gravitational collapse. 1. Scalar and gravitational perturbations.* Phys. Rev. D, 5:2419–2438, 1972.

[94] Carsten Gundlach, Richard H. Price, and Jorge Pullin. *Late time behavior of stellar collapse and explosions: 1. Linearized perturbations.* Phys. Rev. D, 49:883–889, 1994.

[95] Carsten Gundlach, Richard H. Price, and Jorge Pullin. *Late time behavior of stellar collapse and explosions: 2. Nonlinear evolution.* Phys. Rev. D, 49:890–899, 1994.

[96] Bernard S. Kay and Robert M. Wald. *Linear Stability of Schwarzschild Under Perturbations Which Are Nonvanishing on the Bifurcation Two Sphere.* Class. Quant. Grav., 4:893–898, 1987.

[97] Mihalis Dafermos and Igor Rodnianski. *Lectures on black holes and linear waves*. Clay Math. Proc., 17:97–205, 2013.

[98] Ya. B. Zel'Dovich. *Generation of Waves by a Rotating Body*. Soviet Journal of Experimental and Theoretical Physics Letters, 14:180, August 1971.

[99] A. A. Starobinsky. *Amplification of waves reflected from a rotating "black hole"*. Sov. Phys. JETP, 37(1):28–32, 1973.

[100] Richard Brito, Vitor Cardoso, and Paolo Pani. *Superradiance: New Frontiers in Black Hole Physics*. Lect. Notes Phys., 906:pp.1–237, 2015.

[101] William H. Press and Saul A. Teukolsky. *Floating Orbits, Superradiant Scattering and the Black-hole Bomb*. Nature, 238:211–212, 1972.

[102] Vitor Cardoso, Oscar J. C. Dias, Jose P. S. Lemos, and Shijun Yoshida. *The Black hole bomb and superradiant instabilities*. Phys. Rev. D, 70:044039, 2004. [Erratum: Phys.Rev.D 70, 049903 (2004)].

[103] T. Damour, N. Deruelle, and R. Ruffini. *On Quantum Resonances in Stationary Geometries*. Lett. Nuovo Cim., 15:257–262, 1976.

[104] S. W. Hawking and H. S. Reall. *Charged and rotating AdS black holes and their CFT duals*. Phys. Rev. D, 61:024014, 2000.

[105] Vitor Cardoso and Oscar J. C. Dias. *Small Kerr-anti-de Sitter black holes are unstable*. Phys. Rev. D, 70:084011, 2004.

[106] Nami Uchikata and Shijun Yoshida. *Quasinormal modes of a massless charged scalar field on a small Reissner-Nordström-anti-de Sitter black hole*. Phys. Rev. D, 83:064020, 2011.

[107] Y. Angelopoulos, Stefanos Aretakis, and Dejan Gajic. *Horizon hair of extremal black holes and measurements at null infinity*. Phys. Rev. Lett., 121(13):131102, 2018.

[108] Robert M. Wald. *DYNAMICS IN NONGLOBALLY HYPERBOLIC, STATIC SPACE-TIMES*. J. Math. Phys., 21:2802–2805, 1980.

[109] Akihiro Ishibashi and Akio Hosoya. *Who's afraid of naked singularities? Probing timelike singularities with finite energy waves*. Phys. Rev. D, 60:104028, 1999.

[110] Claudio Dappiaggi, Hugo R. C. Ferreira, and Carlos A. R. Herdeiro. *Superradiance in the BTZ black hole with Robin boundary conditions.* Phys. Lett. B, 778:146–154, 2018.

[111] Thomas Hertog and Gary T. Horowitz. *Designer gravity and field theory effective potentials.* Phys. Rev. Lett., 94:221301, 2005.

[112] Ramon Masachs and Benson Way. *New islands of stability with double-trace deformations.* Phys. Rev. D, 100(10):106017, 2019.

[113] Takaaki Ishii and Keiju Murata. *Photonic black resonators and photon stars in AdS_5.* Class. Quant. Grav., 37(7):075009, 2020.

[114] Óscar J. C. Dias and Ramon Masachs. *Hairy black holes and the endpoint of AdS_4 charged superradiance.* JHEP, 02:128, 2017.

[115] Norihiro Iizuka, Akihiro Ishibashi, and Kengo Maeda. *A rotating hairy AdS_3 black hole with the metric having only one Killing vector field.* JHEP, 08:112, 2015.

[116] Kengo Maeda, Shunsuke Fujii, and Jun-ichirou Koga. *The final fate of instability of Reissner-Nordström-anti-de Sitter black holes by charged complex scalar fields.* Phys. Rev. D, 81:124020, 2010.

[117] Ofer Aharony, Micha Berkooz, and Eva Silverstein. *Multiple trace operators and nonlocal string theories.* JHEP, 08:006, 2001.

[118] Edward Witten. *Multitrace operators, boundary conditions, and AdS / CFT correspondence.* 12 2001.

[119] Robert M. Wald. *General Relativity.* Chicago Univ. Pr., Chicago, USA, 1984.

[120] Charles W. Misner and David H. Sharp. *Relativistic equations for adiabatic, spherically symmetric gravitational collapse.* Phys. Rev., 136:B571–B576, 1964.

[121] M. Reed and B. Simon. *Methods of Modern Mathematical Physics. 2. Fourier Analysis, Self-adjointness.* 1975.

[122] A. Ishibashi. private communication, 2020.

[123] James Lucietti, Keiju Murata, Harvey S. Reall, and Norihiro Tanahashi. *On the horizon instability of an extreme Reissner-Nordström black hole.* JHEP, 03:035, 2013.

[124] Peter Zimmerman. *Horizon instability of extremal Reissner-Nordström black holes to charged perturbations.* Phys. Rev. D, 95(12):124032, 2017.

[125] Hadi Godazgar, Mahdi Godazgar, and C. N. Pope. *Aretakis Charges and Asymptotic Null Infinity.* Phys. Rev. D, 96(8):084055, 2017.

[126] Samuel E. Gralla and Peter Zimmerman. *Critical Exponents of Extremal Kerr Perturbations.* Class. Quant. Grav., 35(9):095002, 2018.

[127] Samuel E. Gralla and Peter Zimmerman. *Scaling and Universality in Extremal Black Hole Perturbations.* JHEP, 06:061, 2018.

[128] Shahar Hadar and Harvey S. Reall. *Is there a breakdown of effective field theory at the horizon of an extremal black hole?* JHEP, 12:062, 2017.

[129] James Lucietti and Harvey S. Reall. *Gravitational instability of an extreme Kerr black hole.* Phys. Rev. D, 86:104030, 2012.

[130] Keiju Murata. *Instability of higher dimensional extreme black holes.* Class. Quant. Grav., 30:075002, 2013.

[131] Samuel E. Gralla, Arun Ravishankar, and Peter Zimmerman. *Horizon Instability of the Extremal BTZ Black Hole.* JHEP, 05:094, 2020.

[132] Vitor Cardoso, Tsuyoshi Houri, and Masashi Kimura. *Mass Ladder Operators from Spacetime Conformal Symmetry.* Phys. Rev. D, 96(2):024044, 2017.

[133] Vitor Cardoso, Tsuyoshi Houri, and Masashi Kimura. *General first-order mass ladder operators for Klein–Gordon fields.* Class. Quant. Grav., 35(1):015011, 2018.

[134] Peter Breitenlohner and Daniel Z. Freedman. *Stability in Gauged Extended Supergravity.* Annals Phys., 144:249, 1982.

[135] Peter Breitenlohner and Daniel Z. Freedman. *Positive Energy in anti-De Sitter Backgrounds and Gauged Extended Supergravity.* Phys. Lett. B, 115:197–201, 1982.

[136] Takuya Katagiri and Masashi Kimura. *The Aretakis constants and instability in general spherically symmetric extremal black hole spacetimes: higher multipole modes, late-time tails, and geometrical meanings.* 12 2021.

[137] Michele Maggiore. *Gravitational Waves. Vol. 2: Astrophysics and Cosmology*. Oxford University Press, 3 2018.

[138] Frank W. Olver, Daniel W. Lozier, Ronald F. Boisvert, and Charles W. Clark. *NIST Handbook of Mathematical Functions*. Cambridge University Press, 2010.